Microwave spectroscopy of some maser materials

D. A. Curtis

Microwave Spectroscopy of Some Maser Materials,

by

D.A.Curtis, B.Sc. (Dunelm),

Department of Applied Physics.

A thesis submitted in candidature for the degree of

Doctor of Philosophy

Faculty of Science

University of Durham

September, 1964.

ABSTRACT

Vapour phase rubies were examined by several techniques. X-rays showed that the c-axis varied from place to place in each boule by up to 3°. Superimposed on this was a distribution of mosaic structure with the c-axis varying from grain to grain by up to 3°. Annealing did not improve these imperfections. Boules grown in the 90° orientation showed less mosaic than those grown in other orientations. Polygonisation, observed by Scheuplein and Gibbs (1960), provided an explanation. X-ray examination of corundum gave similar results. The random dislocation density revealed by etching was about 10^{5} dislocations/cm^{2} in corundum and ruby, therefore, adding chromium did not produce dislocations. The imperfections did not correlate with the boules' crystallography. The paramagnetic resonance linewidth increases with the imperfection in the sample and this increase is angular dependent. The basic linewidth depends on the chromium concentration. Sample 337c showed little angular broadening in the $+\frac{1}{2}$ to $+\frac{3}{2}$ and the $-\frac{3}{2}$ to $-\frac{1}{2}$ transitions. In G2a the latter transition showed a maximum broadening of about $2\frac{1}{2}$ times near the polar angle 45°. X-rays showed that each sample had similar c-axis misorientations but G2a contained much more mosaic than 337c.

The misorientation predicted by the broadening G2a is 0° 25'. The $-\frac{1}{2}$ to $+\frac{3}{2}$ transition in 337c was about 22 oersteds wide and did not vary much with angle. In G2a this transition broadened to 33 oersteds at polar angles 45° and 30°. The chromium concentration predicted from the basic linewidth at 55° in both samples is 0.43 weight % of chromium. The concentrations given by chemical analysis are 0.052 weight % for 337c and between 0.02 and 0.032 weight % for G2a.

PREFACE.

My supervisor and I joined the Department of Applied Physics on the same day in October, 1961. Since that day a large number of people have exerted a considerable amount of effort to help us erect the spectrometer and its anciliary units which I have used for the measurements on maser materials reported in this thesis. A few of these are aknowledged on page iv. The spectrometer is described in chapter five and the measurements made with it in chapters six and seven. Chapter four contains the basic theoretical work for the measurements which were made. Besides the microwave resonance work, I have made some X-ray and chemical etching measurements in order to investigate points closely related to the main theme of the thesis. These are reported in chapters two and three. The first chapter is a general survey of the background to the work while the final chapter contains a survey of the work performed and some suggestions for future work.

D.A.Curtis.

ACKNOWLEDGEMENTS.

I wish to express my thanks to the organisations and individuals listed below for the assistance, advice and encouragement which they afforded me during the course of the work reported here. It is impossible to gauge the full extent of their contributions to this work, but it is all deeply appreciated. The organisations are the Department of Scientific and Industrial Research, C.V.D. the Admiralty and the Thermal Syndicate Ltd. The individuals are Professor D.A. Wright, my supervisor Dr. J.S. Thorp, the staff and research students of the Department of Applied Physics, especially L. Clark and D.R. Mason, the technical staff of the Department headed by Mr. F. Spence, the electronics technician Mr.E.Lincoln and Mrs. M.L. Bell who has done the typing. Figure 1 is reproduced by kind permission of the Thermal Syndicate Ltd.

CONTENTS.

CHAPTER ONE.

INTRODUCTION.

Introductory comments; description of the growth process of ruby; X-ray, chemical etching and microwave spectroscopy techniques for examination of single crystal boules; relevance of chemical imperfections.

INTRODUCTION.

Gordon et al. (1954) coined the word maser with reference to a gaseous system. Soon afterwards Combrisson et al. (1956) and Bloembergen (1956) discussed different modes of maser action in solids. It was quickly realised that these solid state devices would have important applications in communications as well as in scientific and defence systems, and a large amount of work was initiated on the research and development of these systems. The obvious uses of masers were as sensitive, low noise amplifiers and as stable, low power signal generators in the millimetre and centimetre wavelength region of the spectrum.

Ruby was one of the materials used in the early masers and it is still a common choice. It is also a common choice for solid state lasers which were developed after the maser. To satisfy the demand for crystals to be used in these devices, several sources of artificial material were developed, and it soon became obvious that techniques must be developed for the examination of the material produced to check its suitability as

maser or laser material.

The work described in this thesis is an examination of crystals of ruby grown by flame fusion from the vapour phase (K.H.Jack and G.W.Stephenson, private communication). The aim was to determine the type and distribution of imperfections in the boules. In particular physical imperfections were studied but chemical imperfections were considered when they were relevant to the work. Also of interest were the effects on the paramagnetic resonance spectrum of physical imperfections in a sample.

GROWTH PROCESS.

Ruby is Al_2O_3 with some of the aluminium atoms replaced by chromium atoms which are usually triply ionised. Most of the material examined was grown by flame fusion from the vapour phase. In this process the chemicals are fed into a furnace as vapours (Figure 1). Inside the furnace they react in an oxy-hydrogen flame and the unwanted chemicals are swept away by the gas flow while the remainder are deposited on a suitably placed seed crystal to form the boule. Normally halides of aluminium and chromium are used as the source vapours because they can be produced easily and are vaporised readily. An example of the reactions involved is

$$2Al + 3Cl_2 \longrightarrow 2AlCl_3,$$

$$2AlCl_3 + 3H_2O \longrightarrow 6HCl + Al_2O_3.$$

A chromium halide is introduced similarly. The advantage of using gaseous feeds is that the starting materials can be produced in a very pure state and so the resulting boule contains very few

A diagrammatic representation of the aluminium bromide generator and furnace subsidiary heating elements.

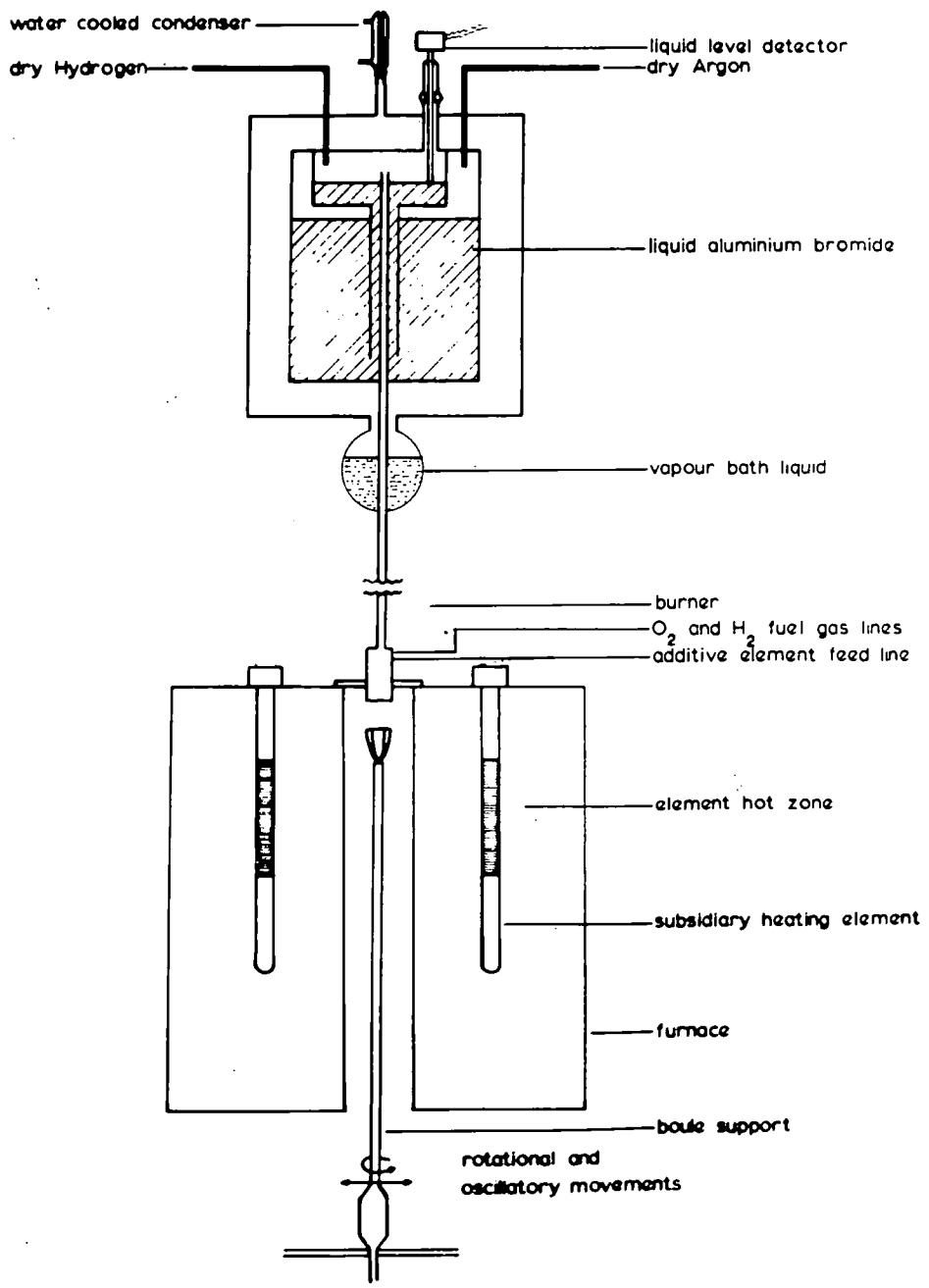

Figure 1.

unwanted chemical impurities.

The seed crystal is carefully orientated in the furnace and during the growth process it is withdrawn at such a rate that the surface on which the fresh material is being deposited is always in the same plane in the furnace. While it is being withdrawn it is also rotated and oscillated laterally in order to help distribute the chromium uniformly across the boule. The growing temperature for the material is 2050°C, and because of the large temperature gradients in the boules, they are highly strained on removal from the furnace and are difficult to handle without fracturing. The temperature gradients within the furnace are reduced as much as possible by using baffles and subsidiary heaters. Due to the nature of the growth process, with its long cooling off period in the furnace, every sample is partially annealed on removal, but even so it is wisest to anneal the samples further after growth by heating them to temperatures approaching 2000°C for several hours and then cooling slowly.

The boules examined were grown in three different growth directions, the so called 0°, 73° and 90° directions. That is the crystallographic c-axis of the seed crystal, and also of the resultant boule, was at 0°, 73° or 90° to the direction of withdrawal of the seed from the furnace.

TECHNIQUES FOR EXAMINING CRYSTALS.

X-ray, chemical etching and microwave spectroscopy techniques have been used to examine the boules of synthetic ruby

produced by the growth process described above.

Many sophisticated X-ray techniques exist for studying defects in solids. Lang (1958) developed a technique by which he was able to observe individual dislocations in the body of a material. Dislocation densities up to 10^8 cm^{-2} can be studied in materials by analysing rocking curves from a double crystal spectrometer using the method developed by Lambot et al. (1953). Strain throughout a volume of crystal lattice can be detected using a method due to Guinier and Tennevin (1949). This technique has been applied to ruby (J.R.Prior, private communication).

The Laue technique is not so sophisticated as these but it is a very versatile technique (K.Lonsdale, 1959) and can furnish information on crystal orientation, polycrystalline structure and strain in a lattice. Thiswas the method employed in the work described in this thesis.

Horn (1952) showed that the position of a pit produced on the surface of silicon carbide by chemical etching indicated where a screw dislocation intersected the surface. Since this demonstration of the relation between chemical etch pits and dislocations in solids many materials have been studied in this way. Scheuplein and Gibbs (1960) carried out an investigation of synthetic corundum, undoped Al_2O_3, using the etching technique. They observed etch pits on the (0001) plane, which they attributed to prismatic slip, and on the $\{10\bar{1}1\}$, $\{20\bar{2}1\}$ and neighbouring planes, which they attributed to basal slip. The

surface density of the pits on the latter was ten times that of the pits on the former.

Ellis (1955) gave two requirements for a chemical if it is to be suitable for use as an etchant. They are, firstly, that the etching shall be slow, and secondly, that the etch must attack some other crystal face faster than the one under study. Méléka (1958) put forward two more conditions for an etch to satisfy in order to give greater clarity, especially when working on materials with low dislocation densities. These are that the etch pits should not be large compared to the distance between them and that they should not be randomly distributed due to a general attack on the surface.

Microwave spectroscopy is the study of materials using the interaction between an electromagnetic wave and a magnetic or an electric moment. Nuclei, atoms, molecules, crystal defects and conduction electrons can have suitable moments. Here the interest was in electron paramagnetic resonance in solids where the interaction was with a magnetic moment produced by an incomplete electron shell in the atoms of one of the elements present in the solid. The resonance interaction between the magnetic moment and the electromagnetic wave can be described in several ways.

Bloch (1946) developed a phenomenological approach which he applied to nuclear magnetic resonance in liquids where the magnetic moments of the nuclei did not interact strongly with one another. The theory showed how the individual magnetic

moments precess around an effective magnetic field produced by a large steady field and a circularly polarised alternating field of frequency ν_0. The precession about the effective field shows amplitude resonance when ν_0 equals the precession frequency ν. This basic theory has now been extended to solids and electron paramagnetic resonance where it is mainly used to describe transient phenomena.

The optical analogy to paramagnetic resonance describes it in terms of the distribution of population of the electrons of the paramagnetic ion in its energy levels. First the energy levels are calculated and then probabilities for transitions from one level to another. The probabilities vary with frequency and increase to large values at resonant frequencies. This is analogous to optical spectroscopy and demonstrates that electron paramagnetic resonance is spectroscopy at microwave frequencies. There are, however, several slight differences. Electron paramagnetic spectroscopy is absorption spectroscopy while optical spectroscopy is usually emission spectroscopy from excited electron states in a gas discharge. Also the microwave technique uses the Zeeman effect to overcome partially the difficulty of obtaining power sources over a wide range of frequencies to suit all energy level splittings. The magnetic field alters the energy levels and this change is adjusted so that the available source of power causes transitions, which is a more flexible technique than trying to alter the source frequency.

Calculation of the energy levels shows the importance of the resonance technique. They are very sensitive to the structure of the solid and so the spectrum is sensitive to the structure as well.

The model of the interaction which is best suited to the description of the spectrometer used in this work depends on the results of the theory of electromagnetism. The mean power P_m absorbed per unit volume by a material whose volume magnetic susceptibility is $\chi_1 - j\chi_2$ from a time varying field of amplitude H is

$$P_m = \frac{1}{2} \omega \mu_0 \chi_2 H^2 \qquad 1.1$$

where ω is the pulsatance of the magnetic field and μ_0 is the permeability of free space. χ_1 and χ_2 vary with frequency, figure 2. . In particular χ_2 shows a sharp peak in its variation with frequency so the power absorption shows a corresponding sharp maximum.

The spectrometer, which will be described fully later, worked at frequencies around 35 Gc/sec. The three main parameters which describe the transmission of power down a waveguide are the power P, the frequency ν and the standing wave ratio r. The last parameter is related to the voltage reflection coefficient Γ which in turn is related to the circuit Q values where Q is a quality factor defined as

$$\frac{\omega \times \text{total energy stored}}{\text{energy losses per second}} \qquad 1.2$$

As the energy losses vary, the value of Q varies, so if the losses

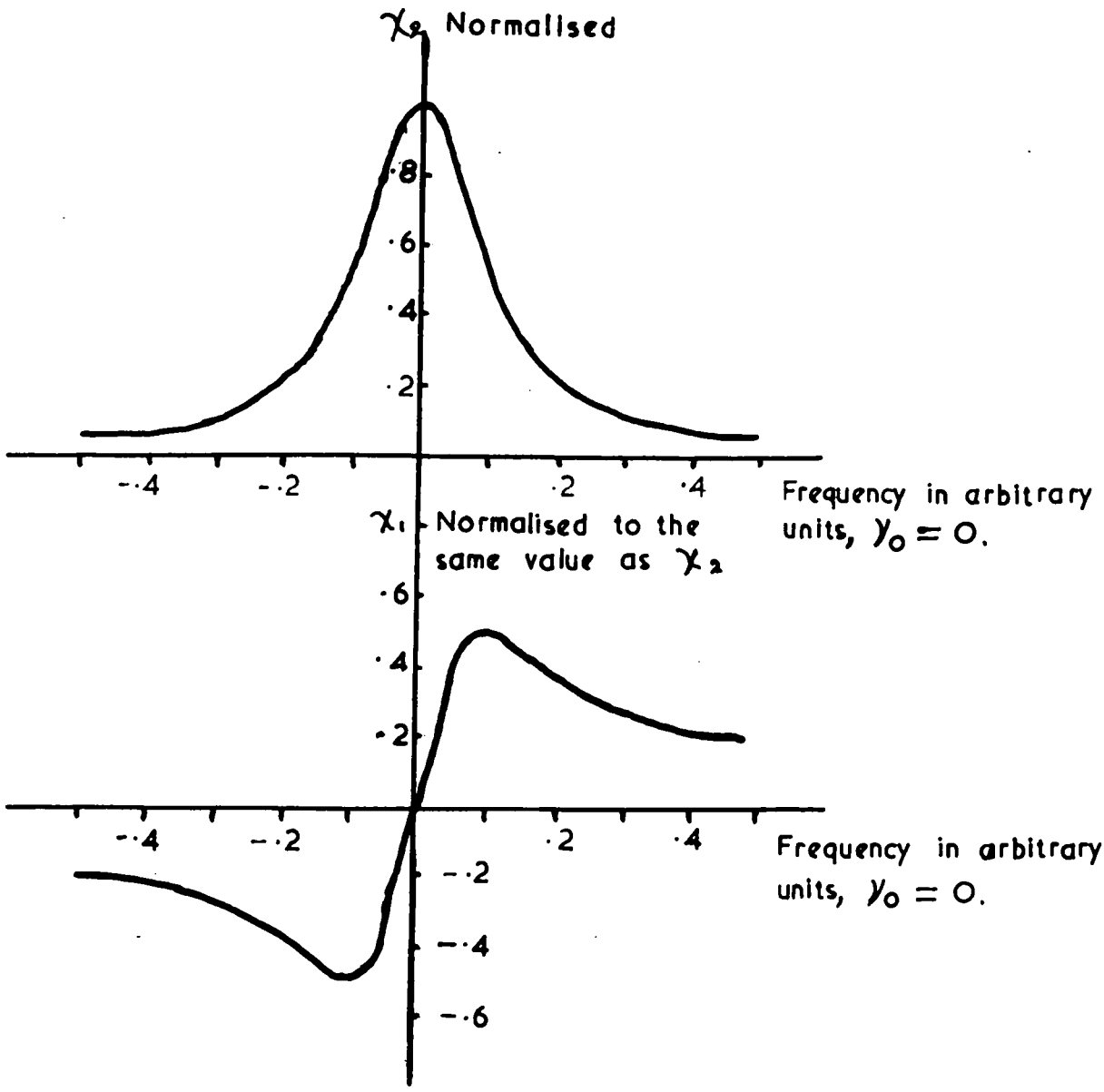

χ_1 AND χ_2 AGAINST FREQUENCY

FIGURE 2

depend partly on γ_2 a measurement of Q provides some information on γ_2.

The curves of figure 2 can be obtained by the method described by Bloembergen et al. (1948). These workers calculated the power absorbed by the electrons from an electromagnetic wave using the quantum mechanical theory of transition probabilities and the Boltzmann distribution of electrons throughout the energy levels. This expression for power absorption is equated to the expression given in 1.1 and so γ_2 is obtained in terms of transition probabilities and electron populations of energy levels. The transition probabilities show maxima at certain frequencies and so does γ_2. By using the Kramers - Kronig relations an expression for γ_1 can be obtained as well, and this also has significant values only near certain resonant frequencies.

The value of the energy stored in a resonant cavity depends on γ_1 so the Q value for the cavity is altered by changes in γ_1. Both γ_1 and γ_2 change rapidly near the resonant frequency and to differentiate between the effects of the two requires great care in the construction of the spectrometer. One way to differentiate between the real and the imaginary parts of the susceptibilities is to vary the signal frequency in such a way that the cavity is always at the peak of its resonance and the terms containing the real part of the susceptibility disappear. An alternative way is to use a waveguide system which

can be adjusted so that only γ_1 or γ_2 is detected but not a mixture of the two. A magic tee can be used in this way.

An important parameter to consider in the construction of a microwave spectrometer is the sensitivity of the instrument. The sensitivity is usually defined as the ratio of signal voltage to noise voltage. For the highest sensitivities a large signal and a system which produces very little noise are required. The best signal is produced by using a cavity with a large unloaded Q value and containing a sample of such a volume that its dielectric losses reduce the Q value to two-thirds its original value. This cavity has to be suitably coupled to the rest of the waveguide system (Feher, 1957). Assuming a suitable arrangement has been made to maximise the signal there are several systems for detecting it which have different noise properties.

Possible sources of noise are the klystron, the detector crystal, the amplifier and the recorder, and if the cavity is in boiling cryogenic liquids or the klystron is cooled by a powerful fan, microphonic noise may be present. By careful choice of the amplifier and careful mounting of the various components, noise due to the amplifier and microphony can be reduced. The klystron noise may be very difficult to improve. Voltage variations on the electrodes of the klystron should be reduced as much as possible. If the system contains a magic tee it can be adjusted so that it rejects the noise carried by the microwave power. It is most effective when detecting γ_2. Feher (1957) described the action of the magic tee in terms of

variations in voltage reflection coefficients, while Bloembergen et al. (1948) preferred to describe the action as a superheterodyne system which had an intermediate frequency of zero which effectively reduced the total bandwidth and also the noise passed by the system. The biggest source of noise is the detector crystal. The noise temperature t of a crystal can be written as (Uhlir, 1963)

$$t = t_w + A/f \qquad 1.3$$

where t_w is the "white" noise or combined Johnson noise of the crystal impedance and shot noise of the barrier. A/f represents the flicker noise of the barrier where A is a constant for any particular crystal and f is the signal frequency, that is the modulation frequency, not the carrier frequency. t_w is approximately equal to unity so t is given closely by A/f when f is very small. By artificially modulating the signal at a high frequency f, the noise temperature becomes almost equal to t_w.

There are four ways of modulating the signal. The magnetic field can be modulated with such a large amplitude that it completely sweeps through the line. This is usually performed at audio frequencies because of the large power required to overcome the self inductance of the modulation coils. After the detector the signal is amplified by an audiofrequency wide band amplifier and then displayed on an oscilloscope. An alternative modulation system uses phase sensitive detection where a small amplitude magnetic field sweep is combined with a slow

sweep of the main magnetic field through the line. In this way a very small part of the line is covered by the small amplitude modulation at any one time while the whole line is swept out by the main sweep in a period of several seconds. After the crystal is a phase sensitive amplifier tuned to the frequency of the rapid modulation and followed by a recorder. It has a very small bandwidth and can be operated at frequencies of the order of 10^5 c/sec because only small subsidiary coils are required to produce the magnetic field sweep. These two factors mean that the system passes very little noise to the recorder. This system records the derivative of the lineshape.

The simple large amplitude audio frequency equipment can be improved by beating the carrier frequency and signal superimposed on it with a second frequency 40 or 50 Mc/sec away. This means that the detector crystal works in a frequency region where its flicker noise is insignificant. The actual frequency used as the intermediate frequency in this superheterodyne system depends on the noise properties of the intermediate frequency amplifier. Amplifier noise usually increases with increasing frequency. Therefore there is an optimum intermediate frequency at which to operate found by balancing the decrease in flicker noise and the increase in amplifier noise.

A fourth modulation technique is to modulate the frequency through the resonance. This method can be adopted

to separate γ_1 from γ_2 as mentioned above. It has the drawback that distortions are introduced by any frequency sensitive part of the circuit. For powers above 100 mW bolometers make excellent detectors. They can only be used at low freqencies and they operate best at higher powers because their conversion gains are best then. However, they have an optimum power level for operation due to signal generator noise. Crystals also have poor conversion gains at low powers, but their noise power increases with power so they have an optimum power level for operation also.

The aim of spectroscopy is to correlate the various observable parameters with the structure of the atoms responsible for the spectrum. The most easily observed parameters are the energy level spacings, the effects of electric and magnetic fields on these spacings, the selection and polarisation rules of the transitions joining the energy levels and the relative intensities and linewidths of the various transitions. In principle all these points are known from the initial and final states of the transition. Here the interest is in the linewidths of the transitions because they are influenced by a variety of mechanisms in the solid which can, therefore, be studied by making careful observations of the linewidth.

The complete theoretical solution to the problem of predicting lineshapes and linewidths is insoluble with present techniques. It requires the solution of the energy levels of many interacting ions. However because of its importance much

work has been done on the problem. The three main aims have been to evaluate the form of the lineshape, or the moments of the lineshape, or the magnitude of the linewidth. The second two aims have received the most attention. Pryce and Stevens (1950) gave a general theory of moments and linewidths which has been applied to the case of ruby by many workers. Anderson and Weiss (1953) performed a calculation which could be applied to the lineshape of ruby, but it does not appear to have been so far.

The work of Van Vleck (1948) on moments and linewidths cannot be applied directly to ruby because he specifically neglected the effects of the crystal field in his calculations. More recently O'Reilly and Tsang (1962) have attempted calculations on the linewidths and moments of nuclear magnetic resonance lines using lattice harmonics and they intend extending their work to electron paramagnetic resonance lines. Bersohn and Das (1963) have used techniques of statistical mechanics to simplify the summations involved in evaluating the moments of lines and Klauder and Anderson (1962) attempted a theory of lineshapes in terms of stochastic processes. All this work has illuminated the various mechanism in solids which can contribute to the width of the lines even if it has not as yet produced the complete solution to the problems.

CONCLUSIONS.

An indication has been given of the general background of the work contained in this thesis. The growth process of the ruby samples used has been described and the techniques which were used to examine the crystals introduced. These techniques were aimed at elucidating the physical imperfections in the crystals but they also have some bearing on the chemical imperfections. This was particularly true of the spectroscopy work. Of the methods used to investigate the samples the spectroscopy seems the most suitable because the material was examined in conditions closely similar to those of maser operation.

CHAPTER TWO.

X-RAY STUDIES.

Experimental technique; method of analysis of measurements; results of measurements; discussion of types and magnitude of imperfection revealed; conclusions.

EXPERIMENTAL TECHNIQUE.

The ruby specimens were examined using the Laue back reflection technique. White radiation from a copper target was used. The focus of the target was 10 mm by 1 mm and it was viewed perpendicularly to the longer side between angles -1° and $+8^{\circ}$. The tube was run at 40 kV and 20 ma. The camera consisted of a flat film holder and a goniometer mounted on a base. Through the centre of the film holder passed a collimator which was held perpendicularly to the holder. The goniometer had facilities for rotation about three mutually perpendicular axes and for translation along two mutually perpendicular horizontal directions. The samples were mounted on the goniometer and the camera adjusted so that the X-rays from the target passed through the collimator, fell onto the sample and were reflected onto the film.

A choice of collimators and of film-sample distances was available and the actual combination used depended on the detailed requirements of the experiment to be performed. Increasing the film-sample distance increased the accuracy with which measurements

of the angles through which the beam was deviated by different planes of the crystal lattice could be measured, but it also increased the size of the image on the film and so made accurate location of the centre of the image more difficult. Another effect of the larger film-sample distance was to increase the exposure time. Increasing the length of the collimator, or decreasing its diameter, increased the accuracy with which the centre of the image could be located but it also increased the exposure time and the gain in accuracy had to be countered against the increased length of the experiment.

The system most often used consisted of a collimator 7·33 cm long with holes 0·0635 cm in diameter and a film-sample distance of 3 cm. The angular diameter of the beam was calculated as 0·0174 radians and it irradiated a circle of diameter 0·09 cm on the samples. If this beam was deviated from the incident direction by 45° when it was reflected, it was calculated that it would produce an image of size 0·16 cm by 0·23 cm on the film. The exposure time for this arrangement was 90 minutes. Using the same collimator and a film-sample distance of 5 cm increased the illuminated diameter on the sample to 0·12 cm and the dimensions of the image to 0·25 cm by 0·35 cm. The exposure required was $4\frac{1}{2}$ hours. Other collimators were available including one which required exposure times of less than one hour. The largest film-sample distance it was convenient to use was 5·5 cm.

To facilitate carrying out the X-ray work, a brass disc

was made which had two 30° sectors diametrically opposite to each other removed. This disc was fitted over the film with the collimator passing through its centre. With this disc three separate exposures could be taken on the same film, figure 3. Usually the specimen was translated horizontally parallel to the film between exposures so that on one film three exposures of adjacent regions on a straight line across the sample were obtained. The fact that only one-sixth of the pattern was revealed in each exposure did not affect its analysis. Enough of the pattern of spots was revealed to allow it to be performed.

The Laue technique has the disadvantages that it is not as sensitive or as accurate as some other methods and that only a small volume at and immediately below the surface of the sample is examined in any one exposure. It has the advantages that it is simple to perform and to analyse the films and that the specimens do not require any special preparation. This meant that it was possible to examine material as received from the manufacturer.

RESULTS.

Each exposure gave information about the orientation of the specimen, the strain present in the specimen and the presence or otherwise of polycrystalline material, referred to as mosaic structure, at the position on the specimen where the X-ray beam was incident. If the volume illuminated was good single crystalline material then good sharp images were produced

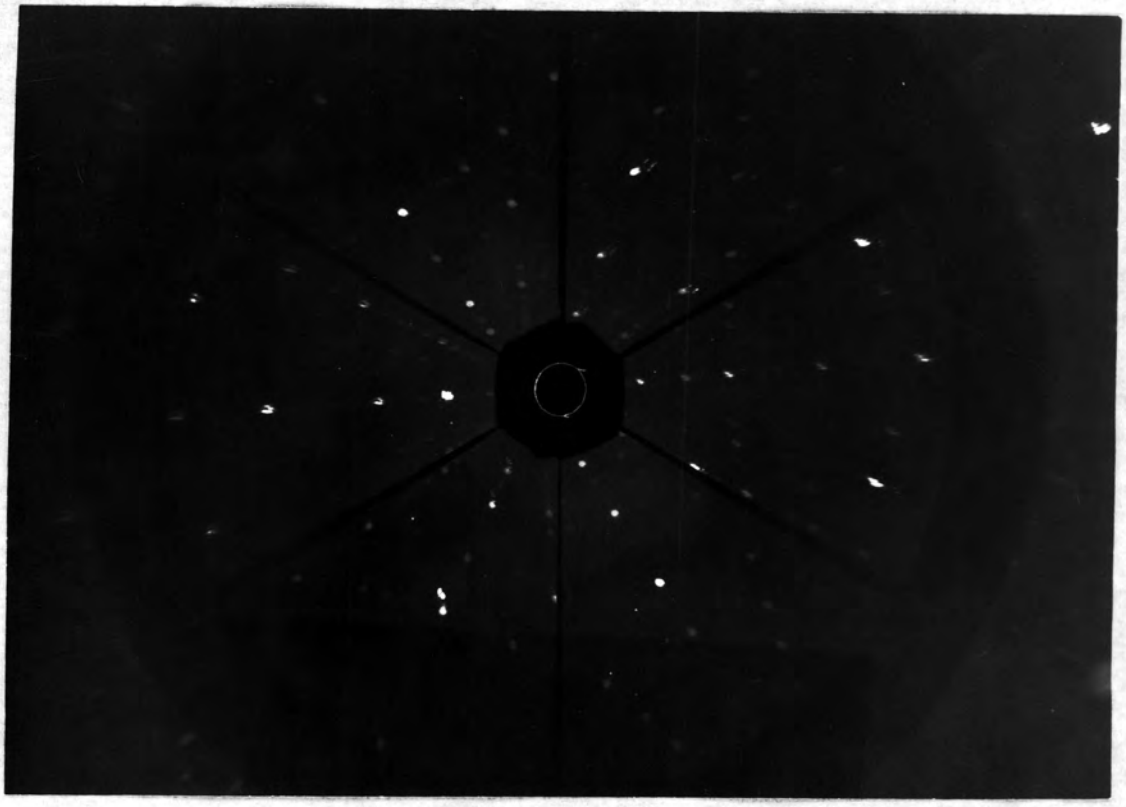

A SECTOR DISC PHOTOGRAPH

FIGURE 3.

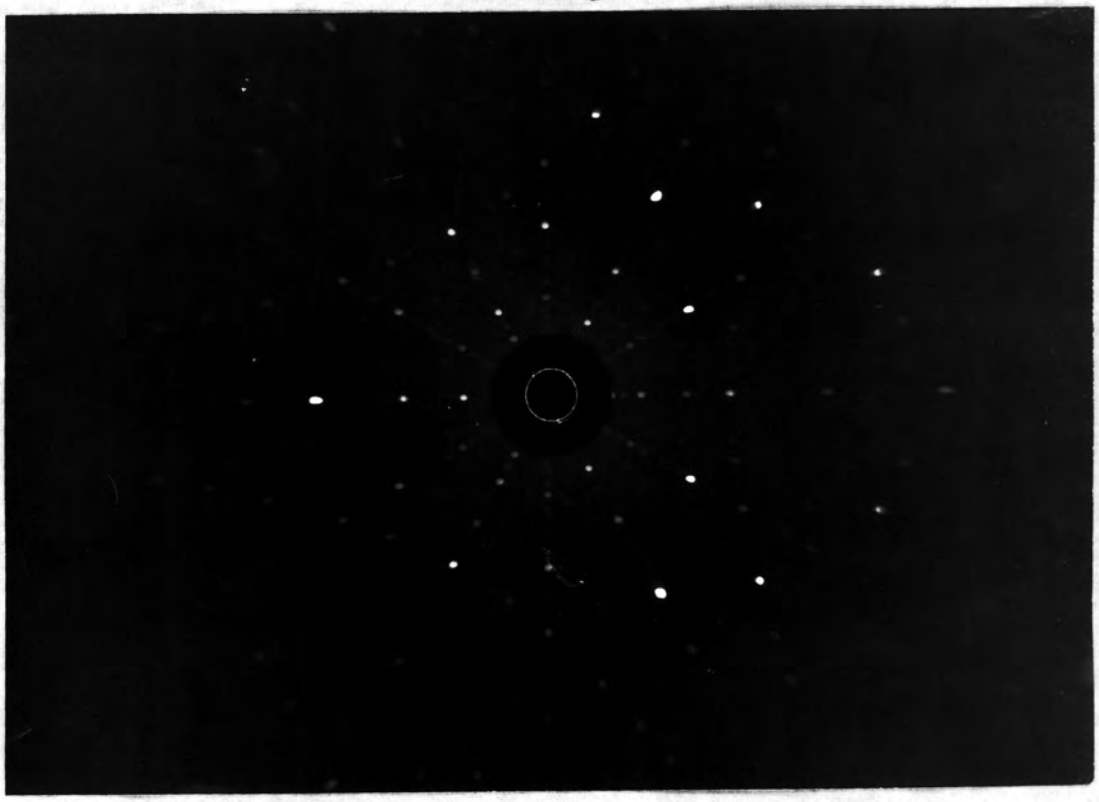

A PHOTOGRAPH OF GOOD MATERIAL

FIGURE 4.

on the film, figure 4. The dimensions of the images agreed with those predicted from the geometry of the system. The angle between the direction of the incident beam and the direction of the c-axis was calculated from measurements of the film-sample distance and the position of the image due to the (0003) plane. This was done in preference to using a Greninger chart (Barrett, 1952) because it gave more accuracy. If strain was present in the material this was revealed by asterism of the images. No quantitative measurements were made of this.

The presence of mosaic structure was revealed when a single image from one set of planes broke up into several separate images due to the presence of several crystallites each slightly misorientated with respect to its neighbours, figure 5. The angle of misorientation between two adjacent elements was calculated using a method based on figure 6. Q' and R' are the images produced by the plane (hkil) in neighbouring crystallites. A and B are the images produced by the (0003) plane in the neighbouring crystallites. Normally they were not visible on a photograph because they were formed near to the centre of the film and were obscured by the collimator. The perpendicular to the (0003) plane is the crystallographic c-axis. It is assumed for this calculation that the c-axis of one of the crystallites is perpendicular to the film. This assumption was rarely correct but the c-axes were never more than two or three degrees from the perpendicular so it is a reasonable approximation to make.

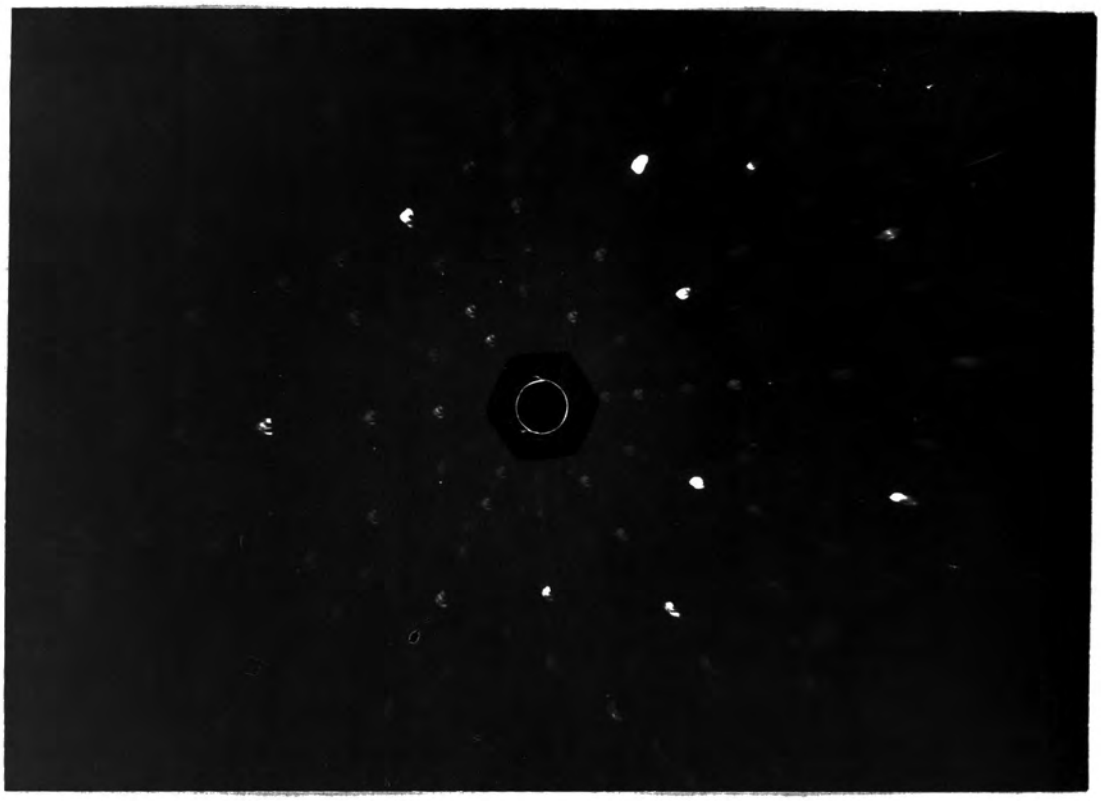

A PHOTOGRAPH OF MOSAIC

MATERIAL

FIGURE 5.

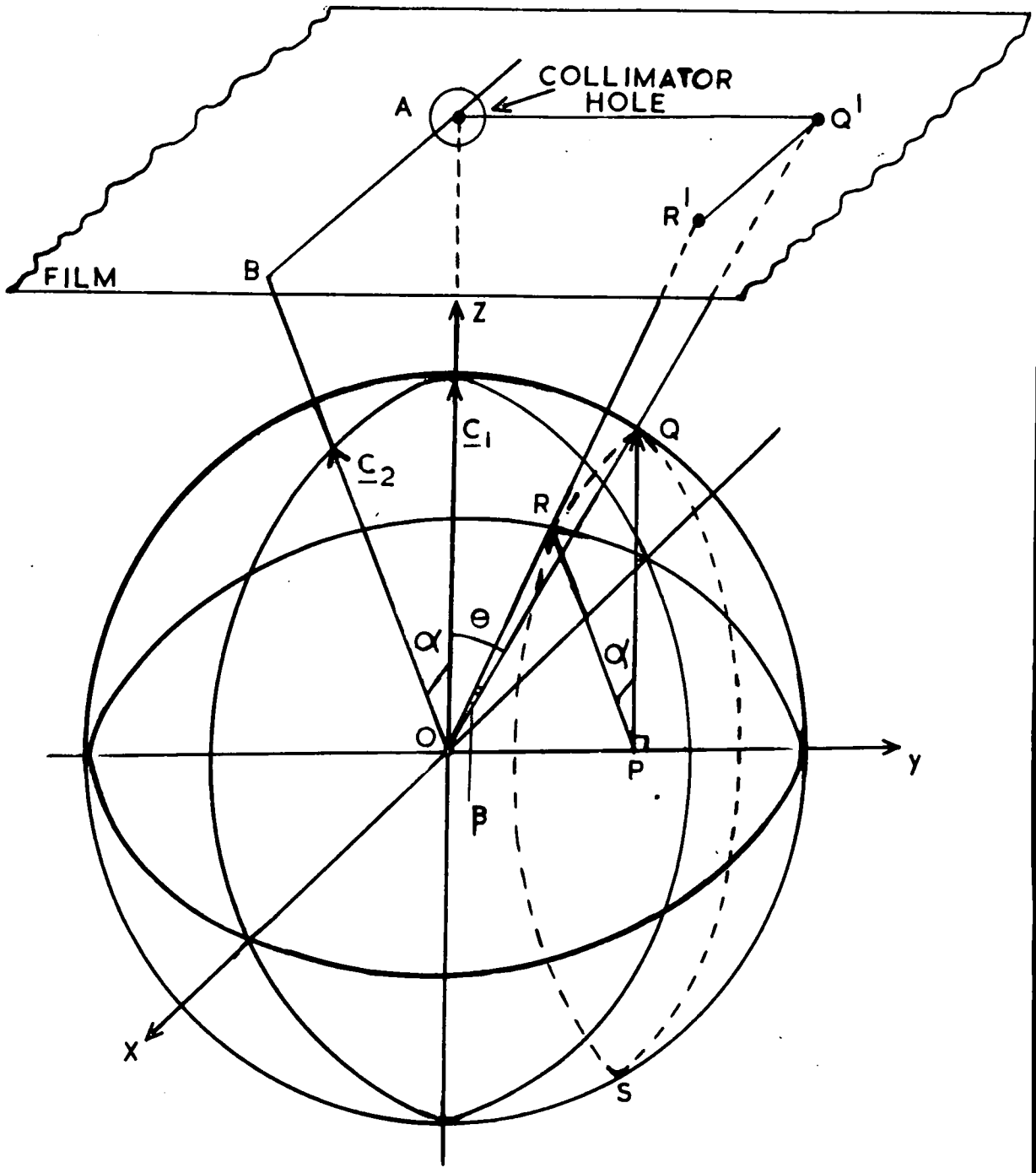

MOSAIC MISORIENTATION .

FIGURE 6

A set of spherical coordinates is constructed such that Oz is perpendicular to the film, the plane Ox Oz contains the other c-axis which is not perpendicular to the film and the plane Oy Oz contains the X-ray beam producing the image Q'. The X-ray beam producing the image A is translated into the beam producing the image B by a rotation of angle α about Oy. The beam OR which is reflected from the (hkil) plane in the second crystallite can also be found by making a suitable rotation of α about Oy from the direction OQ. R and Q are on the surface of a cone which has Oy as its axis of symmetry and $\hat{RPQ} = \alpha$. From figure 6

$$\alpha = \beta / \cos\theta \qquad 2.1$$

where $\beta = \hat{ROQ} = \hat{R'OQ}$ and $\theta = \hat{AOQ'}$. θ and β can be calculated from measurements of the film-sample distance, AQ' and R'Q'.

From the elementary property of reflections which states that the angle of deviation of a beam increases in magnitude at twice the rate of increase of the angle of incidence, the variation in the c-axis direction between two neighbouring crystallites, the mosaic misorientation, is $\alpha/2$.

Q' satisfies the requirement of being in the plane Oy Oz when $\hat{AQ'R'}$ is a right angle. Images which satisfied this requirement were chosen by inspection of the photographs. A simple case of 2.1 occurs when $\theta = 0^\circ$. Then the images Q' and R' lie on a radius of the collimator hole. In this

particular case OQ need no longer be in the plane Oy Oz. If the tangential or radial distribution cannot be observed on a photograph the existing mosaic may be resolved into tangential and radial components and the resultant taken. This can be done because the angles α and β are small. (See figure 7 which shows a similar situation in the case of c-axis misorientations.)

Examination of a series of specimens showed that good single crystal material and poor mosaic material could exist in neighbouring regions in the same specimen. Figure 3 shows this. The exposures in the figure were about 3 mm apart on the same specimen. It was observed that even between two regions of good material there was a misorientation between the c-axis directions at these two positions.

Figure 7 shows the method used for the calculation of the c-axis misorientation between two positions. G and H are the positions of the image produced by the (0003) plane at two different positions in the sample. Normally the images were obscured by the collimator so their positions had to be found by construction from the zones revealed on the film. The x and y axes are constructed in any convenient position as only differences in coordinates are required. The coordinates x_1, y_1, x_2, y_2 and the film-sample distance OS are measured.

Then
$$\hat{GSH} = \sqrt{((x_1 - x_2)^2 + (y_1 - y_2)^2)}/OS, \qquad 2.2$$

and the c-axis misorientation is $\frac{1}{2}\hat{GSH}$. This calculation assumes

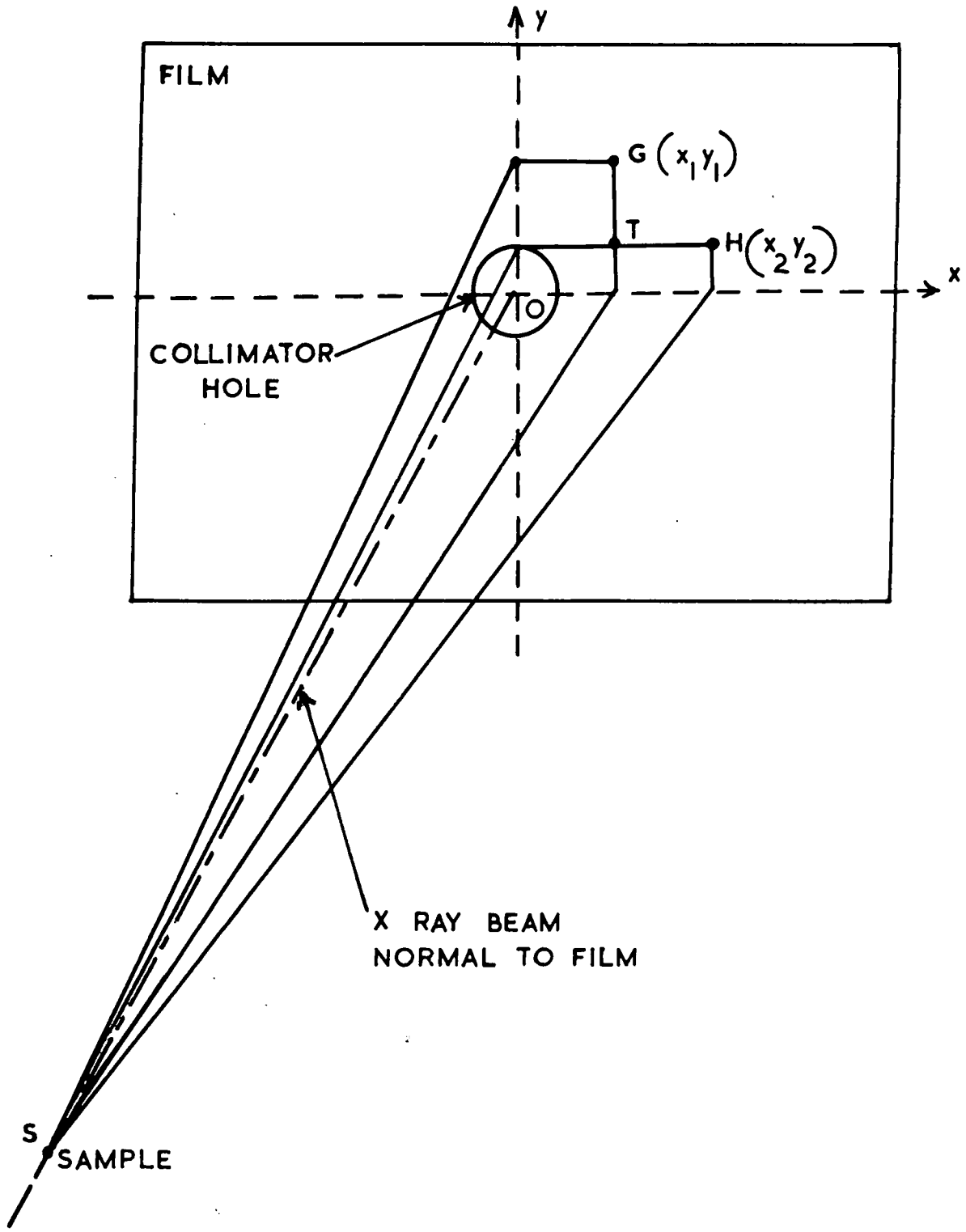

C-AXIS MISORIENTATION

FIGURE 7

that G and H are close to O and that their separation is much less than the distance OS. If the first assumption is not cofrect then OS must be replaced by ST. This was done in those mosaic misorientation calculations where the misorientation was resolved into radial and tangential components and then compounded again.

Tables 1 to 4 show typical results for the c-axis misorientation between neighbouring regions of a specimen and for the mosaic misorientation at various positions in a specimen. The accuracy of the results did not depend on their magnitudes. For values of c-axis misorientation the error was $\pm$ 25' and for mosaic misorientation the error was $\pm$ 15'. These errors are for the 3 cm film-sample distance. Measurements made with the 5 cm distance reduced the two errors to about two-thirds their former values. Because of these magnitudes it seems best to regard those values of c-axis misorientation below 1^{o} and of mosaic misorientation below 45' as order of magnitude only. Figures above these values are more reliable. Their reliability was checked in some cases by repeating some measurements.

Several subsidiary experiments were performed in order to support the main experiments. These included experiments to check the location of the film in the holder, the location of the collimator and the ability to set up the system so that a desired position could be viewed. Also the dimensions and shape of the collimated X-ray beam were checked. The most important subsidiary experiments were those designed to investigate possible surface effects on the specimens. Each exposure investigated only a small

volume of the specimen at and immediately below its surface. If any surface effect existed the results obtained would not be representative of the bulk of the specimen around that particular volume. Any surface layer which was present would be revealed by dissolving it away and comparing X-ray examinations made before and after the chemical action. This experiment was performed on the natural growth surfaces of the specimens, on surfaces prepared by cutting with a diamond wheel and on surfaces prepared by grinding with a diamond grinding wheel. About 0·1mm depth of the surface was removed by boiling the samples in potassium hydroxide for two hours. Examination of the X-ray photographs showed that for as grown surfaces and surfaces prepared by cutting there was very little difference from before to after the chemical preparation of the surfaces. An improvement in the structure would have demonstrated that a damaged surface layer had existed and had been removed by the chemical. This was observed in the case of surfaces prepared by grinding when powder was formed on the surfaces and gave arcs of powder rings on the X-ray photographs. A deterioration in the structure would not have demonstrated conclusively the presence of a surface layer due to the handling of the surface because it seems most unlikely that any of the methods used to prepare the surfaces would produce a layer of perfect material on top of a region of poor material.

The main experiments provided information on several different points. A sequence of measurements was performed to

study the effects of various types of heat treatment on the specimens. Another set of experiments was designed to provide information on the distribution of defects throughout certain types of material while other measurements were made on rubies and corundum grown with their c-axes at various angles to the growth direction.

Every measurement made gave some information on the distribution of c-axis misorientation and mosaic misorientation throughout the various boules examined, but two of the 0° growth direction boules were examined in more detail concerning this point. Boule 1B was cut into slices perpendicular to the c-axis and several of these examined in detail, table 1. Five exposures were made covering a distance of 5 mm parallel to the growth direction, in a position midway between the centre and the surface of the boule. There were traces of arcs of powder rings on one exposure because the surface had been ground. None of the other exposures showed any structure. The results gave no indication of the c-axis misorientation along this line. One slice was examined along a line perpendicular to the radius of the boule about one-third of the way from the centre of the boule. This investigation revealed mosaic misorientation near the natural faces of the boule. There was a slight crack in the material and X-ray examination revealed misorientation across it. This examination was carried out on unannealed slices of the specimen.

Boule 319 was examined throughout as shown in figure 8. Also the natural faces (0001), $\{10\bar{1}0\}$ and $\{11\bar{2}0\}$ were examined.

Table 1

X-Ray Results

Boule 1B, 0° growth direction ruby, chromium concentration unknown.

Photograph	Slice	Mosaic misorientation	C-axis misorientation	Footnote
1	1Bb1	slight arcs	-	A
2	1Bb1	none	-	A
3	1Bb2	none	-	A
4	1Bb2	none	-	A
5	1Bb3	none	-	A
6	1Bb2	1° 0' *	-	B
7a	1Bb2	0° 30' *	7a-7b 0° 15'	B
7b	1Bb2	none	7b-7c 1° 0'	B
7c	1Bb2	0° 30' *	7a-7c 0° 45'	B
8	1Bb1	slight arcs	-	C
9	1Bb1	none	-	D
10	1Bb2	none	-	E
11	1Bb2	0° 30' *	-	F
12	1Bb2	1° 0' *	-	G
13a	1Bb2	0° 15' *	13a-13b 0° 45'	H
13b	1Bb2	none	13b-13c 0° 30'	H
13c	1Bb2	1° 0' *	13a-13c 0° 15'	H

*Values with less accuracy than quoted in the text. 7a, 7b, etc. refer to sectors a, b, etc. of photograph 7. A. Unannealed slices, the photographs taken along a line parallel to the growth direction. B. Unannealed slice, the photographs taken on a plane perpendicular to the growth direction. C. and D. Slice annealed at 1700°C for 24 hours. C. Compare with photograph 1. D. Compare with photograph 2. E, F, G and H. Slice annealed at 1900°C for 24 hours. E. Compare with photograph 3. F. Compare with photograph 4. G. Compare with photograph 6. H. Compare with the sectors of photograph 13 the equivalent sectors of photograph 7.

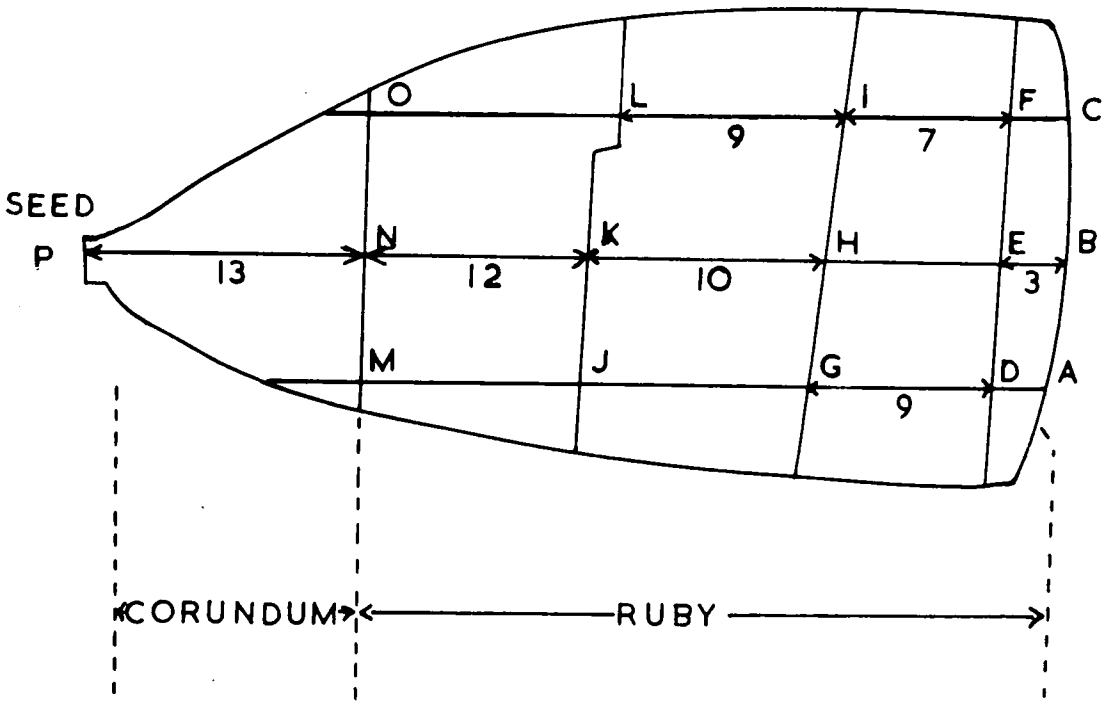

figures are approximate distances in mm .

SECTION THROUGH BOULE 319 SHOWING POSITIONS OF EXPOSURES LISTED IN TABLE 2 ,

FIGURE 8 .

The results for mosaic misorientation only are included in table 2 because of the larger inaccuracy of the determinations of the c-axis misorientations. A quantitative map of the c-axis misorientations would have required the addition of several values which would have rapidly increased the error until the final figure had an error of several hundred per cent. Qualitatively, however, it was observed that the c-axis followed a corkscrew path along the boule. It is to be noted that the seed crystal had mosaic structure, but at the plane where the doping with chromium commenced there was very little mosaic. After this plane the mosaic increased again. This boule had been annealed at 1900°C for about 24 hours.

One slice of boule 1B, 1Bb1, was annealed at 1700°C for about 24 hours and examined after the treatment. The images on the film were sharpened slightly indicating a reduction in the amount of stress in the crystal, but, apart from this, there was no obvious improvement of structure due to the annealing. A second slice of the boule, 1Bb2, was examined after annealing at 1900°C for about 24 hours. The distribution of the c-axis misorientation and of the mosaic misorientation was altered by the annealing, but there was no sign of an improvement. The natural faces of boule 319 were examined before it was annealed, and, in this case also, no improvement in the crystal structure was noticed after the annealing. These measurements are also recorded in tables 1 and 2.

Boules 1B and 319 were 0° growth direction boules.

Table 2

X-Ray Results

Boule 319, 0° growth direction ruby, chromium concentration unknown.

Photograph	Mosaic misorientation	C-axis misorientation	Footnote
14a	2° 20'	14a-14b 1° 35'	I
14b	2° 0'	14b-14c 1° 45'	I
14c	2° 5'	14a-14c 3° 10'	I
15a	2° 40'	15a-15b 2° 10'	J
15b	2° 35'	15b-15c 1° 10'	J
15c	none	15a-15c 1° 55'	J

14a, 14b, etc. are sectors a, b, etc. of photograph 14.

I. Photographs of the natural (0001) surface of the unannealed boule.

J. Photographs of the natural (0001) surface of the boule after annealing at 1900°C for 24 hours. Compare the sectors of photograph 15 with those of photograph 14

Qualitative study of the natural faces $\{1010\}$ and $\{1120\}$.

Each face was examined in one position only. Annealing had very little effect on the mosaic structure of two faces, it removed mosaic structure from two faces, caused mosaic structure on one previously clear face and worsened the mosaic structure on one face.

P.T.O.

Table 2 (Cont.)

Detailed examination of boule 319 after annealing.

Reference in figure 8	Mosaic misorientation
A	$0^{\circ}\ 40'$
B	$1^{\circ}\ 25'$
C	$2^{\circ}\ 20'$
D	$0^{\circ}\ 40'$
E	$0^{\circ}\ 35'$
F	$2^{\circ}\ 40'$
G	$1^{\circ}\ 20'$
H	$1^{\circ}\ 10'$
I	$2^{\circ}\ 30'$
J	0°
K	$2^{\circ}\ 45'$
L	$2^{\circ}\ 50'$
M	0°
N	$0^{\circ}\ 15'$
O	$0^{\circ}\ 15'$
P	$0^{\circ}\ 55'$

From the qualitative study above, four of the six faces $\{1010\}$ and $\{1120\}$ showed mosaic structure at the one position examined on each face.

Table 3 includes measurements made on rubies grown at growth angles of 73° and 90° as well as including a further selection of typical results for 0° growth direction rubies. Table 4 contains the results of measurements made on corundum grown at angles of 0°, 73° and 90°. From the tables it can be seen that the values of the c-axis misorientation and the mosaic misorientation were of similar orders of magnitude throughout the materials examined. No detailed examination of the effects of annealing or the distribution of defects in the 73° and 90° rubies and the 0°, 73° and 90° corundum crystals was made. Only one exposure from nine made on crystals grown in the 90° orientation showed mosaic while in the 73° orientation crystals the number was three from nine. Both these ratios are much smaller than that found in the 0° growth direction crystals.

DISCUSSION.

The X-ray results agree quite well with those obtained by J.R. Prior (private communication). He used the Guinier-Tennevin technique which gave more accuracy and allowed him to investigate a large volume of material at one time. He noticed that the directions of the c-axis in a volume of material tend to form a cone. This was not observed in these measurements because of the small volumes involved, but the apparent spiral in the c-axis observed in boule 319 fits in with the description in terms of a cone.

In the 0° crystals the regions of good or bad material

Table 3.

X-Ray Results.

General results for rubies

A	B	C	D	E	F	G
297	16a	none	16a-16b 0° 15'	unknown	0°	unannealed
	16b	none	16b-16c 0° 15'			
	16c	1° 45'	16a-16c 0° 30'			
337c	17a	none	17a-17b 0° 50'	0·052%	0°	1930°C
	17b	none	17b-17c 0° 55'			
	17c	none	17a-17c 0° 10'			
337c	18a	0° 40'	18a-18b 0° 40'	0.052%	0°	1930°C
	18b	none	18b-18c 1° 5'			
	18c	none	18a-18c 1° 5'			
337a	19a	none	19a-19b 0° 10'	0·052%	0°	1700°C
	19b	none	19b-19c 0° 40'			
	19c	none	19a-19c 0° 35'			
337a	20a	none	20a-20b 0° 45'	0·052%	0°	1700°C
	20b	none	20b-20c 0° 20'			
	20c	0° 30'	20a-20c 0° 40'			
G2a	21a	0° 10'	21a-21b 0° 40'	0·02 to	0°	unannealed
	21b	0° 35'	21b-21c 1° 0'	0·032%		
	21c	0° 10'	21a-21c 1° 10'			
G2a	22a	0° 55'	22a-22b 0° 20'	0·02 to	0°	unannealed
	22b	0° 15'	22b-22c 0° 30'	0·032%		
	22c	0° 20'	22a-22c 0° 25'			
344a	23a	0° 50'	23a-23b 0° 25'	0·02%	0°	unannealed
	23b	none	23b-23c 0° 30'			
	23c	1° 10'	23a-23c 0° 45'			
344a	24a	none	24a-24b 0° 25'	0·02%	0°	unannealed
	24b	none	24b-24c 0° 25'			
	24c	none	24a-24c 0° 10'			

P.T.O.

Table 3 (Cont.)

A	B	C	D		E	F	G
492a	25a	none	25a-25b	0° 20'	unknown	73°	unknown
	25b	0° 30'					
492b	26	0° 15'	26-27	0° 30' *	unknown	73°	unknown
	27	none					
461a	28	none	28-29	0° 30' *	unknown	90°	unknown
	29	none					
461b	30	none	30-31	1° 30' *	unknown	90°	unknown
	31	none					

16a, 16b, etc. refer to sectors a, b, etc. of photograph 16.

* These measurements were made along a diad axis perpendicular to the c-axis.

A. Specimen;

B. Photograph;

C. Mosaic misorientation;

D. C-axis misorientation;

E. Chromium concentration, weight per cent;

F. Growth direction;

G. Previous heat treatment of the sample, the temperatures are those at which annealing has been performed.

Table 4.

X-Ray Results.

General results for corundum (undoped Al_2O_3).

A	B	C	D		E	F
421a	32a	none	32a-32b	1° 0'	0°	unknown
	32b	1° 25'				
421b	33	0° 50'	33-34	2° 15' *	0°	unknown
	34	2° 15'				
420a	35a	none	35a-35b	0°	0°	unknown
	35b	none				
420b	36a	none	36a-36b	0° 10' *	0°	unknown
	36b	none				
426a	37a	none	37a-37b	1° 10'	73°	unknown
	37b	none	37b-37c	0° 30'		
	37c	none	37a-37c	1° 30'		
426b	38	none	38-39	0° 30' *	73°	unknown
	39	0° 15'				
423a	40a	none	40a-40b	0° 35'	90°	unknown
	40b	none	40b-40c	0° 55'		
	40c	none	40a-40c	0° 40'		
423b	41	none	41-42	1° 0' *	90°	unknown
	42	0° 25'				

32a, 32b, etc. are sectors a, b, etc. of photograph 32.

*These measurements were made along a diad axis perpendicular to the c-axis.

A. Specimen; B. Photograph; C. Mosaic misorientation; D. C-axis misorientation; E. Growth direction; F. Previous heat treatment of the sample.

apparently extend parallel to the growth direction. This indicates that they probably originate in or near the seed. Boule 319 was the only boule examined where this effect was looked for, and the result was rather inconclusive. In this boule a plane of good material was found between the mosaic seed crystal and the mosaic boule. It may be that the dislocations in the region immediately around the seed did not form grain boundaries and polycrystalline material because it is such a small region and large temperature gradients could not form across it. When the boule became larger temperature gradients may have formed which encouraged the formation of polycrystalline material. Another possible explanation is that the chromium ions formed the mosaic structure, but this is not supported by the work on corundum or the etch pit studies to be described in chapter three. Further discussion of this is postponed until later.

CONCLUSIONS.

The experiments show that the boules of ruby or of corundum examined consisted of a main lattice over which the c-axis may change direction by up to 3° and superimposed on this lattice a random distribution of mosaic structure with up to 3° spread between the components. There did not seem to be any relation between the mosaic structure and the crystal lattice of the boules. When mosaic structure occurred near the natural surfaces of the boules it was usually more marked than when it occurred in the bulk of the material. The figures for the incidence of mosaic in boules of the three different growth

directions seem to indicate that the 90° crystals contain less mosaic than the 73° crystals which in turn contain less than the 0° crystals. This conclusion is supported in part by J.R.Prior, see chapter three. In the one case examined the exact relationship between the structure of the seed crystal and the boule was not immediately obvious. For the 0° growth direction boules annealing caused a rearrangement in the distribution of the c-axis misorientations and the mosaic structure but it did not improve either. It did, however, improve the handling qualities of the material by removing some of the stress caused by the growth process. It appears that in 0° boules a better impression of the quality of the crystals was obtained by examining in a plane perpendicular to the growth direction rather than in a plane parallel to the growth direction. In this type of crystal this plane is also the easiest to examine.

CHAPTER THREE

ETCHING STUDIES

Experimental technique; results of measurements; correlation between etch pits and dislocations; discussion of this work and its relation to that of other workers; conclusions.

EXPERIMENTAL TECHNIQUE.

The method used to etch the rubies was based on that described by Scheuplein and Gibbs (1960). The (0001) face was polished using diamond impregnated grinding wheels. Several wheels were used, each succeeding wheel having a finer grade of diamond than the one before. The polished specimens were cleaned by immersing them for several hours in benzene and then in nitric acid and finally by washing in distilled water. The etching was performed in orthophosphoric acid (90% A.R.) by placing them in the acid, heating it up to 320°C and then pouring away the acid immediately that temperature was reached. Before washing the remaining acid away with distilled water the specimens were allowed to cool for several minutes. Examination with a microscope revealed etch pits.

In order to obtain the best results, it was important to finish the etching as close to 320°C as possible, so, to ensure this, the correction term for the exposure of the stem of the thermometer was applied to its readings. It was necessary to orientate the samples accurately before polishing

them because etching did not take place if the polished surface was more than 5° from the (0001) plane. Care had to be taken to avoid sudden changes in temperature, especially with unannealed specimens, which could cause cracking in the crystals. Unfortunately the polishing process left scratches on the surfaces of the specimens which sometimes hid structure which would otherwise have been revealed by the etching. Scheuplein and Gibbs were able to remove these scratches by heating their samples for a few seconds at $1600^{\circ}C$, but this was not desirable here due to the danger of cracking the samples and because such treatment would alter the heat history of the specimens. This last point was of interest in the work described here.

RESULTS

The etch pits were triangular in shape with sides parallel to $[10\bar{1}0]$, figure 9. Using a microscope with an interference objective the depths of the pits were measured as close to 5 microns. Figure 9 shows a sample with a random etch pit density of 2.10^5 etch pits/cm^2.

Besides a random distribution of etch pits there were also rows of etch pits, figure 10, presumably related to rows of dislocations forming grain boundary walls, which had linear densities estimated to be up to 5.10^3 etch pits/cm. Including the rows of etch pits in a region increases the total etch pit density to about three times the random etch pit density. There were about 3.10^2 rows of etch pits per cm^2. The linear

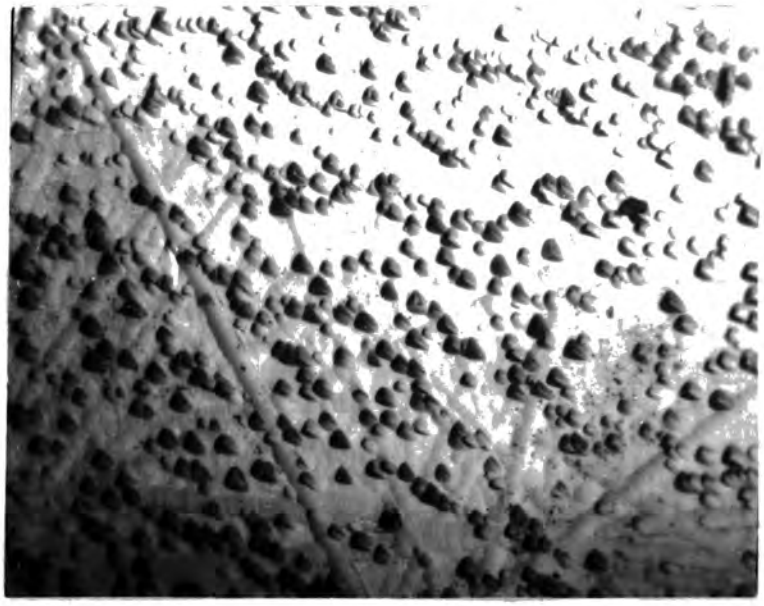

A PHOTOGRAPH OF ETCH PITS RANDOMLY DISTRIBUTED (X160)

FIGURE 9.

A PHOTOGRAPH OF ROWS OF ETCH PITS (X160)

FIGURE 10.

dimensions of the grains, that is the areas bounded by the lines of etch pits, ranged from millimetres to microns with the median value in the range 10^{-2} to 10^{-3} cm. The lines of etch pits were parallel to the $[11\bar{2}0]$ directions and intersected at close to 60^{o} revealing the underlying symmetry of the crystals. These detailed figures are for the various specimens of ruby grown in the 0^{o} growth direction which are listed in table 5. Also included in this table are the random etch pit densities for rubies grown in other orientations and for corundum crystals grown in the three main orientations. There are no results for the total etch pit density or the density of etch pit walls for this second group of ruby samples or for the corundum samples. It is believed that the chromium concentrations of those rubies whose concentrations are recorded as unknown were below 0·1% . The error in all the figures in the table is about $\pm$ 15% .

No attempt was made to examine the dislocations due to basal slip, nor to correlate those due to prismatic slip which were examined with the underlying crystal structure.

The fused potassium hydroxide, used to prepare the surfaces of samples for X-ray work, attacked their surfaces more strongly than the orthophosphoric acid. Occasionally etch pits were seen as a result of this attack, even on previously unpolished specimens, but their occurrence seemed to depend on chance and no attempt was made to use it as an etch for examining dislocations. The potassium hydroxide removed material at a mean

Table 5.

Etching Results.

Ruby.

A	B	C	D	E (1)	E (2)
G2a	0°	ann 1700	0·02 to 0·032	2·3	2·9
G2b	0°	ann 1700	0·02 to 0·032	2·0	2·0
337b	0°	ann 1700	0·052	1·7	2·7
337c	0°	ann 1930	0·052	2·3	2·7
344a	0°	unann	0·02	1·0	1·1
344b	0°	unann	0·02	1·6	1·8
497	73°	unknown	unknown	1·3	1·6
461b	90	unknown	unknown	1·4	-

Corundum.

420a	0°	unknown	none	1·1	0·9	0·9*
430	73°	unknown	none	1·3	1·4	
423a	90°	unknown	none	0·7	0·9	
512	90°	h.t. ann	none	1·6	-	

A. Specimen; B. Growth orientation; C. Previous heat treatment, ann means annealed, unann means unannealed, h.t. ann means annealed at high temperature in the growing furnace, and the figures are temperatures in °C; D. Chromium concentration in weight per cent; E. Random dislocation density, all figures are to be multiplied by $10^5/cm^2$, (1) and (2) refer to values at two different positions on the sample.

* An extra value of the random dislocation density obtained at a third position.

rate of 0·001 in/hour parallel to the c-axis and at a mean rate of 0.002 in/hour perpendicular to the c-axis. This is in agreement with Ellis's second requirement for the production of etch pits on the (0001) face (Ellis, 1955).

THE CORRELATION OF ETCH PITS WITH DISLOCATIONS.

If there is a one to one correspondence of etch pits to dislocations then the figures quoted above for etch pit densities are also the figures for the dislocation densities. It is assumed here that this correspondence does exist and that the figures in table 5 do represent dislocation densities. The main justification for this assumption is that Scheuplein and Gibbs, using a similar technique, obtained similar patterns of etch pits and values of etch pit densities to those obtained here, and they were able to demonstrate the one to one correspondence by means of a series of subsidiary experiments.

Further support for the assumption was obtained from the X-ray studies. Each X-ray photograph which showed mosaic structure gave information on the number of grains forming the mosaic structure in the volume irradiated by the X-ray beam and on the angle of misorientation of one grain with respect to its neighbour. Knowing the diameter of the X-ray beam when it struck the crystal, the value most frequently used was 9.10^{-2} cm, an estimate could be made of the linear dimension of the grains. The values calculated correspond to the higher values of grain size measured by the etching technique. The X-ray method was

not sensitive enough to detect smaller values of grain size. Using the value of the angular misorientation, α , between neighbouring grains and the linear dimensions of the grains, t, obtained from an X-ray photograph, an estimate of the dislocation density, D, in the neighbouring grains can be made by means of a formula due to Hirsch (1956),

$$D = \alpha/Bt. \qquad 3.1$$

The mosaic misorientations observed by the X-ray technique were due to basal slip so the value of B, Burgers vector, is 4·75 angstrom units (Scheuplein and Gibbs, 1960). Values of D calculated from X-ray photographs of some of the ruby specimens examined by the etching technique were about 3.10^6 dislocations per cm^2. These values agree reasonably well with the expected values which for the basal slip system of dislocations are about an order of magnitude greater than for the prismatic slip system of dislocations.

Scheuplein and Gibbs state that the minimum temperature required for generation of prismatic slip dislocations is 2000°C which meant that attempts to produce dislocations on the (0001) surface by piercing it with sharp points or by scratching it were unlikely to succeed. When several scratch marks were made on the surface of a specimen with a diamond no dislocations were observed which would definitely be connected with the scratches.

Woods (1960) suggested using the intersection of three

grain boundaries, as revealed by lines of etch pits, to establish the correlation between etch pits and dislocations. If there is a one to one correspondence and p,q and r are the linear etch pit densities in the three lines of etch pits then

$$p \simeq q + r. \qquad 3.2$$

Most of the intersections examined on the rubies showed approximate agreement with 3.2 but owing to the high density of etch pits in the lines it was difficult to find any clear threefold intersections from which definite conclusions could be drawn.

The assumption of a one to one correspondence in the case of the samples investigated is not directly contradicted by any of the above measurements.

DISCUSSION.

Table 5 shows that there was no large difference between the random dislocation densities of the ruby and corundum samples examined. It appears from this that the inclusion of 0·05 % or less of chromium in the growth process of ruby does not introduce extra dislocations. This is supported by some work performed by D.R. Mason (private communication). He etched a ruby and the seed from which it had been grown and found that both had dislocation densities about 10^5 dislocations/cm^2. Thus it was possible to attribute all the dislocations in the ruby to propagation from the seed crystal and no extra mechanism of

formation of dislocations was required.

Prior (private communication) observed that the density of walls per unit area on the surfaces of 90° growth direction crystals was very low. This supports the conclusion drawn from the X-ray results of the previous chapter concerning the incidence of mosaic structure in these crystals. Unfortunately no measurements of the density of walls on the 90° samples examined in this work were made. The number of walls per unit area in any sample may be a more important parameter than the random dislocation density in any attempt to correlate relaxation times or linewidths with physical defects as the grain boundaries are more prominent defects than single dislocations.

The growth angle of 73° which has been used to grow some of the crystals corresponds to the angle 73° 24' between the c-axis and the normal to the $\{10\bar{1}1\}$ faces. Edge dislocations of the basal slip system intersect these faces. The boules grown in this growth orientation are usually larger than those grown in the 0° orientation. This may be explained by the larger number of dislocations in the basal slip system than in the prismatic slip system which makes the growth process easier and more rapid. The crystals grown in the 90° orientation are usually smaller than those grown in the other two directions and this may be explained by the fact that there is no set of edge dislocations in this direction to aid the growth.

The etching work of Scheuplein and Gibbs on the

polygonisation of corundum crystals seems to offer an explanation to two points of the previous chapter. They observed that mosaic structure was formed when stress was applied to a crystal while it was maintained at about 2000°C and afterwards annealed at 2000°C. Polygonisation also occurs when the crystals are stressed while they are cooling rapidly from 2000°C and are then annealed at 1900°C. The first of these processes could quite easily occur in a growing boule. The stresses in the boule could be produced by the weight of the boule and its constraint at the intersection of boule and seed crystal, but they are more likely to be caused by temperature gradients across it. A boule grown in a particular orientation has a size and shape characteristic of the orientation employed. These characteristic forms, combined with the slight anisotropy in the thermal conductivity in ruby, produce different patterns of temperature gradients and thermal stresses in the boules. Qualitative considerations confirm that the 90° growth boules grow under the least stress and so have the least polygonisation. This was shown by experiment. This process of polygonisation probably explains why the detailed X-ray examination of boule 319 revealed a plane of good single crystal material between the boule and the seed crystal, both of which contained mosaic structure. The overall length from the plane to the tip of the seed crystal was only 1·3 cm. The thermal stresses over this distance were probably much less than those over the whole length of the boule, 4·6 cm, and so there was more likelihood of

polygonisation occurring in the larger volume of the boule than in the small region close to the seed crystal bounded by the clean plane.

The factor of four between the smallest and largest values of the random dislocation density in table 5 is to be expected. Scheuplein and Gibbs reported values for the prismatic slip system from 10^3 to 10^5 dislocations/cm^2. Any attempt to put another explanation on the values in table 5 would be of doubtful validity because the previous heat treatment of several of the samples is unknown.

The work described in chapters two and three combined with the results of work performed by Thorp and Mason form the letter included as appendix one (Thorp et al., 1964).

CONCLUSIONS.

For the samples examined the random etch pit density is about 10^5 etch pits/cm^2. The mode value is in the range 10^5 to 2.10^5 etch pits/cm^2, while the extreme values are 7.10^4 and $2{\cdot}9.10^5$ etch pits/cm^2. Support for the correspondence between etch pits and dislocations was obtained from the X-ray work so the figures in table 5 are the values of the random dislocation density in the samples. These samples included corundum and ruby so the results support the conclusion that the inclusion of chromium in the growth process does not introduce extra dislocations. The different sets of edge

dislocations in the boules and the polygonisation process described by Scheuplein and Gibbs form the basis of an explanation of the physical structure of the boules as revealed by the X-ray and etching work.

CHAPTER FOUR.

LINEWIDTHS.

Line broadening mechanisms; explanation of basic linewidth in ruby; prediction of extra broadening due to imperfections; conclusions.

LINE BROADENING MECHANISMS.

The line broadening mechanisms can be classified according to the type of line they produce or according to the type of mechanism which produces the line. In the first classification the mechanisms are called homogeneous if they produce broadening throughout all the line and inhomogeneous if they produce broadening through part of the line only. An example of the other type of classification is to divide the mechanisms into the following divisions.

1. Mechanisms which limit the lifetime of the states of the system.
2. Mechanisms which cause a spread of the values of the local magnetic field at the sites of the ions.
3. Broadening produced by the spectrometer.
4. Other mechanisms.

In division 1 are included the natural linewidth and the spin-lattice relaxation mechanisms. The natural linewidth can be estimated from Heisenberg's uncertainty principle. Spontaneous emission limits the lifetime of the state which leads to an uncertainty in the energy of the state. This process produces

widths of only 10^{-4} c/sec which in solids can be safely neglected. The phonon interactions which cause the spin-lattice relaxation broaden the energy levels and so contribute to the linewidths. The second division includes interactions between nuclear magnetic moments and the paramagnetic ions and also interactions due to the presence of impurities and imperfections in the solid. The third class includes inhomogeneities in the magnetic field, distortions of the line shape due to power saturation and due to the finite time constants or bandwidths of the associated electronic equipment. The other mechanisms include the dipole-dipole and exchange interactions between the paramagnetic ions. These two can be regarded as being a mixture of the first two divisions because each reduces the lifetime of ions at neighbouring sites as well as producing a spread of magnetic fields at the sites.

The important mechanism here is the one which produces a spread in the values of the local magnetic field due to physical imperfections in the crystals. As already seen, the ruby crystals contain dislocations and mosaic structure and it is desired to correlate these physical imperfections with linewidth measurements made in ruby. In order to do this it is necessary to know how the other mechanisms affect the linewidth.

The contribution due to spin-lattice relaxation is approximately $1/T_1$ where T_1 is the spin-lattice relaxation time. The value of T_1 for all the transitions at $77^{\circ}K$, the temperature

at which the work was performed is 44.10^{-6} sec, Pace et al. (1960), so the broadening due to this mechanism is 2.10^{4} c/sec which can be neglected compared to the total linewidth of about 60.10^{6} c/sec. In the particular ruby samples used the impurity content was very low so there was no need to consider impurities as a source of linewidth. Care was taken to avoid the effects of saturation on the linewidths, see chapters five and six. Also, by a careful choice of bandwidths and time constants in the electronic equipment, most of the distortions due to these factors were eliminated, and those which remained were allowed for as far as possible, see chapters five and six. The magnetic field was homogeneous to one part in five thousand and stable to one part in 10^{5} in time. These values mean that the magnet did not produce any distortions of the true line shape. It is not certain how homogeneous the field due to the secondary coils was, and this is also discussed in chapters five and six.

The remaining mechanisms which have to be considered are the nuclear, exchange and dipole-dipole interactions. These three interactions produce the basic linewidth in ruby. The Al^{27} nuclei interacting with the Cr^{3+} ions produce a width of 9·7 oersteds (Altshuler and Mineeva, 1963) and the Cr^{53} nuclei, even though they are only 9·5% abundant, produce the long tail of the ruby lines (Klyshko, 1964). For some years the dipole-dipole interaction was regarded as the main source of the linewidth in ruby, but the theoretically predicted values were much larger than

the experimentally observed values (Manenkov and Fedorov, 1960). Recently two separate explanations of the basic linewidth in terms of exchange interactions have been put forward, one by Altshuler and Mineeva (1963) and the other by Klyshko (1964).

Before considering the detail of these explanations it may be worthwhile to consider the model of Anderson and Weiss (1953) which accounts for the broadening due to dipole-dipole and exchange interactions together. Their basic explanation did not include crystal field effects but they were able to include these effects roughly at a later stage. They assumed that the ion absorbs at one frequency which is in a certain range determined by the dipole-dipole interactions. The absorption frequency wanders at random over the range available to it under the influence of the exchange interactions. Thus the dipole-dipole interactions are continually interrupted and cannot exert their full influence. Anderson and Weiss computed the general form of the lineshape for this type of double mechanism and they predicted a lineshape with a central portion following a Lorentzian curve and the wings a Gaussian curve. Alshuler and Mineeva and Klyshko based their calculations on the general theory of Pryce and Stevens for the evaluation of moments of the lineshape rather than on the ideas of Anderson and Weiss, but these ideas give a clearer picture than the work of Pryce and Stevens. The approach of the latter included the effects of the crystal field from the beginning of the calculation.

Altshuler and Mineeva predicted the widths of the $-\frac{1}{2}$ to $+\frac{1}{2}$ transition at polar angles 0^{o} and 55^{o} and of the $+\frac{1}{2}$ to $+3/2$ transition at 0^{o}. (The polar angle is the angle between the direction of the main magnetic field and the c-axis of the crystal.) They predicted that the widths ought to depend on the concentration of the chromium ions. The calculations were based on the assumption of a Lorentzian lineshape and isotropic exchange interaction. The latter assumption implies that the spin-orbit coupling is neglected. The exchange interaction was represented by an operator W_{ij} given by

$$W_{ij} = J(r_{ij})(S_i \cdot S_j) \qquad 4.1$$

where S_i and S_j are the spins of the ions at the sites i and j and $J(r_{ij})$ is the exchange integral associated with the spins at sites i and j, a distance r_{ij} apart. They assumed that $J(r_{ij})$ could be written as

$$J(r_{ij}) = J(r_o)/r_{ij}^{n} \qquad 4.2$$

for distances $r_{ij} > r_o$ where r_o is the distance such that $J(r_o) = 2D$, the crystal field splitting. For $r_{ij} < r_o$ the exchange interaction would produce new lines, Statz et al. (1961), while for $r_{ij} > r_o$ it would produce broadening, J_o was given as approximately $2 \cdot 5$ cm^{-1} and $n = 12$.

Klyshko approached the problem from a different point of view. He estimated the mean square width for the $-\frac{1}{2}$ to $+\frac{1}{2}$ transition at 0^{o} by neglecting the dipole-dipole interaction over

the region where the exchange interaction produces fresh lines, and by neglecting the exchange interaction and retaining the dipole-dipole interaction over the region $r_{ij} > r_o$. He stated that r_o can be obtained from the experimental value of $\langle \Delta\nu^2 \rangle_{av}$ and that the assumptions made were supported by experiment for the case of isolated ions. His prediction for the mean square width is also concentration dependent. He carefully analysed the observed line shape of the $-\frac{1}{2}$ to $+\frac{1}{2}$ transition at the polar angle 0^o and demonstrated that it was formed by two Gaussian curves with different constants, one describing the centre portion and the other describing the far wings of the line. Between the Gaussian regions was a long tail, some 20 oersteds long, caused by hyperfine interactions with the Cr^{53} nuclei.

BROADENING DUE TO IMPERFECTIONS.

The amount of broadening due to mosaic and c-axis misorientations may be readily estimated. If the value of the magnetic field H at resonance varies with polar angle θ and there is a distribution of c-axis directions in a crystal represented by $\Delta\theta$ then

$$\Delta H = \Delta\theta . \, dH/d\theta \qquad 4.3$$

where ΔH represents the increase in the linewidth.

Shaltiel and Low (1961) were able to demonstrate that in the case of a cubic crystal the correct value for $\Delta\theta$ was α_o, a constant characterising a Gaussian distribution of

crystallites about an axis referred to as the rotation axis. This distribution was assumed to cut off at a value α and it was also assumed that the rotation axes were isotropically distributed throughout all directions. These assumptions are probably correct for a cubic material.

Figure 11 shows the situation in ruby. The mean direction of the c-axis is the z-axis of the spherical coordinates. The basal slip dislocations form one set of rotation axes in ruby. One of these dislocations is represented by the vector $\underline{b}$ in the figure. The possible directions of $\underline{b}$ are limited to the regions within $70° \leq \theta \leq 80°$ and $\phi \pm 5°$, $120° + \phi \pm 5°$ and $240° + \phi \pm 5°$, Scheuplein and Gibbs (1960). The mosaic blocks are rotated about $\underline{b}$ by up to α so that the c-axis can take up any direction in the region limited by $\underline{c}'$ and $\underline{c}''$. The distribution of c-axes when viewed along the z-axis appears as shown in figure 12.

The prismatic slip dislocations are distributed in a cone about the mean c-axis direction. They also act as axes of rotation but the result of this rotation is to alter ϕ only. This does not affect the spectrum and therefore does not affect the linewidth by the mechanism of 4.3.

The X-ray examinations were carried out in the main on the (0001) face which is perpendicular to the c-axis as shown in figure 11. Therefore the measurements were of the distribution

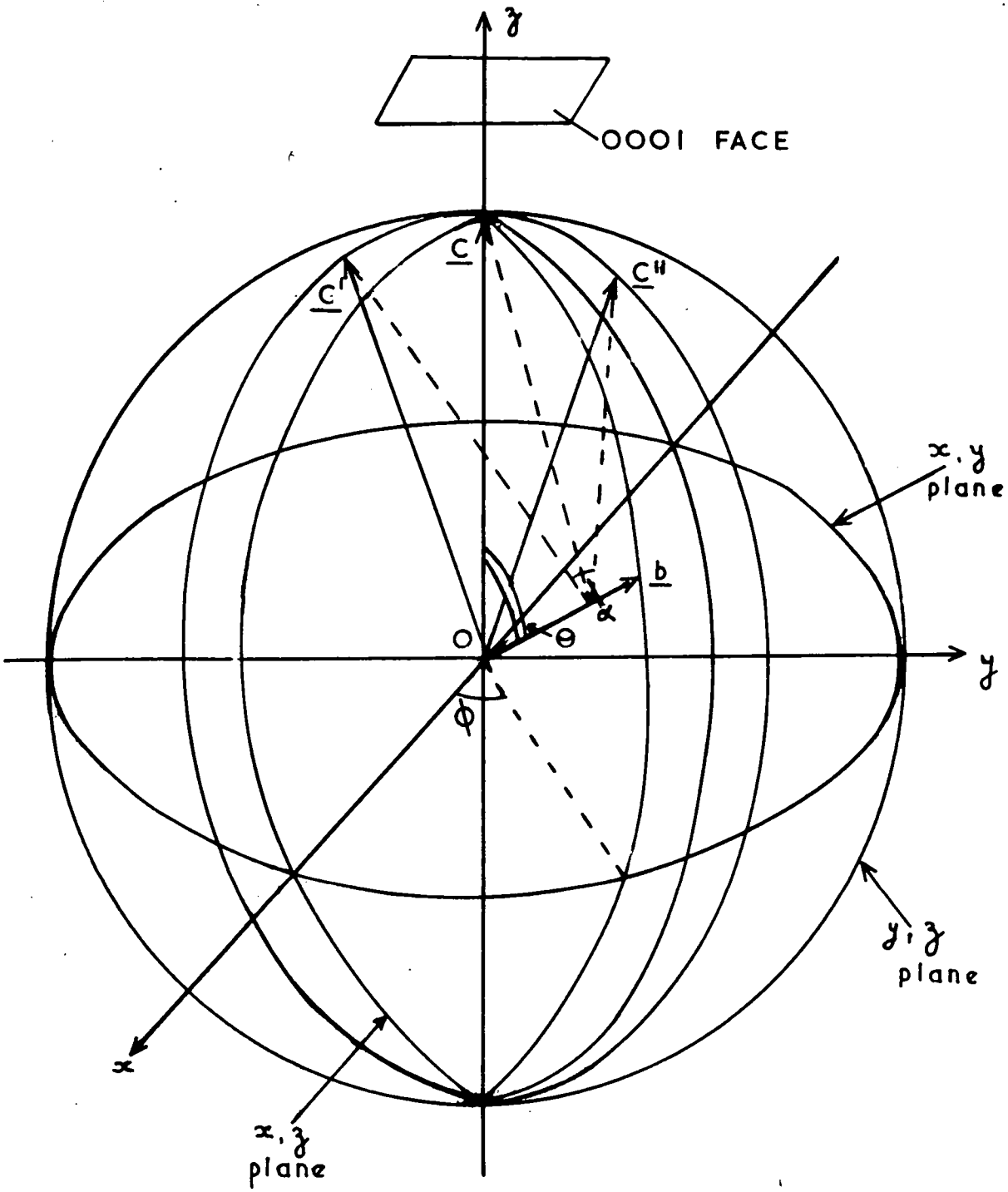

DISTRIBUTION OF PHYSICAL IMPERFECTIONS IN RUBY

FIGURE 11

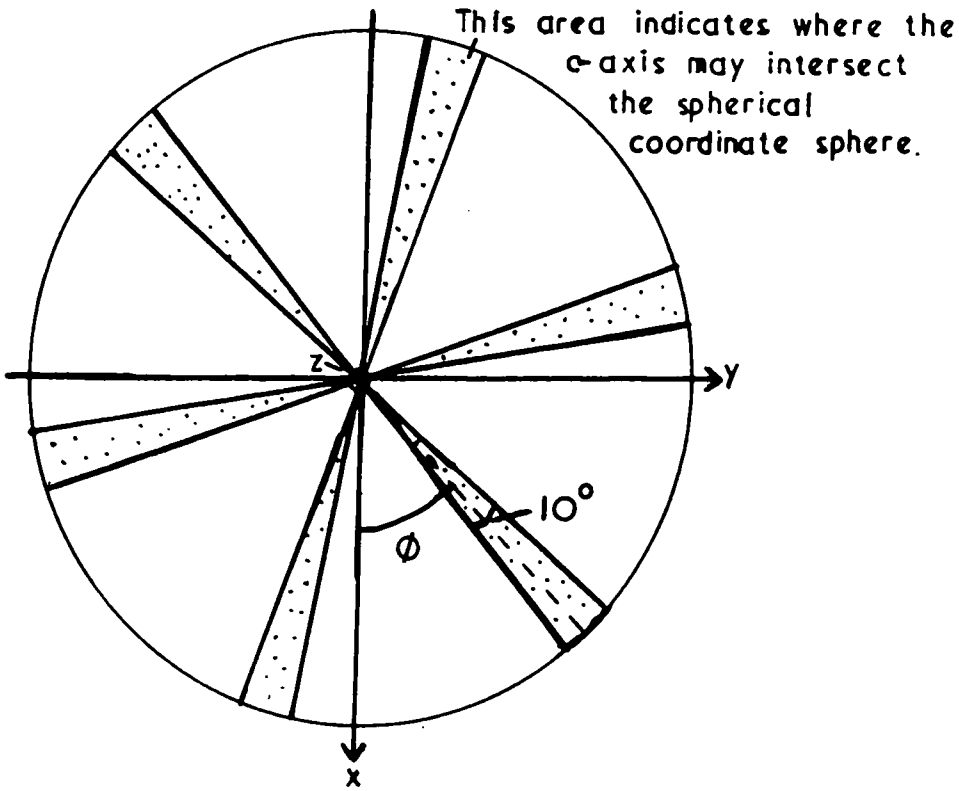

PLAN VIEW OF THE DISTRIBUTION

C-AXIS DIRECTIONS

FIGURE 12

produced by the rotations described above. The value substituted into 4.3 for $\Delta\theta$ has to be a suitable representation of the distribution of c-axes, see chapter seven.

For the $-\frac{1}{2}$ to $+\frac{1}{2}$ transition $dH/d\theta \simeq 0$ so there should be no broadening due to this mechanism in this transition. For the -3/2 to $-\frac{1}{2}$ and the $+\frac{1}{2}$ to +3/2 transitions the gradient of the magnetic field for resonance against angle is proportional to $\sin 2\theta$ (Shaltiel and Low) which predicts a maximum broadening due to this mechanism in these transitions at $\theta = 45^{\circ}$. The gradient $dH/d\theta$ can be measured for the second and third order transitions and so estimates of the amount of imperfection broadening can be made for them also.

From an analysis of the variations of the linewidth of a transition with polar angle it should be possible to estimate the amount of broadening due to physical imperfections and perhaps gain some further information on the nature of the physical imperfections. To perform this analysis, the effects of the dipole-dipole and exchange interactions have to be allowed for. Also it is assumed that the broadening due to physical imperfections is directly additive to the basic linewidth due to other mechanisms.

Another mechanism due to physical imperfections is the one described by Manenkov et al. (1963). The stresses present in a crystal may distort the surroundings of the paramagnetic ion and so alter the values of the parameters in the spin Hamiltonian.

Manenkov et al. have demonstrated how changes in the value of the crystal field splitting parameter D can effect the widths of the $+\frac{1}{2}$ to $+3/2$ and the $-3/2$ to $-\frac{1}{2}$ transitions. They detected this effect by observing the relative intensities of these transitions compared to the $-\frac{1}{2}$ to $+\frac{1}{2}$ transition. For any one sample it may be considered as part of the basic linewidth.

TRANSITION PROBABILITIES.

The line shape will be distorted from that due to 4.3 if the transition probability of the transition varies rapidly with angle. In order to estimate the effect of this the transition probability was calculated against angle. The calculation is based on the work of Schulz-du Bois (1959).

Figure 13 shows the coordinate system related to the pole piece gap and the coordinate system related to the walls of the waveguide. For an H_{10} wave

$$H_x = E_0 \sqrt{(\epsilon/\mu)}\sqrt{(1-\lambda^2/\lambda_c^2)}\sin\frac{\pi x}{a}\exp i(\omega t-\gamma z),$$
$$H_z = -i E_0 \sqrt{(\epsilon/\mu)}(\lambda/\lambda_c)\cos\frac{\pi x}{a}\exp i(\omega t-\gamma z), \qquad 4.4$$
$$\gamma = 2\pi/\lambda_g.$$

If the sample is cut correctly and fits perfedly into the guide then the c-axis is parallel to OX. It is then possible, see chapter six, to orientate the guide so that OX is parallel to Ox. In this case, in the spherical coordinates attached to the pole piece, $\vartheta = 90^\circ$, $\phi = 0^\circ$ and OZ is parallel to Oy. The angle ϑ is the polar angle already defined and the situation at any arbitrary ϑ is shown in figure 14. Following Schulz-du Bois the transition probabilities can be calculated at any angle ϑ.

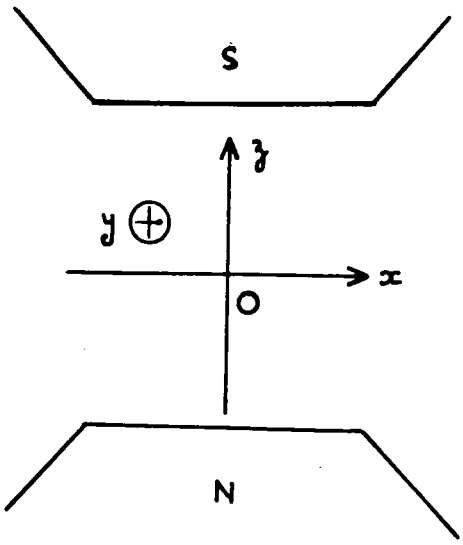

Magnet coordinates. View looking downwards from cryostat head.

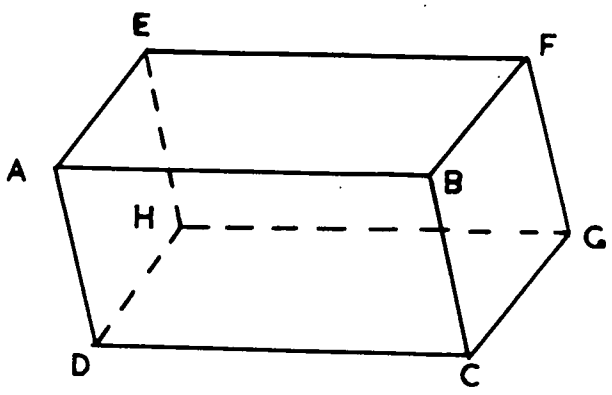

Waveguide. Origin at H; EH // OX, broad dimension a; DH // OY narrow dimension b; GH // OZ, power travels in the positive direction.

COORDINATE SYSTEMS

FIGURE 13

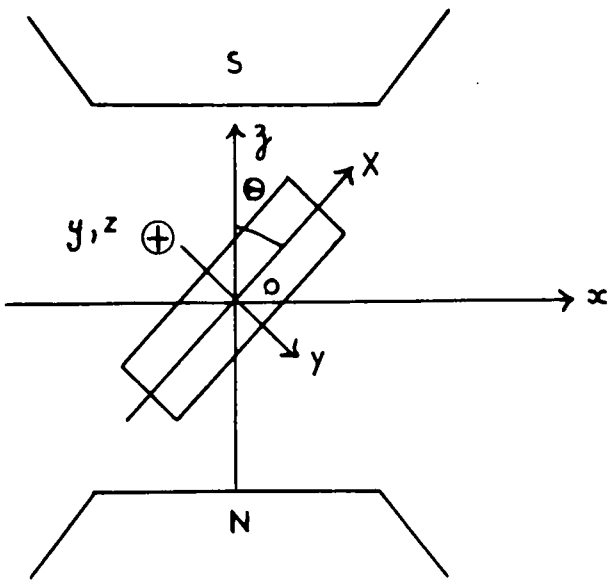

RELATION OF WAVEGUIDE TO MAGNET COORDINATES, VIEW FROM CRYOSTAT HEAD

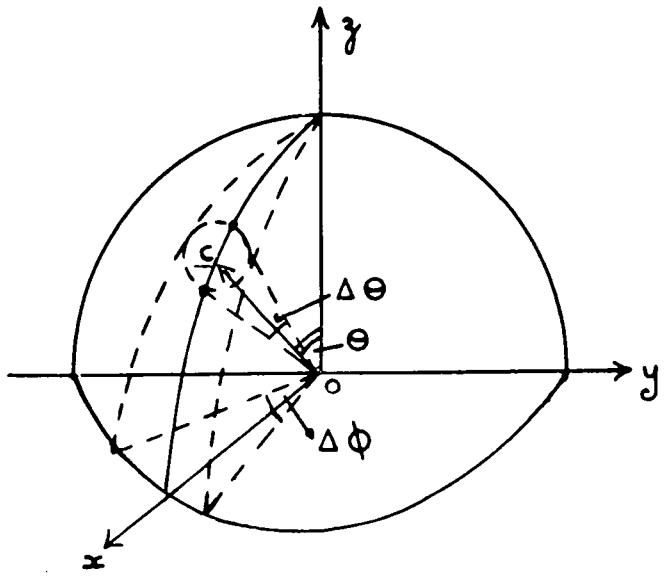

RELATION OF POSSIBLE C-AXIS DIRECTIONS TO THE MAGNET COORDINATES AT THE POLAR ANGLE θ

FIGURE 14

The alternating field which produces the transitions is that due to the X and Z components of the magnetic field in the waveguide. These components have to be resolved along Ox, Oy and Oz. The value of the probability decreases with decreasing value of θ for the main transitions. It was necessary to extrapolate the graphs of eigenvectors beyond the magnetic field value of 10700 oersteds, which is the limit of their range in the paper by Schulz-du Bois, in order to perform the calculations at the higher field values.

Figure 14 shows the effects of the various misorientations on the mean c-axis direction at the general angle θ. The dotted circle around $\underline{c}$ contains the c-axis distribution of figure 12. Study of the graphs of eigenvectors given by Schulz-du Bois shows that for variations in the c-axis direction of $\pm 3^{\circ}$ in θ there are only negligible changes in the transition probability. The effect of a $\pm 3^{\circ}$ variation in ϕ can be calculated using the formula relating values of eigenvectors for different values of ϕ which is given by Schulz-du Bois. It is readily found that at any one value of θ this small variation in ϕ has a negligible effect on the transition probabilities. The figures of $\pm 3^{\circ}$ were chosen after reference to the results of the X-ray work because they are larger than any measured value of mosaic or c-axis misorientation.

These calculations were made on the assumption that the crystal was perfectly cut and inserted in the waveguide. This,

in general, was not the case. Another possible error was that the waveguide might not be aligned exactly in the magnet. The effects of such deviations from the perfect case described above are discussed in appendix two. The main conclusions of this appendix are, firstly, that the perfect case described above is closely approximated to when the waveguide is arranged to be parallel to Oy, that is vertical, and, secondly, that the small angle between the c-axis and the wall of the waveguide, which must be included in any calculation of the absolute transition probability, can be neglected in any calculation of the difference in transition probability between two angles only a few degrees apart.

CONCLUSIONS.

From an analysis of linewidth measurements made at various values of the polar angle it should be possible to estimate the amount of physical imperfection present in a sample. It should also be possible from the basic linewidth to make an estimate of the local concentration of chromium ions. The main features of the line which ought to be measured for a complete description are the lineshape, the width at half the peak intensity or the root mean square width (the two can be related if the lineshape is known) and the moments of the line. The important points in the preparation of the experiments are the alignment of the waveguide as near to the vertical as possible and the correct orientation of the c-axis. These adjustments facilitate the

calculation of the angular variation of the transition probabilities and allow a check to be made of the effects of the various parameters on the angular variation of the linewidths.

CHAPTER FIVE.

THE SPECTROMETER.

Specific requirements for spectrometer design; theory of signal production; discussion of conditions stated in theory; description of apparatus; sensitivity of spectrometer; conclusions.

SPECIFIC REQUIREMENTS FOR THE DESIGN OF THE SPECTROMETER.

The aim was to measure the absorption linewidths and lineshapes in ruby, and to study their variation with polar angle. The work was carried out at frequencies near 35 kMc/sec which meant that magnetic fields up to 17000 oersteds were required and to supply these with the magnet available a pole piece gap no larger than 4·5 cm had to be used. The sample size was the order of size that might be used in a maser, that is up to 1 cc. This size was also suitable for the X-ray and etching techniques described above. A conventional Q-band cavity designed to take this size of sample would have been too bulky to fit between the poles of the magnet and still leave room for the dewars necessary for low temperature work. Because of this it was decided to study the possibility of using a shorted piece of guide as a cavity. The material was known to have a strong signal so sensitivity considerations were not of major importance. The most important factor was to produce a system

which would detect γ_2 only and well enough to allow measurement of the peak intensity of the line, the linewidth at half the peak intensity and the major features in the shape of the line. Also, as noted in chapter four, the guide had to be adjusted correctly in the pole piece gap.

THEORY OF SIGNAL PRODUCTION.

Figure 15 shows a block diagram of a simple spectrometer. Power from a klystron was fed into a magic tee where it was divided into the two side arms. One side arm, the balance arm, contained an E-H tuner and a matched load so that a controllable reflection could be introduced; the other was connected to the sample. An iris of diameter 3·5 mm was placed in the side arm containing the sample, and the length of guide, about 100 cm, between the iris and the short circuit which terminated the guide acted as the cavity. The iris diameter was chosen so that the value of the reflection coefficient of the sample arm off magnetic resonance was 0·5. This value was close to the optimum value for maximum sensitivity of the spectrometer (Feher, 1957). The E-arm of the magic tee was terminated by a detector crystal.

In figure 15 P is the power incident on the magic tee, P_c is the power incident on the detector, Γ_b is the reflection coefficient from the balance arm and Γ_o is the reflection coefficient from the cavity and sample while the sample is off magnetic resonance. Both Γ_o and Γ_b are complex quantities

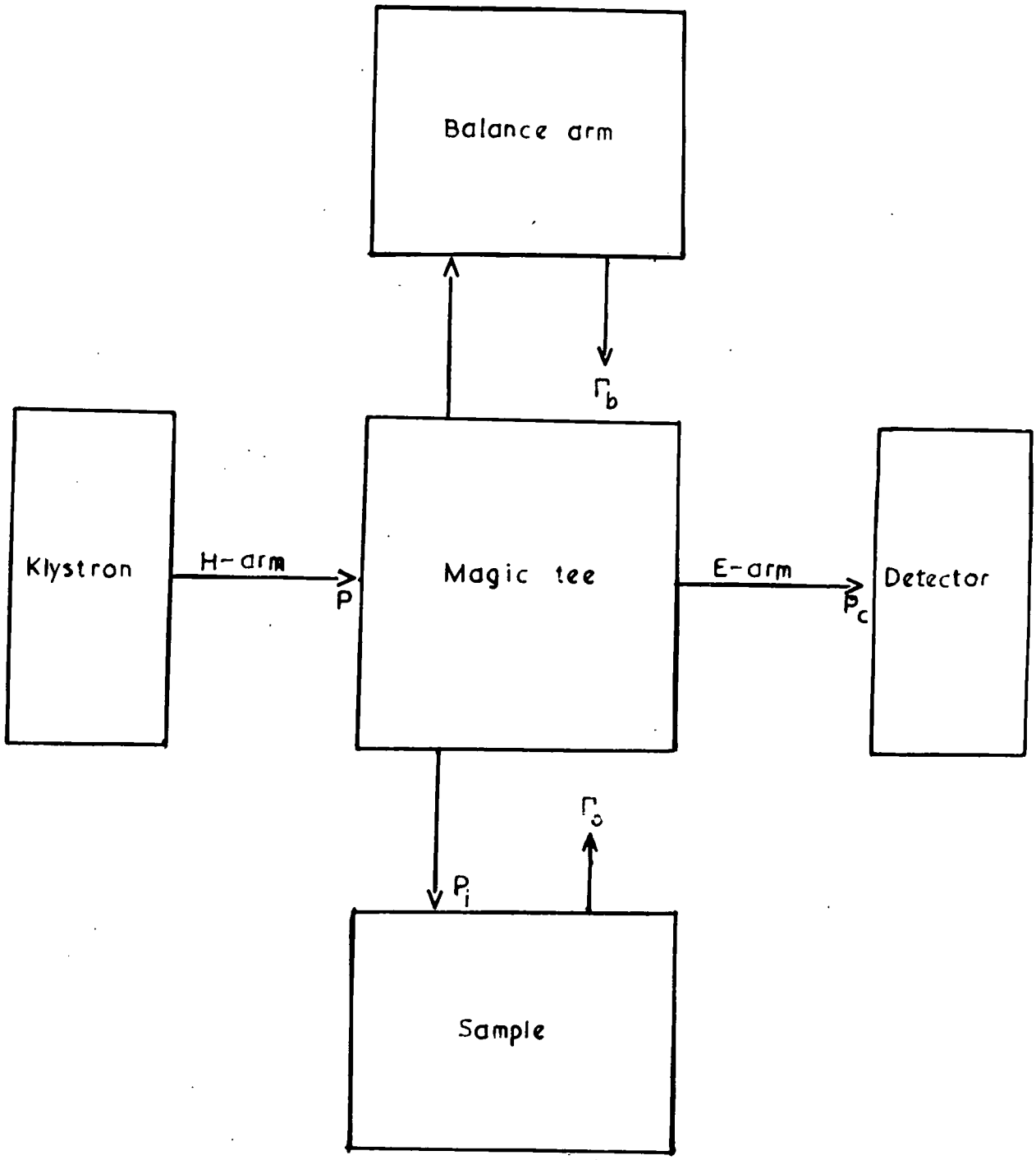

BLOCK DIAGRAM OF THE SPECTROMETER

FIGURE 15

which can be written as $\Gamma_{o1} + j\,\Gamma_{o2}$ and $\Gamma_{e1} + j\,\Gamma_{e2}$.

The reflection properties of the magic tee can be represented by

$$P_c = \frac{1}{4}\left|\Gamma_o \pm \Gamma_e\right|^2 P. \qquad 5.1$$

To avoid saturation of the amplifiers after the detector and to obtain better noise rejection by the tee, the negative sign is taken in 5.1. When the sample is on magnetic resonance Γ_o changes to $\Gamma_m = \Gamma_{m1} + j\,\Gamma_{m2}$ and the power incident on the detector changes to P_{cm}, where

$$P_{cm} = \frac{1}{4}\left|\Gamma_m - \Gamma_e\right|^2 P. \qquad 5.2$$

The power incident on the detector due to magnetic resonance only P_s, is given by

$$P_s = P_{cm} - P_c . \qquad 5.3$$

Write $\Delta\Gamma = \Gamma_m - \Gamma_o$, then

$$P_s = \frac{1}{4}\left[2\,Re\left\{\Delta\Gamma(\Gamma_o - \Gamma_e)^*\right\} + \left|\Delta\Gamma\right|^2\right] P \qquad 5.4$$

where * represents the complex conjugate. If the condition

$$\left|\Delta\Gamma\right|^2 \ll 2\,Re\left\{\Delta\Gamma(\Gamma_o - \Gamma_e)^*\right\} \qquad (A)$$

is satisfied

$$P_s = \frac{1}{2} P\, Re\left\{\Delta\Gamma(\Gamma_o - \Gamma_e)^*\right\}. \qquad 5.5$$

By adjusting the termination of the balance arm to make $(\Gamma_o - \Gamma_e)$ real, $(\Gamma_o - \Gamma_e)^*$ is made real, and the instrument only detects

$$Re\left\{\Delta\Gamma\right\} = Re\left\{\Delta\Gamma_1 + j\,\Delta\Gamma_2\right\} = \Delta\Gamma_1 . \qquad 5.6$$

If β is the current sensitivity of the detector, the current S due to magnetic resonance is given by

$$S = \beta P_s = \frac{1}{2} \beta P (\Gamma_{o1} - \Gamma_{e1}) \Delta\Gamma_1 . \qquad 5.7$$

A convenient expression for $\Delta\Gamma_1$ can be obtained by writing $\Delta\Gamma$ in terms of the real and imaginary parts of the reflection coefficients Γ_o and Γ_m.

$$\Delta\Gamma = \Gamma_{m1} - \Gamma_{o1} + j(\Gamma_{m2} - \Gamma_{o2}). \qquad 5.8$$

At the peak of a cavity resonance $\Gamma_{o2} = 0$ and at the peak of magnetic resonance $\Gamma_{m2} = 0$. From 5.8

$$\Delta\Gamma_1 = \Gamma_{m1} - \Gamma_{o1}. \qquad 5.9$$

To derive an expression for $\Delta\Gamma_1$ requires the use of the equivalent circuit of the sample arm shown in figure 16. Equivalent circuits for resonant cavities are considered by Montgomery et al. (1947). The plane AB across the guide is chosen so that the admittance of the iris, guide and sample viewed from AB is equivalent to that of the series resonant circuit. The guide on the other side of the plane is represented by a transmission line of impedance equal to its characteristic impedance, Z_o. The iris was placed at least 12 mm from the tee because the guide wavelength for the frequencies used was less than 12 mm. The admittance of a terminated length of transmission line goes through all possible values as its length is increased from zero to λ_g, the guide wavelength, so

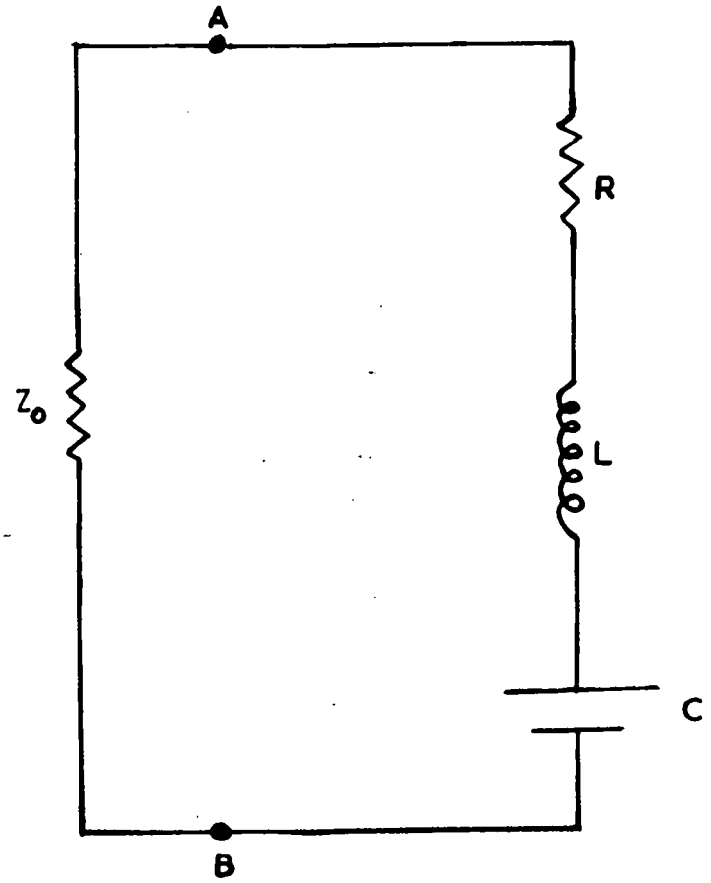

EQUIVALENT CIRCUIT OF THE CAVITY ARM

FIGURE 16

12 mm was the least distance from the iris in which the correct plane AB could be located.

From figure 16

$$\Gamma_o = \frac{R + j(\omega L - 1/\omega C) - Z_o}{R + j(\omega L - 1/\omega C) + Z_o} \qquad 5.10$$

where ω is the pulsatance of the signal. At the peak of the cavity resonance $\omega L - 1/\omega C = 0$ so 5.10 becomes

$$\Gamma_o = \frac{R - Z_o}{R + Z_o} . \qquad 5.11$$

During the magnetic resonance the inductive component in the circuit is altered to a new value L' given by

$$L' = L(1 + 4\pi\eta(\chi_1 - j\chi_2)) \qquad 5.12$$

where η is the filling factor defined as

$$\eta = \int_s H^2 dV_s \Big/ \int_c H^2 dV_c . \qquad 5.13$$

5.12 can be demonstrated by considering the energy stored in the cavity first away from the magnetic resonance and then during the magnetic resonance. In the former case the energy can be written as

$$E_o = \tfrac{1}{2} \mu \int_c H^2 dV_c \qquad 5.14$$

where c represents integration over the cavity volume and H the magnetic field vector at a position in the cavity. In C.G.S. units $\mu = \mu_o + 4\pi(\chi_1 - j\chi_2)$ where μ_o has dimensions but equals unity. Far from a magnetic resonance χ_1 and χ_2 are

very small and may be neglected, see figure 2. At magnetic resonance these quantities become appreciable and the energy can be written as

$$E_m = \frac{1}{2}\int_c H^2 dV_c - \frac{1}{2}\int_s H^2 dV_s + \frac{1}{2}\left[1 + 4\pi(\chi_1 - j\chi_2)\right]\int_s H^2 dV_s \qquad 5.15$$

where s indicates integration over the sample volume. E_o can be equated to the energy $\frac{1}{2}Li^2$ of a coil of self-inductance L and E_m to the energy $\frac{1}{2}L'i^2$ of a coil of self-inductance L'. Eliminating $\frac{1}{2}i^2$ leaves equation 5.12 above with η defined as in 5.13.

During magnetic resonance

$$\Gamma_m = \frac{R + j(\omega L' - 1/\omega C) - Z_o}{R + j(\omega L' - 1/\omega C) + Z_o}. \qquad 5.16$$

The real part Γ_{m1} is given by

$$\Gamma_{m1} = \frac{(R - Z_o + R_m)(R + Z_o + R_m) + (4\pi\eta\omega L\chi_1)^2}{(R + Z_o + R_m)^2 + (4\pi\eta\omega L\chi_1)^2} \qquad 5.17$$

at the peak of the cavity resonance, where $R_m = 4\pi\eta\omega L\chi_2$. It can now be seen that Γ_{m1} contains the effects of χ_1 unless the two conditions

$$(R - Z_o + R_m)(R + Z_o + R_m) \gg (4\pi\eta\omega L\chi_1)^2 \qquad (B)$$

and

$$(R + Z_o + R_m)^2 \gg (4\pi\eta\omega L\chi_1)^2 \qquad (C)$$

are satisfied. It should be noted that if (B) is satisfied then so is (C).

Defining the various resistances R, R_m and Z_o in terms of the unloaded cavity Q, Q_u, the external Q, Q_e the loaded Q, Q_L, the magnetic Q, Q_m and the pulsatance ω, the following

relations are obtained.

$$Q_u = \omega L/R, \quad Q_e = \omega L/Z_o, \quad Q_L = \omega L/(R+Z_o),$$
$$Q_m = \omega L'/R_m = \omega L/R_m. \qquad 5.18$$

The last of equations 5.18 is correct when the relation

$$4\pi\eta\,|\chi_1 - j\chi_2| \ll 1 \qquad (D)$$

is satisfied. From 5.11 and 5.18

$$R - Z_o = \frac{\Gamma_{o1}\,\omega L}{Q_L}. \qquad 5.19$$

Using equations 5.18 and 5.19 (B) becomes

$$\left(\frac{\Gamma_{o1}}{Q_L} + \frac{1}{Q_m}\right)\left(\frac{1}{Q_L} + \frac{1}{Q_m}\right) \gg \left(4\pi\eta\chi_1\right)^2. \qquad (E)$$

When (E) is correct equation 5.17 becomes

$$\Gamma_{m1} = \frac{R - Z_o + R_m}{R + Z_o + R_m}. \qquad 5.20$$

Then, as shown by Goldsborough and Mandel (1960), but using the notation of this paper,

$$\Delta\Gamma_1 = \frac{k Q_u \chi_2 v (1 - \Gamma_{o1}^2)}{1 + k Q_u \chi_2 v (1 + \Gamma_{o1})}$$
$$= \frac{K Q_u (1 - \Gamma_{o1}^2)}{1 + K Q_u (1 + \Gamma_{o1})} \qquad 5.21$$

where $K = k\chi_2 v$. 5.22

In 5.22 k is a constant given by ωC_1, where C_1 is another constant depending on the geometry of the cavity and the mode in the cavity, and v is the sample volume.

From 1.2 the unloaded Q, Q_{um}, of the cavity in the presence of magnetic resonance is given by

$$Q_{um} = \frac{\omega \mathcal{E}}{P_i(1 - \Gamma_m^2)} \qquad 5.23$$

where $\mathcal{E}$ is the total energy stored and P_i is the power

incident on the cavity. Goldsborough and Mandel introduced Q_{um} and stated that

$$H^2 = C_2 Q_{um} \rho_i (1 - \Gamma_m^2) \qquad 5.24$$

where H^2 is the mean square amplitude of the magnetic field vector in the cavity, and $C_2 = 4C_1$. The factor 4 occurs because Goldsborough and Mandel used the half amplitude of the magnetic field vector while here the amplitude is used. It should be noted that during the course of their derivation they tacitly assumed the validity of (D) to compare Q_{um} with Q_e.

From 1.2

$$Q_u = \frac{\omega \mathcal{E}}{\rho_i (1 - \Gamma_{01}^2)} \qquad 5.25$$

where once again (D) has been assumed to hold to give the same value of the energy stored as in 5.23. From 5.21 and 5.25

$$\Delta\Gamma_1 = \frac{K\omega\mathcal{E}}{\rho_i} \Big/ \left(1 + \frac{K\omega\mathcal{E}}{\rho_i(1-\Gamma_{01})}\right). \qquad 5.26$$

The power absorbed by the sample due to magnetic resonance is given by 1.1 Using equations 5.22, 5.23 and 5.24 in 1.1 and remembering that $C_2 = 4C_1$

$$\rho_m = 2K\omega\mathcal{E}. \qquad 5.27$$

Therefore, substituting for $K\omega\mathcal{E}$ from 5.27

$$\Delta\Gamma_1 = \frac{\rho_m}{2\rho_i} \Big/ \left(1 + \frac{\rho_m}{2\rho_i(1-\Gamma_{01})}\right). \qquad 5.28$$

Putting 5.28 into 5.7, remembering that $P_i = \frac{1}{2}P$ because of the action of the magic tee, gives on rearranging

$$\rho_m = \frac{S}{a - bS} \qquad 5.29$$

where $a = \frac{1}{2}\beta(\Gamma_{01} - \Gamma_{b1})$ and $b = 1/\{\rho(1-\Gamma_{01})\}$.

As long as there is no saturation P_m is directly proportional to χ_2 as shown in 1.1, so measurement of the variation of P_m with magnetic field also gives the variation of χ_2 with magnetic field. The apparatus had to be designed and operated so that saturation did not occur and so that any instrumental errors, due to finite bandwidths and the time constants of various parts of the electronic circuits, were reduced to a minimum.

If bS << a equation 5.29 becomes

$$\rho_m = \frac{S}{a} . \qquad 5.30$$

Equation 5.30 is correct if the condition

$$\frac{\rho_m}{2\rho_i(1-\Gamma_{01})} << 1 \qquad (F)$$

is satisfied. This condition can be rewritten using equation 5.25 and the definition of Q_m in equation 1.2. It then becomes

$$Q_u(1+\Gamma_{01}) << 2Q_m . \qquad (G)$$

Of the seven conditions stated above it is only necessary to consider (A), (D), (E) and (G). This is because (E) and (G) are alternative forms of (B) and (F), and if (E) is satisfied so also is (C). It is useful to rewrite (A) as

$$\left(\frac{1}{Q_L} + \frac{1}{Q_m}\right)^{-1}\left[\left(\frac{1-\Gamma_{01}}{Q_m}\right)^2 + \left(\frac{8\pi\eta\chi_1}{Q_e\left(\frac{1}{Q_m}+\frac{1}{Q_L}\right)}\right)^2\right] << 2\left(\frac{1-\Gamma_{01}}{Q_m}\right)\left(\Gamma_{01}-\Gamma_{b1}\right). \qquad (H)$$

The experimental work was performed with the cavity on a

resonance so $\Gamma_{02} = 0$ and equation 5.8 simplifies to

$$\Delta\Gamma = \Gamma_{m1} - \Gamma_{01} + j\Gamma_{m2}. \qquad 5.31$$

(H) was obtained from (A) by using equations 5.16 and 5.31 and carrying out similar steps to those by which (E) was obtained from (B). If (H) is not satisfied the signal contains the effects of γ_1 as well as γ_2 through the influence of $|\Delta\Gamma|^2$. At the peak of the magnetic resonance $\gamma_1 = 0$ and (H) simplifies considerably. It can then be seen that in order to satisfy the condition, the magic tee must be adjusted so that $(\Gamma_{01} - \Gamma_{e1})$ is as large as possible and $Q_L \ll Q_m$. The inequality requires that the filling factor be as small as possible. In practice a value of approximately 10^{-2} was used. For a detailed numerical discussion see chapter six.

Condition (D) is easily satisfied, especially with a small filling factor. The validity of (E) determines whether Γ_{m1} will contain the effects of γ_1 as well as of γ_2. When it is satisfied the terms containing γ_1 are small enough to be neglected and it is shown in chapter six that the experimental values do satisfy it. Once more a small filling factor is a help in satisfying the relation.

The seventh condition (G) is the one concerning the simplification of the expression for the signal by reducing 5.29 to 5.30. This condition does not have to be satisfied because the lineshape can be evaluated from 5.29 quite easily. If it is satisfied then the signal recorded is proportional to

the lineshape. Physically the condition means that the energy losses due to paramagnetic resonance must be very much less than those due to the cavity. This condition also is more easily satisfied for small values of the filling factor.

Many workers have discussed aspects of the theory of microwave resonance spectrometers, among them Bloembergen et al. (1948), Feher (1957), Goldsborough and Mandel (1960) and Misra (1963). Feher was more concerned with the design of a sensitive spectrometer and the parameters which affect such a design. He only considered the signal due to γ_2, and in his derivation of the signal he never indicated what possible effects γ_1 might have. Although he did mention briefly that the apparatus had to be set up in such a manner that the two were separated, he did not discuss how this could be done.

The present theory is based on the approach of Goldsborough and Mandel. It should be noted that equation 5.4 above is equivalent to their equation (19) where the conjugate complex is omitted. This has no affect on their final conclusions, but there appears to be an error in their conclusions concerning the neglecting of $|\Delta\Gamma|^2$. Before it can be neglected (H) above must be satisfied rather than the condition $\Delta\Gamma \ll 1$ which they gave.

The derivation of 5.20 above is not given by Goldsborough and Mandel, nor are the conditions which have been assumed to hold in order to obtain this equation. It was quoted as (9) in

their paper. Their derivation of an expression for $\Delta\Gamma_1$ has been reconsidered by stressing different parameters so that an exact expression, equation 5.29, for P_m in terms of readily observable parameters of the spectrometer could be obtained. The derivation of 5.29 from 5.21 depends on (D) being true. Saturation of the transition and instrumental distortions which make it incorrect to apply 5.29 can be detected by subsidiary experiments and allowance made.

Goldsborough and Mandel made one assumption in deriving their equation (15) from their equation (9). This assumption is equivalent to (D), which can be complied with, so their equation (15) is justified. It is written out in terms of γ_2 and a constant which depends on the geometry of the cavity and the mode pattern in it. This expression can be used to describe a saturated line. Equation 5.29 above can be rewritten if necessary to give an expression in terms of γ_2 suitable for saturation measurements, but if it is so rewritten in order to evaluate H^2 a constant depending on the geometry of the cavity and mode pattern in it must be introduced. So, in order to use 5.29 two more conditions had to be placed on the spectrometer. It had to be designed and operated so that:-

γ_2 was not a function of H^2, (I)

and instrumental distortions were kept to a minimum. (J)

It is probably impossible to design an instrument which does not at some time violate these conditions, but it was quite

easy to make experimental checks to see if violations were occurring. See below in chapter six.

Misra has recently published a discussion and extension of Goldsborough and Mandel's work. He treated signal production in transmission and reflection cavity systems and he also considered briefly the sensitivity of these systems. The reflection system he considered was identical to that of figure 15 but the equivalent circuit he used for the cavity arm was a parallel resonant circuit. He obtained the reflection properties of the magic tee by considering the absolute voltages in the side arms of the tee, and then set out to evaluate $|\Delta\Gamma|$ by finding the expression for $|\Gamma_m|$. (The discussion here is in terms of the notation used in this paper.) The derivation was performed in terms of admittances which caused difficulties because the binomial expansion for index -1 has to be carried out several times, each time imposing a new condition on the final result. He eventually obtained a result similar to that obtained here and by Goldsborough and Mandel, but it seems to be rather fortuitous because his derivation of the reflection properties of a magic tee appears to be incorrect. This component forms the voltages in its E- and H-arms by adding the amplitude and phase of the voltages in the side arms, not their absolute magnitudes. This was done above and as a result it became necessary to find an expression for $Re\{\Delta\Gamma\}$, not $|\Delta\Gamma|$ as Misra did. This error probably also accounts for the difficulties Misra had in eliminating terms in γ_1. He was able to eliminate them in the expression for $|\Delta\Gamma|$, but when it became

necessary to show that if the signal depended on $|\Delta\Gamma|^2$ it contained the effects of γ_1, he had to reconsider his assumptions The approach used here avoids this difficulty. (E) is the condition for eliminating γ_1 from the expression for Γ_{m1}, and even when it is satisfied it can be seen that γ_1 occurs in the expression for $|\Delta\Gamma|^2$.

APPARATUS.

Figure 17 shows a block diagram of the spectrometer built to do the measurements. It operated at Q-band, the klystron producing about 10 mW at 34 to 35 kMc/sec. To reduce noise in the klystron output the heaters were driven from a battery. Frequencies were measured by means of a Midcentury Microwavegear wavemeter, type MC 22/2A. The power level was monitored by using a directive feed to tap off part of the power to a crystal, and it was adjusted by varying the calibrated attenuator. The iris in the sample arm was placed in the first waveguide junction at least 12 mm from the tee. As the samples were about 1 cm long their filling factor was approximately 10^{-2}. The cross-section of the samples, 0·280 in. by 0·140 in., was such that they were a close sliding fit into the guide. A G.E.C. crystal, type VX 3171, was used as the detector.

Three types of system were available after the detector crystal, a simple D.C. system with display of the lineshape on a pen recorder, a video system with display of the lineshape on an oscilloscope and a phase sensitive detection system with display of the derivative of the lineshape on a pen recorder.

KEY TO FIGURE 17.

A Cavity to help stabilise the klystron.

B Isolator.

C Sample.

D Short circuit.

E Secondary coils to make the field more homogeneous.

F Main modulation coils.

G Small modulation coils for the phase sensitive detector.

E/H E-H tuner.

W/M Wavemeter.

ATT Attenuator.

1, 2 and 3 Alternative routes for the signal.

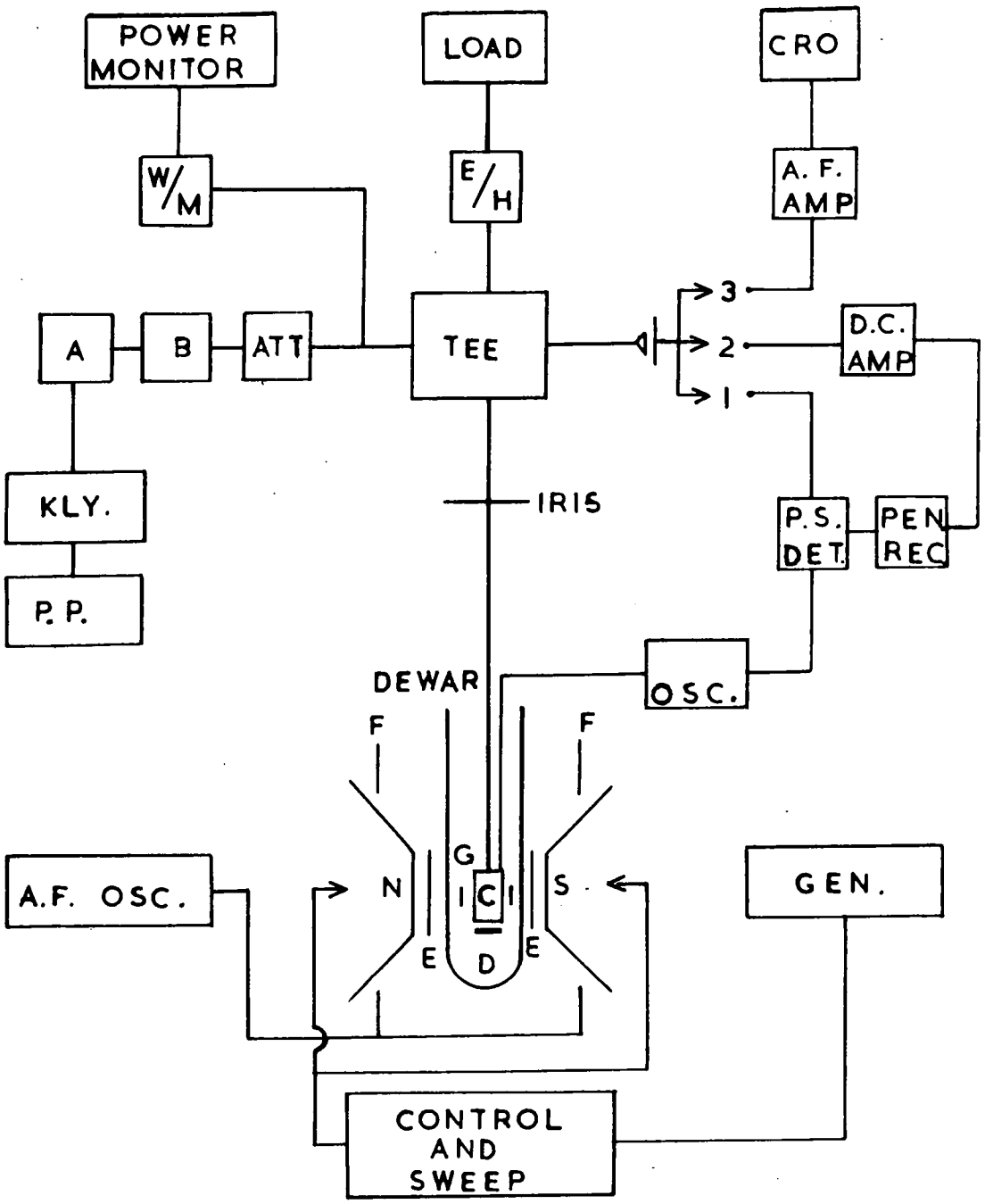

BLOCK DIAGRAM OF THE SPECTROMETER.

FIGURE 17

In the first system the current from the detector crystal was taken to a Solartron AA 900 D.C. amplifier and then to an Everett Edgcumbe pen recorder with an internal impedance of 7 ohms, a time constant for full scale deflection of 3 seconds, speeds of 1 or 6 in./minute and a full scale deflection of 5 mA. The output impedance of the amplifier was 1 ohm, so wire wound resistors with values varying between 22 and 128 ohms were placed in series with the recorder. All values below about 70 ohms increased the time constant of the recorder. The effect of this is discussed further below. In order to avoid saturation of the amplifier a backing off system was included between the detector crystal and the amplifier to reduce the steady D.C. current, produced by the crystal from the steady D.C. power level incident on it, to nearly zero. This backing off could be supplied either by the power monitoring crystal or a separate D.C. source.

The steady D.C. power level on the crystal meant that it was operating over a region of its characteristics which was neither linear nor square law. The current change due to resonance was so small, however, that the value of the gradient at the working point on the power versus current characteristic was taken as the value of β with no loss of accuracy. The input impedance of the amplifier was 3.10^5 ohms so the steady crystal current was about 5.10^{-7} amps while the change in current due to the signal was about 10^{-9} amps. The signal was produced by sweeping the magnet slowly through the value of magnetic field at which resonance occurred. In the video system the signal was produced

by modulating, at 30 c/sec, the main magnetic field about the value at which resonance occurred. This was done by feeding current from a power oscillator into the main modulation coils of the magnet, which provided amplitudes up to 100 oersteds at this frequency. From the detector crystal the current was passed through a wide band amplifier, bandwidth 0 to 40 kc/sec, and then displayed on an oscilloscope. This method was mainly used for rapid location of the lines, but some measurements were taken using it, see chapter six.

The phase sensitive system worked at 160 kc/sec. The main magnetic field was varied slowly through the resonance value as in the D.C. method, but it was also modulated at 160 kc/sec by means of a pair of small, subsidiary coils attached to the outside of the waveguide close to the position of the sample. From the detector crystal the signal was taken through the phase sensitive detector and then displayed on the pen recorder. In this case it was not necessary to use the wire wound resistors to avoid damping the recorder as the output impedance of the phase sensitive unit was large. In this system and the video system there was no need for a backing off circuit between the detector and the first amplifier unit. The output of the phase sensitive unit did possess a meter zero for backing off the signal to any required value at that stage.

The magnet was a Newport 8 inch Electromagnet type D which could produce 16000 oersteds over a 4·5 cm gap. The pole

pieces were coned down at an angle of 65° to a 3·5 in. diameter pole face. Originally the homogeneity of the field was only about one part in 500 so two small coils were designed to fit on the pole faces and produce a small field, about 10 oersteds, opposite to the main field and in this way reduce the field gradient across the gap. Each coil consisted of eight turns of copper wire, 21 S.W.G., wound on a tufnol former in a flat pancake of mean diameter (4·4 - 2d) cm, where d is the diameter of the wire. They were worked as a Helmholtz pair with current supplied by two 12 volt batteries through a rheostat. The maximum working current was 8 amps. It was found best to move the coils so that they were no longer opposite to each other. In their best position, found empirically, they improved the homogeneity at the centre of the gap to one part in 5000. The reduction in working space between the pole faces by 0·180 in. was rewarded by an increase in the homogeneity of the field.

The magnet was calibrated by a combined proton/lithium resonance magnetometer which allowed the field value to be measured at any setting of the current control unit to ± 1 oersted. A very useful facility of the current control unit was its ability to sweep the current of the main magnet coils through a range of values and over a range of times. With this facility the magnetic field was swept through the resonance lines at such a rate that they were traversed in a time at least ten times longer than the time constant of the recorder. Because it was possible to alter the field sweep rates easily this allowed

compensating changes to be made when the value of the line width changed or when the time constant of the recorder was changed by the alteration of the load resistors mentioned above. Long sweep times through the lines were required to overcome any smoothing of the line by the time constant of the recorder. A second check on this was to sweep through the line from both above and below.

Facilities for low temperature work were available. The system was a conventional cryostat for liquid helium work but as no helium temperature results are included here it will not be described further. The measurements were performed at liquid nitrogen temperatures with the liquid in the outer dewar and helium acting as a heat transfer gas in the interspace of the inner dewar and inside the inner dewar. The samples were placed in the guide, resting on a short circuit, which went into the tail of the inner dewar.

SENSITIVITY OF THE SPECTROMETER

The work was concerned with ruby samples containing about 10^{19} spins per sample and it was performed at Q-band and $77^{\circ}K$ where the magnetic susceptibilities were quite large. This meant that a strong signal could be expected.

The signal voltage across the recorder is given by

$$V_s = \frac{S \cdot R_i \cdot R_T \cdot g_2}{R_o + R_T + R_l} \qquad 5.32$$

where S is the signal due to the magnetic resonance, R_1 and R_o

are the input and output impedances of the amplifier, R_1 and R_r are the load and recorder impedances and g_2 the gain of the amplifier.

The calculation of the noise voltage is more complex as each system has its own noise sources. The calculation performed here is for the case of the simple D.C. system with no modulation as this is the noisiest system used. The other two systems were more sensitive.

A non-linear element cannot have a noise figure (Uhlir, 1963) so a noise temperature has to be defined for the detector crystal, as it was not operating over its linear region. Following closely the arguments of Torrey and Whitmer (1947a) the noise figure of the crystal and amplifier combined can be calculated. Let dN_o be the output noise power of a component, G its power gain, F its noise figure, df its bandwidth, T the absolute temperature, k Boltzmann's constant, t the noise temperature of the crystal, subscript 1 represent the crystal and subscript 2 the amplifier. Then for the two components in series

$$dN_{o(1+2)} = F_{1+2}\ G_{1+2}\ k\,T\,df. \qquad 5.33$$

At any one incident power P_i,

$$G_{1+2} = G_1(P_i).\ G_2. \qquad 5.34$$

For the crystal

$$dN_{o1} = t\,k\,T\,df. \qquad 5.35.$$

Considering the noise ouput through the system due to the crystal only

$$dN_{o'(1+2)} = G_2 t k T df \qquad 5.36$$

and similarly the noise output due to the amplifier only is

$$dN_{o''(1+2)} = F_2 G_2 k T df - G_2 k T df \qquad 5.37$$

where the second term is introduced in order not to include twice the Johnson noise of the output resistance of the crystal. Now

$$dN_{o(1+2)} = dN_{o'(1+2)} + dN_{o''(1+2)} \qquad 5.38$$

and substituting in 5.38 from 5.33, 5.34, 5.36 and 5.37 and simplifying gives

$$F_{1+2} = \frac{(t + F_2 - 1)}{G_1(\rho_i)} \qquad 5.39$$

which represents the noise figure for the combined system.

The effective noise figure is given by

$$F'_{1+2} = \frac{\int_0^\infty G_1(\rho_i).\, G_2.\, (t + F_2 - 1)/G_1(\rho_i).\, df}{\int_0^\infty G_1(\rho_i)\, G_2\, df} \qquad 5.40$$

where G_2 is now taken to be the gain of the amplifier - output meter combination so that the integrals converge. This combination had a bandwidth of 4.10^4 c/sec or 3.10^{-1} c/sec depending on condition (K) quoted below. Whichever value is chosen it is very much less than that of the crystal which is about 10^9 c/sec. Therefore it is possible to consider $G_1(P_i)$ and F_1 as constants over the range of the integration. Then

$$F'_{1+2} = \frac{(t + F_2 - 1)}{G_1(\rho_i)} \qquad 5.41$$

and the noise power output of the crystal and amplifier - meter

combination is given by

$$N_o' = G_2 k T df (t + F_2 - 1). \qquad 5.42$$

Even though a magic tee was used which helped reduce the noise in the waveguide, there was still some noise left which was incident on the crystal. If the noise figure representing the noise in the waveguide is F_g then the noise power N_o'' at the output of the crystal - amplifier - meter system due to the guide noise only is

$$N_o'' = F_g G_1(P_i). G_2 k T df. \qquad 5.43$$

From 5.42 and 5.43 the total noise power output N_o is

$$N_o = [G_2(t + F_2 - 1) + F_g G_1(P_i). G_2] k T df. \qquad 5.44$$

This noise power in the amplifier output produces a noise voltage, V_n, in the recorder and load impedances given by

$$V_n = (R_e + R_r) \sqrt{\left(\frac{N_o}{R_o + R_r + R_e} \right)}. \qquad 5.45$$

To this noise must be added the ndse voltage of the recorder and load impedances due to Johnson noise and given by

$$V_{re} = \sqrt{\{4 (R_r + R_e) k T df\}}. \qquad 5.46$$

The total noise voltage is the root of the sum of the squares of 5.45 and 5.46, therefore, the noise voltage across the recorder is

$$V_n = \sqrt{\left\{ \frac{N_o (R_r + R_e)^2}{R_o + R_r + R_e} + 4(R_r + R_e) k T df \right\}} \cdot \frac{R_r}{R_r + R_e}. \qquad 5.47$$

Feher gives the condition for distinguishing between the amplifier and recorder bandwidths for the value df. It

states that if the carrier voltage V at the output of the amplifier is large enough, then the amplifier bandwidth may be ignored with respect to the recorder bandwidth. In symbols the condition is

$$V^2 > \tfrac{1}{2} R_i 2k T_d F \qquad (K)$$

where dF is the amplifier bandwidth. (K) was satisfied in the measurements made, see chapter six, so the bandwidth of the recorder represented the bandwidth of the system.

The power monitor crystal when used to provide a backing off current also introduced noise, but it can be shown that this noise source can be neglected. The crystal introduced noise at the input of the amplifier due to its own noise and the noise present in the guide. The available noise power due to two sources in parallel can be calculated by following Torrey and Whitmer (1947b). If the dynamic resistance of a noise source in parallel with other noise sources is ρ_k and the noise power is P_k then the total available noise power of the sources in parallel is

$$P = \sum_k \frac{P_k}{\rho_k} \Big/ \left(4 \sum_k 1/\rho_k\right). \qquad 5.48$$

The impedances of the two crystals were equal but their noise powers were not,as one, the power monitor crystal,was used as a video detector, and the other was used to detect the signal. The noise produced by a video crystal is that due to the Johnson noise of the barrier impedance $\frac{1}{4}$ kTdf, where df is the bandwidth of the crystal (Torrey and Whitmer, 1947c). The noise from the

detector crystal is $4kTdf$, where t is the noise temperature of the crystal under its operating conditions. Thus the detector is t times noisier than the video crystal. The value of t for the crystals used was about 10^7, obtained from interpolation on a graph given by Uhlir. This meant that the detector crystal was much noisier than the other crystal and indeed it was much noisier than any of the other noise sources in the system, so 5.47 simplifies with the use of 5.44, to

$$V_n = R_t \sqrt{\left\{ \frac{G_2 . t k T df}{R_0 + R_t + R_l} \right\}} . \qquad 5.49$$

The ratio of the signal to noise voltage is

$$\frac{V_s}{V_n} = \frac{S . R_i . q_2}{\sqrt{\{ G_2 t k T df (R_0 + R_l + R_t) \}}} \qquad 5.50$$

which becomes

$$\frac{V_s}{V_n} = \frac{\beta (\Gamma_{01} - \Gamma_{el}) P_m . R_i . q_2}{2 \sqrt{\{ G_2 . t k T df (R_0 + R_t + R_l) \}}} \qquad 5.51$$

on using 5.30 and the definition of a in 5.29. Equating 5.51 to one and using 1.1 gives

$$\gamma_2 = \frac{4 \sqrt{\{ G_2 t k T df (R_0 + R_t + R_l) \}}}{\beta (\Gamma_{01} - \Gamma_{el}) \omega \mu_0 v H^2 R_i . q_2} . \qquad 5.52$$

Inserting suitable values into 5.52 gives the minimum value of γ_2 which could be detected, theoretically, by the equipment. This can be compared with the actual value of the susceptibility to obtain some idea of the signal to noise ratio. Details are given in chapter six.

THE EFFECT OF ERRORS IN THE MEASUREMENTS.

Detailed consideration of 5.29 showed that P and Γ_{01}

had little effect on the calculated value of P_m. This was confirmed by the experimental work carried out, see chapter six.

The analysis was carried out by means of the general formula for combining errors given by Topping (1958). Putting the approximate figures in the resulting expressions and assuming each measured quantity had 5% error gave a final error in the value of P_m of nearly 15% , but only 4% of this total error was contributed by the assumed errors in P and Γ_{01} . Thus for accurate quantitative values of P_m, S, β and $(\Gamma_{01} - \Gamma_{e1})$ had to be measured as accurately as possible. Further discussion of errors is postponed until chapter six.

DISCUSSION.

Feher has given an excellent discussion of noise in spectrometers. Besides one or two errors involving numerical constants in equations, he has made two errors in stating equations. He describes his equation (35) as being the noise power at the output of a microwave detector, but if this is the case it should not contain the noise figure of the amplifier, while if it is the output of the detector and amplifier it should contain the gain of the amplifier. Dividing both sides of this equation by kTdf gives the expression for the noise figure of the combined system of amplifier and detector. Later in the paper he compares the noise produced by a square law detection system with the signal produced by a linear detection system.

Torrey and Whitmer have discussed the noise figure of a detector crystal and amplifier combined. Strictly their arguments apply only to linear detection systems because non-linear systems cannot have a noise figure. However, the derivation given above in terms of the noise temperature does eventually reduce to the same answer.

Equation 5.48 above differs from the equation given by Torrey and Whitmer by a factor of $\frac{1}{2}$. This must be included because the theorem is for the available noise power from a set of noisy impedances in parallel. This power is at a maximum, given by one-quarter the power in the source output impedance, when the source output impedance equals the load impedance. This theorem was not used in the derivation of the noise figure for the combined amplifier-detector system because the available power present in different parts of the system was considered. Thus in 5.37 noise powers could be subtracted without reference to the dynamic impedances of the various components.

Goldsborough and Mandel did not consider the details of the sensitivity of their system. Misra, on the other hand, did consider the sensitivities of the transmission and reflection systems and concluded that the reflection system was five to ten times more sensitive than the transmission system.

Other workers have described spectrometers not using a conventional cavity. They include Ingram (1954) who described systems for work on gases, Schulz-du Bois (1959) who examined Cr^{3+} in beryl by placing the sample directly in the guide and

examining the transmitted signal, and Elliston et al. (1963) who used a magic tee system, different from the above, with a sample in a shorted guide.

CONCLUSIONS.

This discussion of a simple reflection spectrometer using a magic tee can be readily extended to cover more complicated magic tee systems. During the course of the discussion several conditions were stated, but it is only necessary to adhere to (A), (D) and (E). Of these three, (D) and (E) are easily satisfied when the filling factor is small, but (A) is more difficult to satisfy, although a small filling factor is a help towards satisfying it. The apparatus for the resonance work was described and an expression was derived for its signal to noise ratio.

CHAPTER SIX.

LINEWIDTH MEASUREMENTS.

Experimental technique; satisfaction of the conditions stated in chapter five; sensitivity of the spectrometer; results.

EXPERIMENTAL TECHNIQUE

The sample was placed on the short circuit terminating a length of thin walled copper-nickel guide. The guide was arranged so that it was vertical and the sample was in the centre of the magnet gap. With the small correction coils in use this was the most homogeneous region of the field. The dewars were then put in position and the system cooled down to liquid nitrogen temperatures.

The frequency of the power from the klystron was set so that the cavity was at the peak of a resonance and then the E-H tuner was adjusted so that the signal incident onto the detector crystal fell to zero. After this balancing the tuner was deliberately unbalanced in amplitude only, to give the largest signal possible. Measurements of Q_u, Q_L, Γ_{01}, the power incident onto the tee and the output power from the tee were made. A crystal previously calibrated against a power meter was used for the power measurements, and from these measurements $(\Gamma_{01} - \Gamma_{02})$ was calculated. The gradient of the crystal's current against power characteristic at the value of the output

power from the tee was taken as β .

The video system was used for rapid location of the transitions and also the adjustment of the magnet to the polar angle 90°. The $+\frac{1}{2}$ to +3/2 transition was the most convenient to use for this adjustment. At $\vartheta = 90°$, $dH/d\vartheta = 0$, where H is the value of the magnetic field at which the transition occurs and ϑ is the polar angle. By plotting H against the magnet setting around the position $\vartheta = 90°$, the magnet setting equivalent to $\vartheta = 90°$ was rapidly located to an accuracy of $\pm 1°$. Having located the transition at a known angle ϑ the line was recorded in one of three ways.

The D.C. technique required a backing off circuit to reduce the steady D.C. current produced by the steady power level incident onto the crystal to zero. This was to avoid overloading the amplifier. The signal amplified and displayed on the pen recorder was produced by the magnetic resonance. The magnetic field was swept through the line in about 70 seconds which was long compared to the time constant of the recorder, so there was very little distortion of the signal. A second check on this possible cause of distortion was to sweep the magnetic field both up and down through the line and observe the shapes produced. If no distortion was present the shapes were identical on both sweeps. Knowing the values of the various circuit components, the detector current could be calculated from the current recorded by the pen recorder. The full width

of the line at half the peak intensity, $\Delta H_{\frac{1}{2}}$, was calculated by measuring it in seconds from the pen recorder and using a calibration of the magnetic field sweep in oersteds/sec. This calibration was made using a proton/lithium magnetometer. Subsidiary experiments were performed to check the linearity of the sweep and the speed of the recorder. The first fifteen to twenty seconds of the sweep were non-linear, so care was taken to ensure that the passage through the line did not begin during this time. Another possible cause of distortion was saturation of the transition produced by too much power incident onto the sample. This was checked by varying the power level and repeating the sweep through the line. An increase in the size of the signal as the power was decreased would have signified that saturation was present. At the powers employed, about 10^{-3} watts, the transitions were not saturated. Figure 18 is an example of a line measured in this way.

Difficulties were encountered using the D.C. technique because of the poor frequency stability of the klystrons available and the backing off circuits used. A variation in the frequency caused a variation in the steady power level incident onto the crystal and after amplification this produced a large change in the baseline on the pen recorder. The current produced by the power monitor crystal could not follow these changes and so could not be used as a source of backing off current, nor could the separate backing off circuit

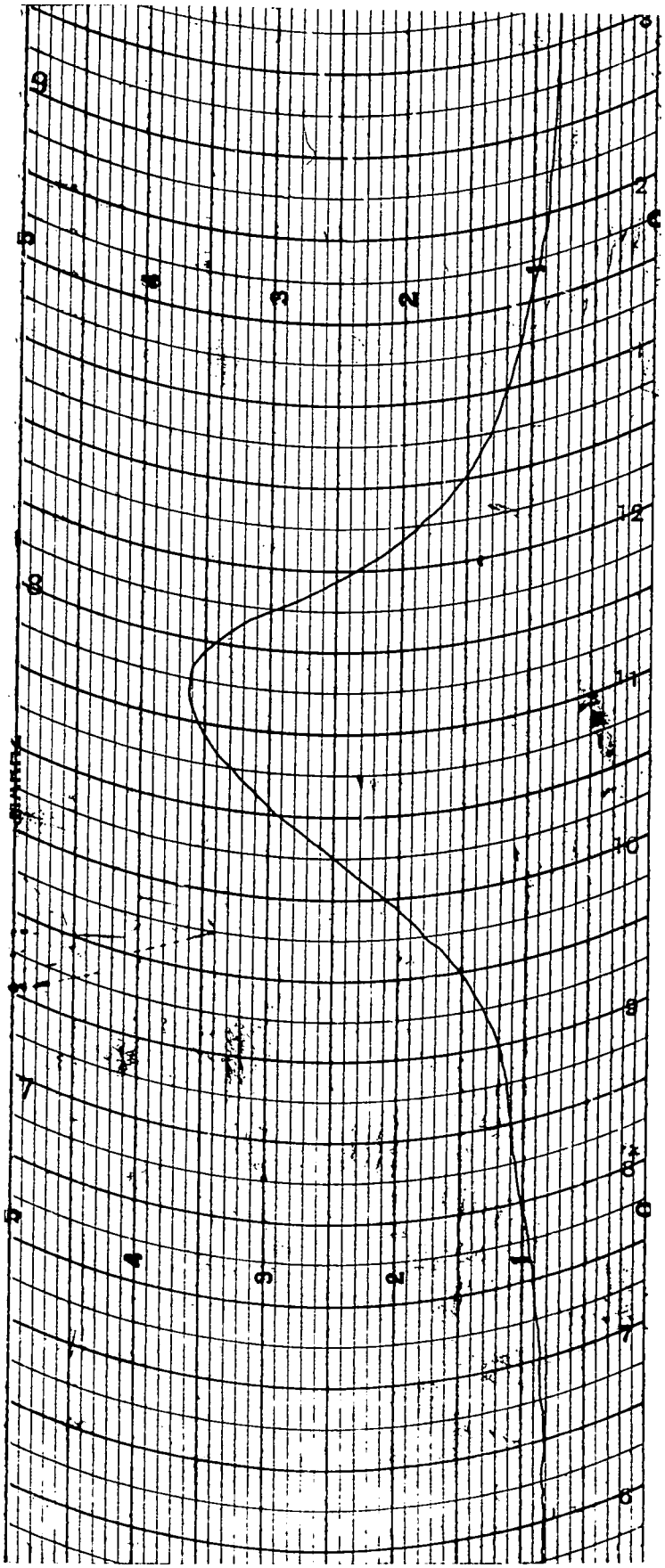

D.C. Chart

Figure 18.

which was used, follow the changes. The frequency changes also made it more difficult to obtain the correct line shape because they altered the balance of the tee.

The video system did not require a backing off circuit. Also, the lines were recorded photographically and the frequency changes were not rapid enough to affect the measurements once the balance had been obtained. The differences between this method and the D.C. method were the modulation of the magnetic field at 30 c/sec using separate modulation coils and the display of the line on an oscilloscope. The slow sweep was not used. An amplifier with a bandwidth of 40 kc/sec was used to amplify the signal. This bandwidth did not distort the signal. The amplitude of the magnetic field modulation was measured using the D.C. current equivalent to the peak A.C. current through the coils, and the proton/lithium magnetometer. During the analysis of the photographs to obtain the value of the linewidth, corrections had to be applied to allow for the non-linearity of the oscilloscope sweep and the uneven spacing of the lines on the trace. The length of the analysis, together with the fact that not enough power was available at 30 c/sec to sweep completely through some of the transitions which it was desired to examine, meant that this method was rarely used for measurements. The subsidiary coils which produced the modulation field had a similar diameter to the main coils, therefore, the variation in the field at the position of the

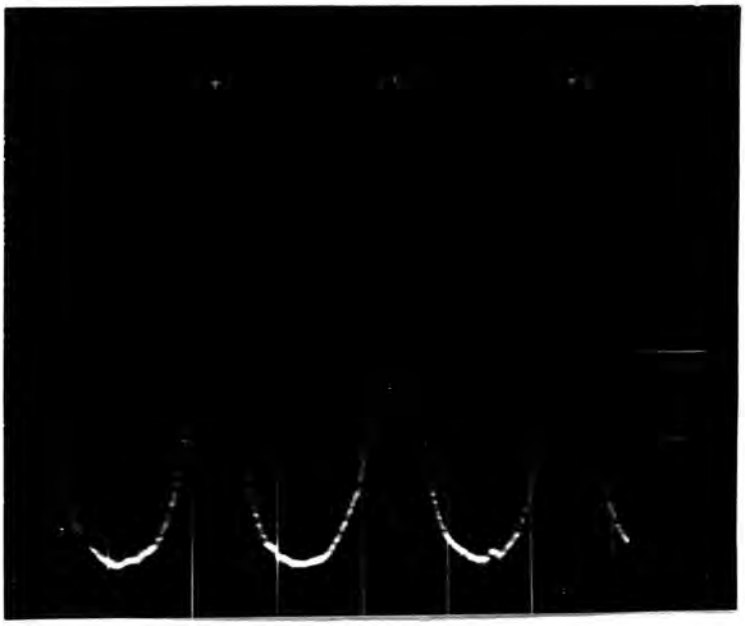

A TRANSITION RECORDED BY THE VIDEO SYSTEM

FIGURE 19.

the line had to be integrated numerically and the half height value located. The values in oersteds were obtained from the calibration against time of the field sweep. This method is the best of the three because it includes the tails of the lines. The other two methods tend to obscure them, and they are important for a full analysis of the line shape and its moments. An idea of the shape of the line observed can be obtained by comparing the values of $\Delta H_{\frac{1}{2}}$ and $\Delta H_{m.s.l.}$. Figure 20 shows an example of a transition recorded by the phase sensitive equipment.

The coils used to produce the 160 kc/sec modulation field were fitted onto the outside of the guide as it was not possible to insert them into the guide. The coils were formed into a low cone so that they fitted into the tail of the dewar. Their overall diameter was 1 cm. The samples were also 1 cm long, so the field produced by the coils was not uniform over them. A calculation of this field, assuming that the coils were plane, gave a value of about 5 oersteds at the centre of the sample. This calculation neglected the presence of the walls of the guide which would reduce the value of the field enormously. A reduction of up to 50% in the magnitude of the field probably occurred, and in this case the field in the sample would be reduced to 2.5 oersteds, and so the inhomogeneity of the modulation field across the sample could not be greater than this. The inhomogeneity

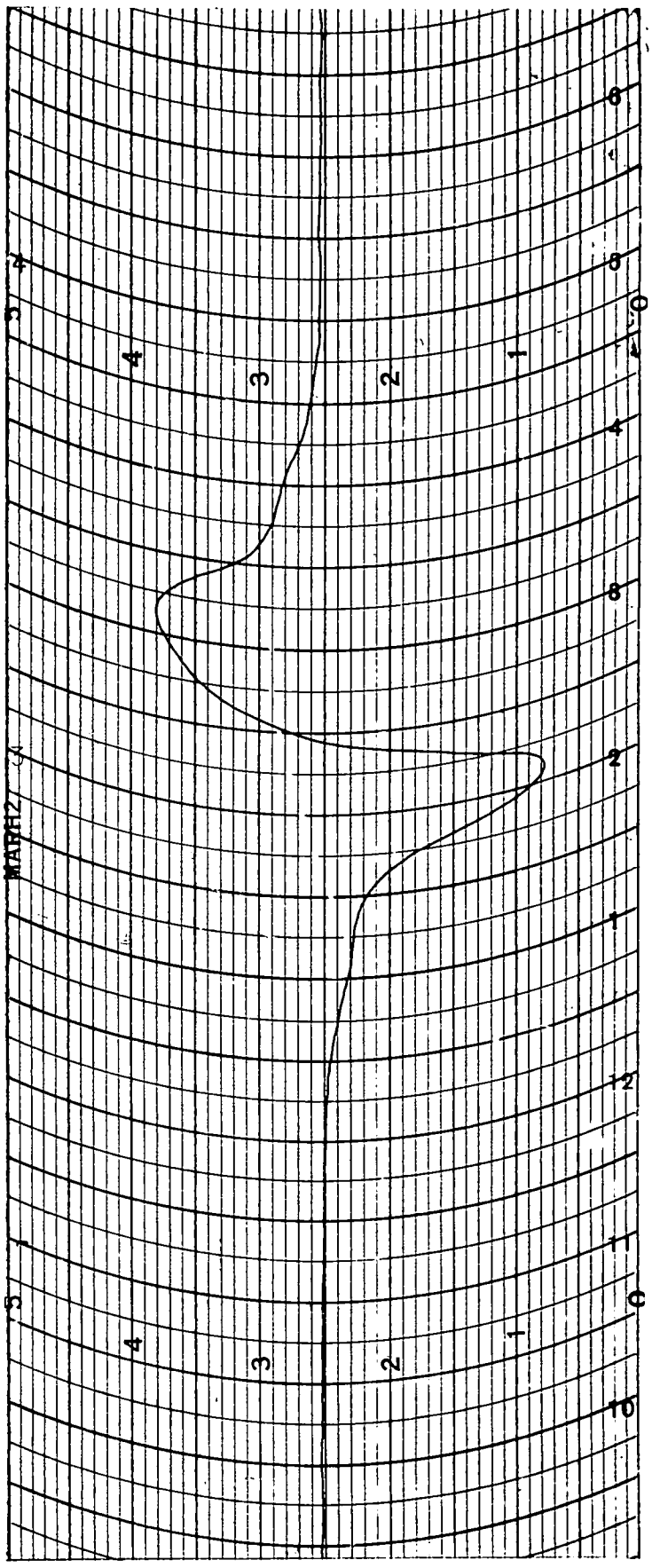

Phase Sensitive

Chart

Figure 20.

of the main field was about this value.

Flynn and Seymour (1960) described a method of correcting for any distortion introduced by the finite value of the amplitude of the modulation field. The larger this amplitude, the more necessary is the correction. In this case the amplitude was usually only 2% or 3% of the total linewidth suggesting that the cofrection was not necessary, and it was not applied to the measurements reported here. As a justification for this, one line was corrected. The correction was calculated twice using values of 1 oersted and 2 oersteds for the amplitude. The latter value gave the largest correction, but the ordinates were only altered by 1% or 2% which was less than their error anyway. This correction may be rather doubtful because it required a value of the field amplitude to apply it, and this was not known with certainty, nor was it constant over the specimen.

The phase sensitive detector unit had to be adjusted carefully to avoid introducing distortions into the line shape. It was most important to adjust the frequency of the modulation to be the same as the reference frequency. The particular equipment used also had facilities for altering the bandwidth and it was usually operated with a bandwidth of 100 c/sec.

An attempt was made to stabilise the output of the klystrons by placing a cavity with a large Q-factor at the output and so locking the frequency and power output. A

similar system was described by Richardson (1964). A wavemeter was used as the cavity because it could be adjusted to resonate whatever the frequency. The system improved the frequency stability, but it was difficult to adjust to one particular frequency because the two cavities interacted with one another in a complex fashion. A sequence of adjustments had to be made to obtain the correct frequency. Even with this system, the frequency drift was enough to cause difficulties in balancing the tee.

THE CONDITIONS OF CHAPTER FIVE.

In chapter five three conditions were put forward, (D), (E) and (H), which must be satisfied in order to eliminate γ_1 from the signal. A further condition, (G), was put forward which, if satisfied, meant that the signal was directly proportional to the power absorbed, as long as the apparatus was operated so that it did not violate conditions (I) and (J). The mode of operation which satisfies these last conditions has been described above. The other conditions are considered in the following numerical example.

The $+\frac{1}{2}$ to $+3/2$ transition in sample 337c at the polar angle 90° and at $77^{\circ}K$ was measured, using the D.C. technique. The half width was nearly 30 oersteds. The values of the various parameters of interest were (the symbols are those of chapter five), $\beta = 4{\cdot}6.10^{-2}$ amp watt^{-1},

$(\Gamma_{01} - \Gamma_{\theta 1}) = 0{\cdot}76$, $\Gamma_{01} = 0{\cdot}51$, $P = 6{\cdot}7.10^{-4}$ watts, $Q_u = 1900$, $Q_L = 1450$, $Q_e = 6100$, the peak value of the recorded current 2·8 ma, allowing for the networks of resistors and the gain of the amplifier, the detector current $S = 3{\cdot}4.10^{-8}$ amps, $\eta \simeq 10^{-2}$ and $\gamma_2 = 1{\cdot}3.10^{-4}$ erg gauss^{-2} cm^{-3}.

The value of γ_2 was estimated using the formula of Bleaney and Stevens (1953)

$$\gamma_2 = \frac{\pi \nu g^2 \beta^2 N [S(S+1) - M(M-1)] f(\nu)}{8 k T (2S+1)} \qquad 6.1$$

with $\nu = 3{\cdot}5.10^{10}$ c/sec, $g = 2$, $\beta = 9{\cdot}3.10^{-21}$ erg gauss^{-1}, $S = 3/2$, $M = 3/2$, $f(\nu) = 1/\Delta\nu$, where $\Delta\nu$ is half the width at half the peak intensity in c/sec, the total number of spins in the specimen $N = 1{\cdot}6.10^{19}$, $k = 1{\cdot}4.10^{-16}$ erg deg^{-1} and $T = 77^{\circ}$K. Using figure 2, estimates of the value of γ_1 and γ_2 at various positions on the resonance curve were made. From values of η and γ_2 a value of Q_m can be calculated since

$$Q_m = \frac{1 + 4\pi\eta\gamma_1}{4\pi\eta\gamma_2} \simeq \frac{1}{4\pi\eta\gamma_2} . \qquad 6.2$$

At the peak of the magnetic resonance, when $\gamma_1 = 0$, condition (H) is satisfied with the larger expression 133 times the smaller. At the peak of the γ_1 curve, when γ_1 is about $6{\cdot}5.10^{-5}$, the larger is 138 times the smaller, while at a point in the tails of both curves, when $\gamma_1 = 1{\cdot}6.10^{-5}$ and $\gamma_2 = 6{\cdot}5.10^{-6}$, the larger is 460 times the smaller. So for this transition condition (H) is satisfied at all parts of the

line. To satisfy (H) in any experimental arrangement, it is important to keep the value of $(\Gamma_{01} - \Gamma_{b1})$ as large as possible and the fraction Q_L/Q_m as small as possible. This fraction is small when η or γ_2 is small.

Condition (D) is satisfied as the expression $4\pi\eta\,|\gamma_1 - j\gamma_2|$ has the value $1{\cdot}6.10^{-5}$ at the peak of the magnetic resonance and this is much less than unity as is required.

Condition (E) is obviously satisfied at the peak of the magnetic resonance when $\gamma_1 = 0$. At the maximum value of γ_1 the larger expression is 3700 times the smaller so this condition is also easily satisfied.

Condition (G) is least likely to be satisfied at the peak of the magnetic resonance. In this example the larger value is 42 times the smaller at this point. Therefore it seems reasonable to take the signal as being directly proportional to the power absorbed. Another expression which can be examined to see if the proportionality is correct is $bS \ll a$, where a and b are defined in chapter five, equation 5.29. In this case at the peak value of the signal, a is 167 times bS. The difference between this and (G) may be because it was necessary to calculate a suitable value of Q_m which in turn depended on the calculation of a value of γ_2. If γ_2 had been calculated four times too large,

or η estimated four times too large, or there was inaccuracy in both, then (G) would reduce to the same values in the inequality. Decreasing the value of η or of γ_2 increases the ease with which the other conditions are satisfied.

Condition (K) is the condition which decides whether the bandwidth of the amplifier or of the recorder represents the bandwidth of the system. The larger value is $2{\cdot}3.10^{8}$ times the smaller when V = 0·21 volts, $k = 1{\cdot}4.10^{-23}$ joule deg^{-1}, T = 290°K, $g_2 = 20$, $R_i = 3.10^5$ ohms and the bandwidth of the amplifier $dF = 4.10^4$ c/sec. This means that the bandwidth of the recorder represents the bandwidth of the system. This example is for the components of the D.C. system.

SENSITIVITY OF THE SPECTROMETER:

Equation 5.52 gives the expression for the minimum value of γ_2 which theoretically can be detected by the simple D.C. system. Using the figures from the same transition as above, and the following values, R_o = 1 ohm, $R_i = 3.10^5$ ohms, R_1 = 68 ohms, R_r = 7 ohms, df = 0·3 c/sec, $\mu_o = 4\pi.10^{-7}$ henry m^{-1}, H = 1·24 amp m^{-1}, $v = 2{\cdot}53.10^{-7}$ m^3, $g_2 = 20$ $G_2 = (R_i/R_o)g_2^2 = 1{\cdot}6.10^6$ and $t = 5.10^7$, then $\gamma_2 = 2{\cdot}1.10^{-6}$ erg $gauss^{-2}$ cm^{-3}. This is 60 times smaller than the theoretically estimated value of γ_2 for the specimen. Therefore, the signal to noise ratio predicted theoretically is 60:1. Figure 18 shows that the observed value was about 250:1.

The discrepancy may be due to the values of H and t used in the calculation since these values had to be

estimated from other information. From equation 1.3, t is given approximately by A/f for small values of f. The value of f used here was estimated from a rough Fourier analysis of the line. The main part of the line was traversed in about 30 seconds so the main Fourier components had frequencies less than $3{\cdot}3.10^{-2}$ c/sec. Bell (1960) has stated that 1/f noise has been detected down to about 10^{-3} c/sec. Therefore, values of f about 10^{-2} c/sec could contribute to the noise in this case. The value of A was obtained by interpolation from a graph given by Uhlir at a bias of 1 μa. It was estimated as 5.10^{5} c/sec. The value of t obtained from these figures could be an order of magnitude out, so explaining some of the error between theory and experiment in the prediction of the signal to noise ratio.

H is the mean value of the amplitude of the magnetic field vector in the cavity. It was estimated by first evaluating the population difference, n, in the specimen under the steady state conditions with the signal incident. The evaluation was performed using

$$P_m = (n_0 - n) h\nu / 2T_1 \qquad 6.3$$

which was obtained by rearranging an equation given by Bloembergen et al. (1948). P_m is the power absorbed by magnetic resonance and is given by $P_m = S/a = 1{\cdot}93.10^{-6}$ watts, the thermal equilibrium population difference $n_o = 9{\cdot}3.10^{16}$,

the relaxation time $T_1 = 4{\cdot}4.10^{-5}$ sec, the frequency $\nu = 3{\cdot}5.10^{10}$ c/sec and Planck's constant $h = 6{\cdot}6.10^{-34}$ joule sec. The value of H which produces this difference of population n can be obtained from a rearrangement of a second equation given by Bloembergen et al. (1948)

$$\frac{n}{n_0} = \left[1 + \left(\frac{\pi g \beta}{h}\right)^2 H^2 T_1 T_2\right]^{-1} \qquad 6.4$$

where T_2 is the spin-spin relaxation time related to the half width at half the peak intensity Δf by $T_2 = 1/2\Delta f$. Any error in this value of H may help explain the observed difference between theory and experiment. It should be noted that 6.3 is based on a two level scheme which is not true in ruby.

The video system is more sensitive than the D.C. system because the modulation of the signal at 30 c/sec reduces the value of t. The phase sensitive system is more sensitive still, as the signal is modulated at 160 kc/sec and the value of t is reduced further.

RESULTS.

The results of the linewidth measurements are contained in figures 21 and 22, and table 6. Samples G2a and 337c were examined in detail and the results for $\Delta H_{\frac{1}{2}}$ of the major transition studied are shown in detail in figure 21. In figure 22 are the results of an examination of the $-\frac{1}{2}$ to $+3/2$ transitions in these samples. Table 6 contains

KEY TO FIGURE 21.

337c
+½to +3/2

337c
-3/2 to -½

G2a
-3/2 to -½

1
and
4 — 337c +½ to +3/2

2
and
5 — 337c -3/2 to -½

3
and
6 — G2a -3/2 to -½

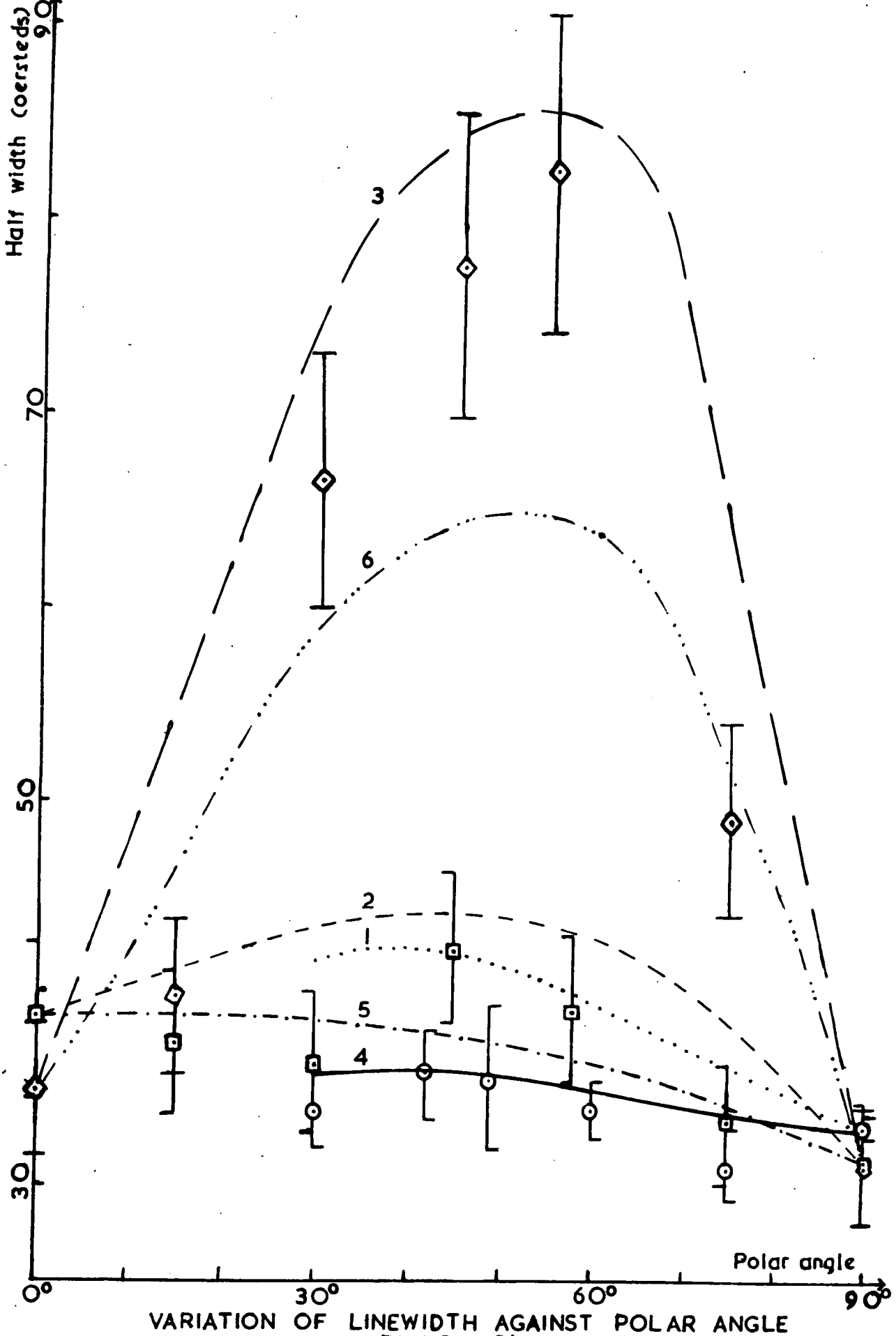

VARIATION OF LINEWIDTH AGAINST POLAR ANGLE
FIGURE 21

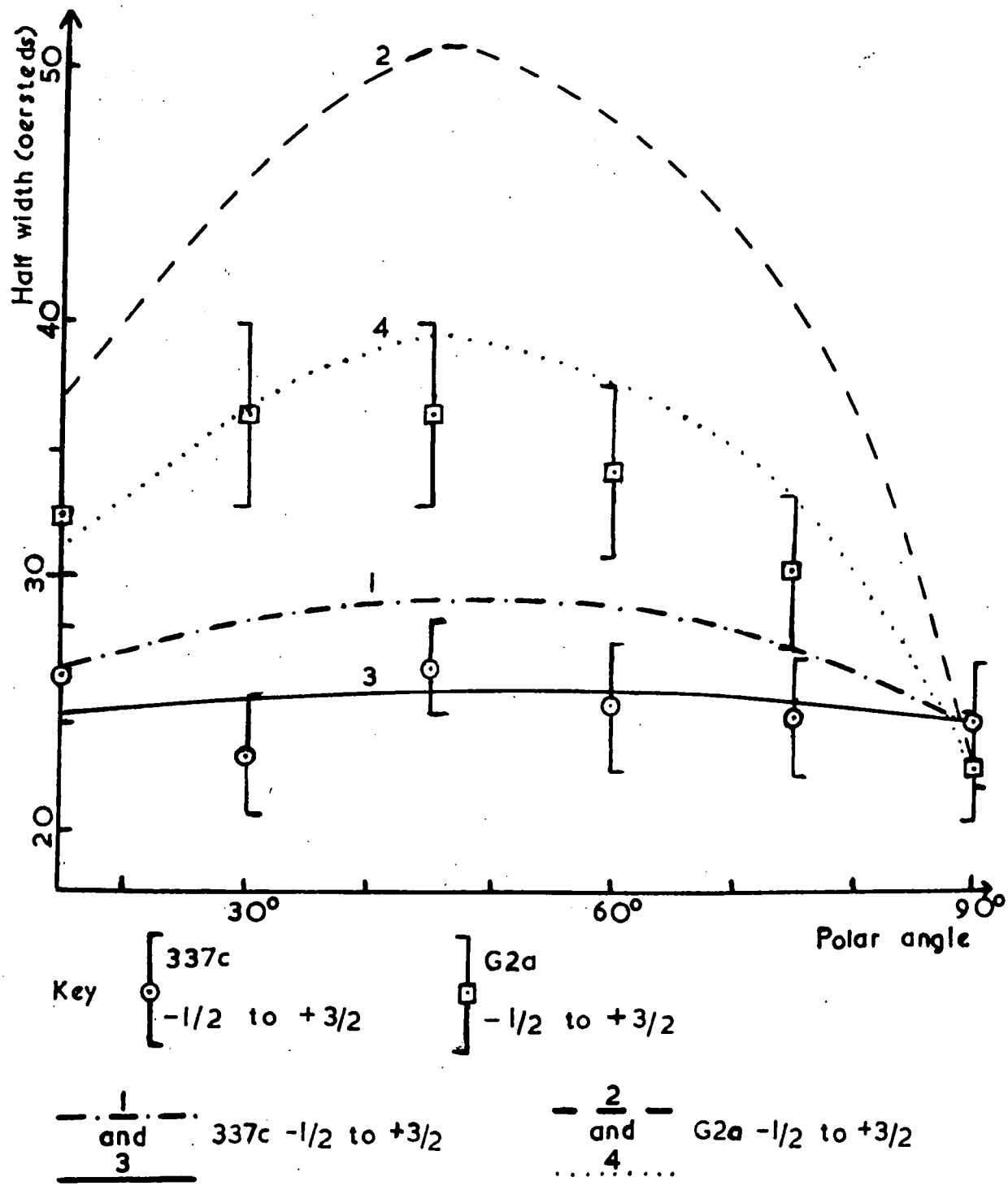

VARIATION OF LINEWIDTH AGAINST POLAR ANGLE

FIGURE 22

TABLE 6.

LINEWIDTH MEASUREMENTS.

Sample 337c.

Transition	$+\frac{1}{2}$ to $+3/2$		$-3/2$ to $-\frac{1}{2}$		$-\frac{1}{2}$ to $+3/2$	
Polar angle	$\Delta H_{m.s.l.}$	R	$\Delta H_{m.s.l.}$	R	$\Delta H_{m.s.l.}$	R
0°	-	-	-	-	-	-
15°	-	-	-	-	16·3	1·6
30°	26·4	1·3	-	-	17·1	1·35
42°	25·8	1·4	-	-	-	-
45°	-	-	31·8	1·35	18·9	1·4
49°	29·0	1·2	-	-	-	-
58°	-	-	23·9	1·65	-	-
60°	-	-	-	-	14·9	1·45
75°	-	-	28·9	1·15	16·9	1·45
90°	26·4	1·25	21·3	1·45	17·5	1·35

Transition	$-\frac{1}{2}$ to $+\frac{1}{2}$		
Polar angle	$\Delta H_{\frac{1}{2}}$	$\Delta H_{m.s.l.}$	R
0°	33·0	24·1	1·35
55°	28·9	19·6	1·45

Sample G2a

Transition	$-3/2$ to $-\frac{1}{2}$		$-\frac{1}{2}$ to $+3/2$	
Polar angle	$\Delta H_{m.s.l.}$	R	$\Delta H_{m.s.l.}$	R
0°	23·0	1·5	-	-
15°	28·6	1·4	23·1	1·4
30°	46·1	1·45	29·1	1·25
45°	61·0	1·25	29·0	1·25
55°	84·0	1·0	-	-
60°	-	-	28·8	1·2
75°	31·9	1·55	24·0	1·25
90°	28·0	1·1	17·8	1·25

Transition	$-\frac{1}{2}$ to $+\frac{1}{2}$		
Polar angle	$\Delta H_{\frac{1}{2}}$	$\Delta H_{m.s.l.}$	R
0°	24·4	21·6	1·15
55°	29·2	19·8	1·5

R is the ratio ΔH / $\Delta H_{m.s.l.}$ For a Gaussian line R = 1·175, for a Lorentzian line R = 1·734.

the values of $\Delta H_{m.s.l.}$ which were measured, the ratio $\Delta H^{\frac{1}{2}} / \Delta H_{m.s.l.}$ and the values of $\Delta H^{\frac{1}{2}}$ for the $-\frac{1}{2}$ to $+\frac{1}{2}$ transition at polar angles 0° and 55°. The results are discussed in chapter seven. Both samples were grown in the 0° growth orientation, but 337c had been annealed at 1930°c while G2a had been annealed at 1700°c.

The errors in $\Delta H^{\frac{1}{2}}$ and $\Delta H_{m.s.l.}$ measured by the phase sensitive equipment are $\pm$ 10%. This means that the error in the ratio is $\pm$ 14%. The major source of this error is the calibration of the magnetic field sweep against time. The error introduced when locating the half height and measuring the width in seconds at this height is much less than this. The measurements made by the video system are also accurate to $\pm$ 10%, but the error in the D.C. measurements was better than this. Because some transitions were measured more than once, a better estimate of the error in the final value of the width could be made. An indication of the error in each value is given on the graphs. The most accurate value was for the transition used as the example in the two sections above. This transition was measured seven times and the final error was $\pm$ 1·7%. Only one of the seven measurements was used in the numerical example given above.

CHAPTER SEVEN

DISCUSSION OF THE LINEWIDTH RESULTS.

Description of the results; comparison with results of other workers; correlation with crystal imperfections; predictions of chromium concentration; conclusions.

DESCRIPTION OF THE RESULTS.

Values of $\Delta H_{\frac{1}{2}}$ for the -3/2 to $-\frac{1}{2}$ transition were measured at several different polar angles from 0° to 90° in samples 337c and G2a. The $+\frac{1}{2}$ to +3/2 transition was examined at several angles between 30° and 90° in 337c. The results are in figure 21. It was not possible to measure this transition at lower angles than 30° because the magnetic fields required were beyond the working range of the magnet. All the transitions followed the same general form in their variation against angle. The value of the linewidth, in oersteds, was in the lower thirties at 90°, rose to a maximum value, which depended on the transition and the sample, around 45° to 55°, and then decreased again. For the -3/2 to $-\frac{1}{2}$ transition the value of the linewidth at 0° was in the upper thirties. In sample 337c the width of the -3/2 to $-\frac{1}{2}$ transition showed a local minimum at 30° and the $+\frac{1}{2}$ to + 3/2 transition had a minimum at 75°.

$\Delta H_{m.s.l.}$ was not measured at every polar angle

for these two transitions. In some cases it was difficult to measure $\Delta H_{m.s.l.}$ because the maximum slope of the line did not occur at one precise value but over a region of several oersteds. Then the mean position of the maximum slope was used in the calculation of $\Delta H_{m.s.l.}$. Any doubt in the value of $\Delta H_{m.s.l.}$ was reflected in the value of R, the parameter which gives some indication of the shape of the line. In sample 337c the few values of $\Delta H_{m.s.l.}$ which were examined showed broadening as the polar angle was altered towards 45°. The values of R which were evaluated were closer to the value for a Gaussian line than to the value for a Lorentzian line. The -3/2 to $-\frac{1}{2}$ transition in G2a showed a definite increase in $\Delta H_{m.s.l.}$ towards 55°. It also showed a wide range of values of the shape factor R. This may be because the line deviated from being a smooth, nearly symmetrical, curve to having definite asymmetry at certain polar angles. This asymmetry was most noticeable at the 45°, 55° and 75° polar angles. The transitions at each of these angles had a hump on the high magnetic field side.

The four values of $\Delta H_{\frac{1}{2}}$ for the $-\frac{1}{2}$ to $+\frac{1}{2}$ transition which were measured are in table 6. This transition was measured at 0° and 55° in the two samples. In 337c the linewidth at 55° was less than at 0°, while in

the other sample the 55° value was larger than the 0° value. The shape of the line in both samples at 55° was nearer Lorentzian than Gaussian, but at 0° it was nearer Gaussian than Lorentzian. The $-\frac{1}{2}$ to $+\frac{1}{2}$ transition at 0° was narrower in G2a than in 337c, and in both samples this transition was narrower than the -3/2 to $-\frac{1}{2}$ transition at that angle.

The $-\frac{1}{2}$ to +3/2 transition was examined in both samples. The results are in figure 22. $\Delta H_{\frac{1}{2}}$ was about 22 oersteds in both samples at 90° and broadened to a maximum in the region of 45° to 30°, the value of the maximum depending on the sample. The transition probability for this transition at 0° is zero, so it was not possible to examine the line at this angle. In 337c the linewidth at 30° has a local minimum. The width between maximum slopes had a similar variation with polar angle. At all the values of the polar angle, the line in G2a was nearer to a Gaussian shape than the equivalent line in 337c.

COMPARISON WITH OTHER WORK.

Manenkov and Fedorov (1960) performed some linewidth measurements on ruby at 77°K and X-band frequencies. They examined the $-\frac{1}{2}$ to $+\frac{1}{2}$ and the $+\frac{1}{2}$ to +3/2 transitions at a polar angle of 0° in several samples with different chromium concentrations. They established that the half width of the latter transition was from 1·3 to 1·5 times the half width

of the former. In 337c this ratio was 1·2 and in G2a it was 1·4. Their results showed that the $+\frac{1}{2}$ to +3/2 transition was marginally closer to a Lorentzian shape than the $-\frac{1}{2}$ to $+\frac{1}{2}$ transition and that as the concentration increased both lines tended towards a Lorentzian shape. At very low concentrations the widths tended towards constant values and the lines were almost Gaussian in shape. The G2a results agree with these conclusions of Manenkov and Fedorov. The $-\frac{1}{2}$ to $+\frac{1}{2}$ transition is nearly Gaussian and the $+\frac{1}{2}$ to +3/2 transition is nearly Lorentzian, which is equivalent to the above conclusions for the higher concentration samples.

Altshuler and Mineeva (1963), from theoretical considerations, stated that the lineshape should be close to a Lorentzian shape and that the $-\frac{1}{2}$ to $+\frac{1}{2}$ transition should be wider at 0^{o} than at 55^{o}. More detailed consideration will be given to this later when the concentration of chromium is considered.

Manenkov et al. (1963) reported measurements which revealed broadening from 4 to 25 oersteds produced by non-uniformity of the crystalline field which in turn is produced by strain in the lattice. The ratio of the linewidth of the $+\frac{1}{2}$ to +3/2 and $-\frac{1}{2}$ to $+\frac{1}{2}$ transitions deviated from 1·3 for lines broadened by this mechanism. This ratio was close to 1·3 in the samples investigated here, so the effects of non-uniformity of the crystalline field were absent from the

samples.

CRYSTAL IMPERFECTIONS AND LINEWIDTHS.

Equation 4.3 is a relation between the spread in directions of the c-axis, $\Delta\theta$, and the extra broadening of the line produced by this spread in c-axis directions. The physical imperfections in the samples produce the spread as shown in figure 11. In order to establish which parameter from the X-ray results was most suitable for use as $\Delta\theta$, estimates of the broadening produced by nine possible parameters were made. The parameters used were the mean value of the c-axis misorientation in the sample, the standard deviation of the values of the c-axis misorientation σ_a, $\sqrt{2}.\sigma_a$, a parameter related to the constant of a Gaussian distribution, the mean value of the mosaic misorientation, its standard deviation σ_b, $\sqrt{2}.\sigma_b$, the mean of the combined c-axis and mosaic misorientation, the standard deviation of the combined misorientations σ_c and $\sqrt{2}.\sigma_c$. The values of these parameters for the two samples are listed in table 7 together with the predicted broadening of the -3/2 to $-\frac{1}{2}$ transition at 45°. When the values for $\Delta\theta$ were calculated, some extra X-ray results were used which are not recorded in table 5. In order to make the predictions, values of $dH/d\theta$ had to be used. They were obtained from graphs, which were constructed from experimental results, of magnetic field for resonance against polar angle and are listed in table 8.

TABLE 7.

PREDICTIONS OF LINEWIDTH BROADENING.

$-3/2$ to $-\frac{1}{2}$ transition at the polar angle 45°.

$\Delta\Theta$ parameter	Sample 337c $\Delta\Theta$ radians	Sample 337c broadening oersteds	Sample G2a $\Delta\Theta$ radians	Sample G2a broadening oersteds
c-axis misorien.				
mean	0·0127	77·5	0·0119	72·6
σ_c	0·0063	38·4	0·0054	32·9
$\sigma_c\sqrt{2}$	0·0089	54·3	0·0076	46·5
mosaic misorien.				
mean	0·0015	9·2	0·0084	51·2
σ_b	0·0041	25·0	0·0052	31·7
$\sigma_b\sqrt{2}$	0·0058	35·4	0·0074	44·8
c-axis and mosaic misorien.				
mean	0·0067	40·9	0·01	61·0
σ_c	0·0077	47·0	0·0056	34·2
$\sigma_c\sqrt{2}$	0·0109	66·5	0·0079	48·4

σ standard deviation, $\sigma\sqrt{2}$ a constant related to a Gaussian distribution.

TABLE 8.

VALUES OF $dH/d\theta$.

Polar angle	$dH/d\theta$ (oersteds/radian) Transition			
	$-3/2$ to $-\frac{1}{2}$	$+\frac{1}{2}$ to $+3/2$	$-\frac{1}{2}$ to $+\frac{1}{2}$	$-\frac{1}{2}$ to $+3/2$
0°	0	0	0	0
15°	$2{\cdot}4.10^3$	-	-	$-1{\cdot}8.10^3$
30°	$5{\cdot}0.10^3$	$-5{\cdot}9.10^3$	-	$-2{\cdot}8.10^3$
45°	$6{\cdot}1.10^3$	$-6{\cdot}2.10^3$	-	$-3{\cdot}4.10^3$
55°	$6{\cdot}3.10^3$	$-4{\cdot}8.10^3$	$-8{\cdot}7.10^2$	-
60°	$6{\cdot}3.10^3$	$-4{\cdot}4.10^3$	-	$-3{\cdot}0.10^3$
75°	$3{\cdot}8.10^3$	$-2{\cdot}1.10^3$	-	$-2{\cdot}2.10^3$
90°	0	0	0	0

The predicted values of the extra broadening ΔH were compared with the experimental values. In obtaining the experimental values an assumption had to be made concerning the basic linewidth at the polar angle 45°. This is discussed further, below. The measured values of ΔH are $(44{\cdot}6 \pm 8{\cdot}5)$ oersteds for G2a and $(7{\cdot}4 \pm 5{\cdot}5)$ oersteds for 337c. Comparison with table 7 shows that the mean of the mosaic misorientation is the most suitable parameter for $\Delta\Theta$.

In figure 21 the curves numbered 1,2 and 3 are predictions of the linewidth of the transitions using the mean mosaic misorientation and values from table 8 in 4.3, and adding the values onto a suitable basic width. The curves 1 and 2 in figure 22 are similar predictions for the $-\frac{1}{2}$ to $+3/2$ transition. The assumption was made that the basic linewidth at any angle, that is the width in a sample which did not show mosaic broadening, could be obtained by interpolation from the known values at 0° and 90°. The widths at 0° and 90° did not contain any broadening caused by physical imperfections because $dH/d\Theta = 0$ at these angles. If both widths were known, the basic width at any intermediate angle was estimated by simple proportion from these values. For those transitions which did not have a value of linewidth at 0°, the value at 90° was used as the basic linewidth for all the other polar angles. The predictions are overestimates of the measured values. That for the $+\frac{1}{2}$ to $+3/2$ transition is the most inaccurate while those for the $-3/2$ to $-\frac{1}{2}$ transitions

are the best fits. The $-\frac{1}{2}$ to $+3/2$ transition in both samples is overestimated by about two times.

The maximum value of the linewidth in G2a for the $-3/2$ to $-\frac{1}{2}$ transition occurs in the region of the maximum value of $dH/d\Theta$, that is near to 55°. For 337c, which has a smaller value of $\Delta\Theta$, the decrease in the basic linewidth between 45° and 55° is larger than the difference in values of ΔH at these two angles, so the maximum occurs at 45° in this case. For the other two transitions considered in detail, the maximum value of $dH/d\Theta$ occurs at 45°, so the maximum broadening occurs at this angle also. Even so, the maximum linewidth may occur at another angle in samples with small values of $\Delta\Theta$, when the assumed basic width varies from angle to angle.

In G2a the distortion of the lines at 45° and higher angles in the $-3/2$ to $-\frac{1}{2}$ transition is related to the physical imperfections in the sample and the asymmetry in the values of $dH/d\Theta$. The gradient is larger at most angles above 45° than for angles below 45°. The values of $dH/d\Theta$ for the $+\frac{1}{2}$ to $+3/2$ transition are less, in most cases, than the values for the $-3/2$ to $-\frac{1}{2}$ transition at the same value of polar angle, so the former does not broaden as much as the latter in any one sample.

The differences in shape of the $-\frac{1}{2}$ to $+3/2$ transition in the two samples lend support to the relation

between the extra broadening in the line and the mosaic structure of the samples. The more perfect sample produced a line tending towards Lorentzian in shape. G2a, on the other hand produced a line tending towards a Gaussian shape. This would be expected if the second sample consisted of a large number of blocks, each one misorientated with respect to its neighbour in a random fashion so that the local fields at the sites of the chromium in each block also varied in a random fashion. A variation of static local fields of this type produces a Gaussian line shape. This is what was observed in the more imperfect of the two samples.

From the experimental values of ΔH, obtained using the same assumption concerning the basic widths as above, several values of $\Delta\theta$ for each sample were calculated. For G2a, from ten values, $\Delta\theta = 5{\cdot}1.10^{-3}$ radians, for 33%c, from nine values, $\Delta\theta = 4{\cdot}6.10^{-4}$ radians. Using these values the linewidths of the transitions were predicted again and they are plotted as curves 4,5 and 6 on figure 21 and curves 3 and 4 on figure 22. The predictions are now a better fit to the experimental results. The only major deviation is in the -3/2 to $-\frac{1}{2}$ transition in G2a which is now underestimated at the central values of the polar angle. Even in this case the values are not as far out of agreement as may appear from a cursory examination of the graph. The measured value

of ΔH is $(44{\cdot}6 \pm 8{\cdot}5)$ oersteds at the polar angle 45° and the predicted value is 31 oersteds, so the difference is about 1·5 times.

The $-\frac{1}{2}$ to $+\frac{1}{2}$ transition in G2a shows broadening caused by mosaic structure because $dH/d\vartheta$ is not exactly zero and $\Delta\vartheta$ is large. For more perfect samples such as 337c, the broadening from this source is very small.

The agreement between the second set of predicted linewidths and the measured values cannot be taken as a justification of the assumptions about the basic linewidth at polar angles away from 0° and 90° because the parameter used to make the predictions was based on this assumption. This lack of support for the assumption does not invalidate the conclusion concerning the use of the mean of the mosaic misorientation as the parameter $\Delta\vartheta$ since the other parameters suggested could not be made to fit the results. In order to estimate the true value of the basic linewidth at any angle, measurements must be made on a perfect sample, or perhaps a detailed theoretical prediction of the linewidth at the various angles could be made as Altshuler and Mineeva have done for the $-\frac{1}{2}$ to $+\frac{1}{2}$ transition at 0° and 55°, and the $+\frac{1}{2}$ to +3/2 transition at 0°. Their predictions for the $-\frac{1}{2}$ to $+\frac{1}{2}$ transition indicate that the basic linewidth increases 1·8 times from 55° to 0°. This predicted variation was not in fact observed, see below for

further details, but the experimental work and the theoretical work both indicated that the basic linewidth could vary with angle for one transition and this variation is not necessarily in the simple way assumed above. Working backwards from the measured linewidths, the basic linewidths were predicted using the X-ray values for $\Delta\theta$. Their values are in table 9.

The values of $\Delta\theta$ obtained from the X-ray and linewidth measurements are in reasonable agreement. The X-ray values were obtained from eight exposures which examined about one-twentieth of the area of the (0001) and the (000$\bar{1}$) faces. The linewidth values were obtained from measurements which included the whole of the sample, but their accuracy may be marred by the assumption of a basic linewidth made above.

CHROMIUM CONCENTRATIONS.

The predictions of linewidth mentioned above, which were made by Altshuler and Mineeva (1963), were based on the assumption that the major contribution to the linewidth was the exchange interaction. The prediction for the $-\frac{1}{2}$ to $+\frac{1}{2}$ transition at 0° agrees with experiment over a certain concentration interval. Theory and experiment only agree for this transition at 55° if the linewidth produced by hyperfine interactions is subtracted from the measured linewidth. The prediction for the $+\frac{1}{2}$ to $+3/2$ transition at 0° does not agree with experiment and this is thought to be due to lattice defects and other sources of broadening making a major contribution to

TABLE 9.

PREDICTIONS OF THE BASIC LINEWIDTH.

Sample 337c.

Polar angle	Basic linewidth (oersteds) Transition $-3/2$ to $-\frac{1}{2}$	$+\frac{1}{2}$ to $+3/2$	$-\frac{1}{2}$ to $+\frac{1}{2}$	$-\frac{1}{2}$ to $3/2$
0°	38·6	-	32·0	-
15°	33·9	-	-	23·4
30°	28·9	24·9	-	18·8
45°	33·0	-	-	21·3
55°	-	-	27·6	-
58°	29·6	-	-	-
60°	-	27·3	-	20·3
75°	27·6	28·3	-	21·0
90°	31·1	33·0	-	24·0
Sample G2a.				
0°	35·0	-	24·4	-
15°	19·6	-	-	17·3
30°	24·6	-	-	12·8
45°	26·4	-	-	7·7
55°	29·5	-	21·9	-
60°	-	-	-	8·8
75°	17·1	-	-	11·5
90°	31·0	-	-	22.2

the line.

The interesting results from the work of Altshuler and Mineeva are the relations between the linewidth, in c/sec, and the chromium concentration f, defined as the ratio of the number of chromium ions to the number of aluminium ions, for the $-\frac{1}{2}$ to $+\frac{1}{2}$ transition at the polar angles 0° and 55°. They are

$$\begin{aligned} \theta &= 0^{\circ}, \qquad \Delta\nu_{\frac{1}{2}} = 4.10^{10} f. \\ \theta &= 55^{\circ}, \qquad \Delta\nu_{\frac{1}{2}} = 2{\cdot}2.10^{10} f. \end{aligned} \qquad 7.1$$

At 55° the widths of this transition in both samples are about 30 oersteds, so a first estimate of the concentration in both samples is about 0·4 weight per cent. This figure is in the region where the theoretical predictions are reasonable. The refined estimates are in table 10. In this table allowance was made for the effects of mosaic structure and hyperfine interactions on the linewidth at 55°. The concentration in 337c predicted from 7.1 is five times the concentration estimated chemically and in G2a it is from six to nine times the chemical concentration. The estimates of the concentration made chemically can be regarded as a mean for the sample. The values in table 10 are at the lower end of the concentration region over which Altshuler and Mineeva established that their predictions were reasonable. It is thought that the larger values of concentration represent the congregation of chromium in the grain boundaries and dislocations, Thorp et al.

(1964). In this paper the authors reported variations in concentration of up to sixty times, and the positions with the higher concentrations were correlated with the regions of distorted material containing grain boundaries and large numbers of dislocations. The highest concentration reported was 2 %, therefore, the values obtained here are not unreasonable.

Klyshko (1964) has also made predictions relating the chromium concentration to the root mean square linewidth. His predictions are only for the $-\frac{1}{2}$ to $+\frac{1}{2}$ transition at 0°. Using the value of the linewidth at this angle, and the value of the local concentration estimated from the linewidth, the mean spacing of the chromium ions can be estimated from the table given in Klyshko's paper. The values obtained from the results of this work are not in this table, so the best estimate is that the mean spacing is greater than 7·27 angstrom units with the spacing in G2a greater than the spacing in 337c.

As a check to see whether the estimated concentrations in table 10 are the concentrations in the distorted material of the samples, two estimates were made of the volume of distorted material. From the estimated value of the concentration the number of chromium ions in the distorted material was calculated and compared to the total number of chromium ions in the specimen obtained from the

ERRATA

Page 102, line 9, for 10^{15}_{20} read 10^{13}_{18}.
Page 102, line 22, for 10^{20} read 10^{18}.
Page 102, line 22, et seq., delete from the new sentence on this line until the end of the paragraph, page 103, line 4, and substitute, "This is the same order as the number of chromium ions known to be in the sample, so it appears that a large proportion of the chromium ions congregate in the distorted region associated with the dislocations. This supports the evidence in the paper by Thorp et al. It is difficult to make a better estimate of the distorted volumes in the samples."

chemical concentrations. The first calculation was based on an estimate of the number of dislocations in a sample and the volume of distorted material associated with each dislocation. Most of the dislocations in each sample belong to the basal slip system which has about 3.10^{6} dislocations per cm^2. Assuming the dislocations pass through the specimen and that they distort the material in a radius of 15 angstrom units around their path, the volume of distorted material is about 6.10^{-8} cm^3. This volume contains about 10^{15} chromium ions. The spectrometer would have had difficulty in detecting this number of spins. Also it is the same order as the number of spins which in a random distribution of chromium ions would occupy sites some eight angstrom units apart. If the estimated volume of distorted material is correct, these figures seem to indicate that the collection of chromium ions in the grain boundaries has little influence on the linewidth. However, the volume may have been underestimated. The second attempt to evaluate it was based on the observed area of grain boundaries revealed by the etching on the surface of the material. This area was assumed to pass right through the specimen. The volume estimated in this fashion was 10^{-2} cm^3 which would contain 10^{20} chromium ions. This is larger than the number of chromium ions known to be in the sample, so in this case the volume of distorted material seems to have been overestimated.

The evidence in the paper by Thorp et el. pointed towards the chromium ions congregating in the dislocations, so the true volume of distorted material is probably between the two estimates.

Altshuler and Mineeva assumed a Lorentzian shape for the line when they gave the relationship between the half width and the chromium concentration. The results given here for the $-\frac{1}{2}$ to $+\frac{1}{2}$ transition are in closest agreement with this assumption at 55^{o}. Their calculation assumed that the main contribution to the linewidth came from the exchange interaction. Here it has been assumed that the broadening caused by the mosaic structure can be added directly to this basic linewidth to produce the total linewidth. The exchange integrals, which occurred in the theory of Altshuler and Mineeva, were evaluated by means of a relationship involving two constants. The constants were evaluated empirically from a known value of the integral at a certain interionic spacing and a known value of the half width at a certain concentration. No values for the integrals were calculated in the region where the exchange interaction produced new lines rather than broadening. The critical value of the spacing of the chromium ions where the exchange altered from splitting the transitions to broadening the transitions was obtained by comparing the energy of the exchange interaction with the energy of the crystal field splitting. When the exchange energy was larger,

the lines were split, and when it was smaller, the lines were broadened. Having established in this way the critical spacing of the ions, their prediction of the linewidths required only a knowledge of the local concentration in order to compare them with experiment.

Klyshko also used the concept of critical spacing, but he assumed that the exchange interactions between ions spaced further than the critical spacing were negligible with respect to the dipole-dipole interactions between these ions. He suggested that the value of the critical spacing could be obtained from the measured value of the linewidth. This was done, with the help of the table given by Klyshko, in the analysis given above. Two parameters, the critical spacing and the concentration, have to be inserted into his prediction of the linewidth before it can be compared with experiment, and also, an assumption has to be made concerning the shape of the line. The figures which he quoted in the paper were for a Gaussian line shape. The $-\frac{1}{2}$ to $+\frac{1}{2}$ transitions at 0° polar angle were close to Gaussian in shape.

CONCLUSIONS.

The widths of the various transitions examined, including the $-\frac{1}{2}$ to $+\frac{1}{2}$ transition, vary with polar angle, and have a maximum in the region of 45° to 55°. The amount of the broadening depends on the imperfection in the sample and has been correlated with the mean value of the mosaic

misorientation. Using the theoretical predictions of Altshuler and Mineeva, the local concentrations of chromium in the two samples were evaluated. These concentrations were several times the chemical concentrations in the samples, and they are thought to be concentrations of ions accumulated in the dislocated material. Sample G2a, which was the more imperfect sample, had a larger ratio of local to chemical concentration than 337c, indicating that in G2a the grain boundaries accumulated more chromium from the surrounding good material than they did in 337c.

The two volumes calculated in the previous section represent two different regions of the crystal. The smaller is the volume in which the dislocations have obliterated the crystal structure. The larger is the volume over which the dislocations have produced elastic strains. From the strength of the observed signal, the measured concentrations and the estimated volumes, it appears that the chromium ions which contribute most to the linewidth congregate in the elastically strained region. This region is related to the mosaic structure not the c-axis misorientation, which explains why $\Delta\Theta$ is related to the mosaic structure only.

The dislocation pattern depicted in figure 11 was assumed to be formed from simple edge dislocations. More complex systems probably existed in the samples, but neither the X-ray nor the linewidth measurements could detect these readily.

CHAPTER EIGHT.

CONCLUSIONS.

Conclusions drawn from the experimental work; discussion of the growth process; comments on maser action in these materials; thoughts about possible future work.

CONCLUSIONS DRAWN FROM THE EXPERIMENTAL WORK.

The X-ray work revealed that in every type of boule examined the c-axis changed direction from place to place by as much as 3° and that superimposed on this was a random distribution of mosaic with variations in the c-axis direction from crystallite to crystallite of up to 3°. The linear dimensions of the crystallites varied from microns to millimetres. The boules grown in the 90° growth direction were observed to contain less polycrystalline material than those grown in the other directions. Annealing of the 0° growth direction ruby boules did not improve their structure but it did improve their ability to withstand handling. There was no apparent connection between the distribution of mosaic structure in a boule and its crystallographic structure. In 0° growth orientation boules the regions of good or poor material extended parallel to the growth direction. This would be consistent with the propagation of dislocations from the seed crystal during growth. In boule 319 a plane of good

material was observed between the seed crystal and the main part of the boule. This was explained as follows, when the boule reached a certain size thermal stresses would be large and would form grain boundaries by polygonisation. The plane of good material occurred in the region close to the seed where the stresses were less and the polygonisation process was unlikely to take place.

Chemical etching revealed the sites of edge dislocations on the (0001) plane of the boules. The random dislocation densites in boules of every type, and in one seed crystal, were similar. The similarity of the imperfections in ruby and corundum, together with evidence that the chromium is found in larger amounts in the distorted regions of the ruby boules, was taken as demonstrating that the chromium does not form the dislocations but tends to congregate in the dislocations during the growth process.

Paramagnetic resonance linewidth measurements were performed on two samples, 337c, which had been annealed at 1930°C, and G2a, which was from the same boule as the first rod of English made ruby to be used in a laser. All the transitions examined showed broadening as the polar angle was altered from either 0° or 90° towards 45°. The amount of broadening depended on the sample as well as the transition examined and it reached a maximum in the region of 45° or 55° depending on the transition. The linewidth was fitted to an

expression of the form

$$\Delta H_{\frac{1}{2}} = H_{basic} + \Delta\theta . dH/d\theta . \qquad 8.1$$

H_{basic} was estimated at the various polar angles from the values of linewidth at the angles where $dH/d\theta = 0$ and $\Delta\theta$ was the mean value of the mosaic misorientation. C-axis misorientation of nearly 1^{o} did not appear to produce any angular dependent broadening. The value of $\Delta\theta$ calculated from the linewidths agreed quite well with the value calculated from the X-ray results. Broadening caused by non-uniformity of the crystalline field was not present.

The shapes of the lines examined were usually closer to Gaussian than Lorentzian. Some of the lines in the less perfect sample, G2a, were distorted from their usual near symmetrical shape by the mosaic broadening.

A more complete analysis of the width of the $-\frac{1}{2}$ to $+\frac{1}{2}$ transitions revealed values of the chromium concentration which helped to produce the linewidth. These values were larger than the values revealed by chemical methods and were taken as being the values of the local concentration in the grain boundaries and dislocations.

DISCUSSION OF THE GROWTH PROCESS.

The basal and prismatic slip systems encourage the growth of large boules in the 0^{o} and 73^{o} growth orientations. The 90^{o} boules are usually smaller. Because of the difference

in size, the thermal stresses in the 90° boules are likely to be less than in the other boules and so the action of polygonisation in the 90° boules is likely to be less. The polygonisation process can generate dislocations as well as form existing groups of dislocations into grain boundaries. Therefore, even with an almost perfect seed crystal, if the boule is under stress during the growth process, dislocations and grain boundaries are likely to occur. As thermal stresses are least likely in small 90° boules, it appears that the best material should result from using the seed crystal with the lowest dislocation density to grow a small boule in the 90° orientation.

Any attempt to reduce thermal stresses by reducing the temperature gradients in the furnace is usually very difficult to put into operation and it may make the growth process longer by slowing the cooling rate. It is the thermal gradients within the boule which have to be adjusted to reduce the thermal stresses, not those within the furnace, although it is obvious that altering the latter will alter the former. Sometimes it may be advantageous to have a large temperature gradient within the boule so that the inner regions of the boule cool to the solidification point rapidly.

COMMENTS ON MASER ACTION.

Crystals of the type described here would have several effects on maser action. The angular broadening of

the - $\frac{1}{2}$ to + 3/2 transition, which could be used as a pump transition, would mean that at some angles pump power would be lost in the wings of the transition. The angular broadening of the major transitions, on the other hand, may be useful in allowing a wider bandwidth for the signal. The spread in the directions of the c-axis may mean that at any one orientation where the angular position is critical part of the crystal is not undergoing maser action. The higher local concentrations in the poor material mean that cross-relaxation is more effective and this too may cause a loss of pump power. For ruby masers working at temperatures above those of liquid helium the extra cross-relaxation may be an advantage. These comments show that the effects may or may not be advantageous depending on the exact requirements of the maser system.

If the small 90° growth boules are of better quality than the ones described here it may be possible to fabricate large pieces of ruby suitable for use in masers or lasers. The accuracy required in aligning the various blocks with respect to one another will discourage attempts at a widespread use of this technique.

The quality of any sample of ruby can be judged from three measurements of the half widths of transitions. They are the -3/2 to - $\frac{1}{2}$ and the - $\frac{1}{2}$ to + $\frac{1}{2}$ at 0° polar angle, and the - $\frac{1}{2}$ to + $\frac{1}{2}$ at 55°. From these, the magnitudes of the

TABLE 10.

CHROMIUM CONCENTRATIONS PREDICTED FROM LINEWIDTHS.

	Sample 337c			Sample G2a		
Polar angle	0°	55°(a)	55°(b)	0°	55°(a)	55°(b)
Measured linewidth (oersteds)	32·0	28·9	28·9	24·4	29·2	29·2
Adjusted + linewidth (oersteds)	32·0	18·8	17·9	24·4	12·2	15·1
Concentration (weight %)	0·23	0·24	0·23	0·17	0·16	0·2

+ Adjusted linewidth applies to the values at 55° where allowance has been made for the broadening of the line caused by mosaic structure and the contribution to the width from hyperfine interactions. This latter contribution was taken as 9.7 oersteds, its theoretical value. In calculating the broadening caused by mosaic structure, case (a) is the value estimated from the X-ray value of the mosaic misorientation, case (b) is the value estimated from the linewidth value of the misorientation.

mosaic misorientation, the non-uniformity of the crystalline field and the chromium concentration can be calculated. If more accuracy is required in the value of the mosaic misorientation, it would be advantageous to measure the half width of the -3/2 to - ½ transition at the polar angle 45° also.

FUTURE WORK.

One of the projects which could be started immediately with the spectrometer used for the measurements described here is a similar investigation of the -3/2 to + ½ and the -3/2 to +3/2 transitions and a full investigation of several more samples to confirm the importance of mosaic structure as compared to the c-axis misorientation. It would also be interesting to investigate some samples from 90° growth orientation boules and from boules with low dislocation densities. The quality test suggested at the end of the last section could be applied to small pieces taken from different regions of the same boule in order to check the distribution of mosaic structure and chromium concentration and their correlation. By experimental or theoretical methods the basic linewidth in undistorted samples ought to be estimated. This parameter had to be assumed above. One last suggestion is to attempt to correlate the measured linewidths to the strain around the dislocations in the samples and the displacement of the atoms connected with the dislocations.

APPENDIX ONE

A letter to the editor, reprinted from the British Journal of Applied Physics, Volume 15, page 775, 1964.

Reprinted from

British Journal of Applied Physics

The Institute of Physics and The Physical Society

Printed in Great Britain by Adlard & Son, Ltd., Dorking

are caused by local high concentrations of chromium. Thus to achieve better homogeneity of doping the mosaic imperfection should be reduced, for example by better control of the temperature gradients occurring in the growing crystal.

Similar arguments apply to the distribution of iron impurity concentrations.

Acknowledgments

We wish to acknowledge the co-operation received from The Thermal Syndicate Ltd. throughout this work.

Two of us (D. A. C. and D. R. M.) also wish to thank the Department of Scientific and Industrial Research for its award of maintenance grants.

Department of Applied Physics,
University of Durham.

J. S. THORP
D. A. CURTIS
D. R. MASON

29th January 1964, *in revised form* 18*th March* 1964

DILS, R. R., MARTIN, G. W., and HUGGINS, R. A., 1962, *Appl. Phys. Letters*, **1**, 75.
DODSON, E. M., 1962, *Analyt. Chem.*, **34**, 966.
SCHEUPLEIN, R., and GIBBS, P., 1960, *J. Amer. Ceram. Soc.*, **43**, 458.
THORP, J. S., and CURTIS, D. A., 1964, 3*rd International Symposium on Quantum Electronics, Paris* 1963. (New York: Columbia University Press), in the press.
YONEMITSU, H., and MARUYAMA, T., 1962, *J. Chem. Soc. Japan*, **65**, 1729.

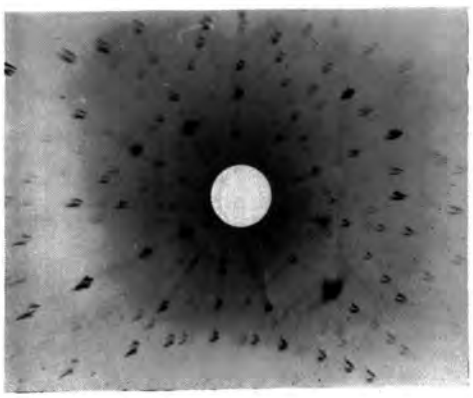

Figure 1. Specimen 1. Outer region of ruby boule (concentration 20 μg Cr per mg Al_2O_3). Back reflection photograph taken 0·5 mm from boule outer surface. Beam parallel to c axis, CuKα radiation.

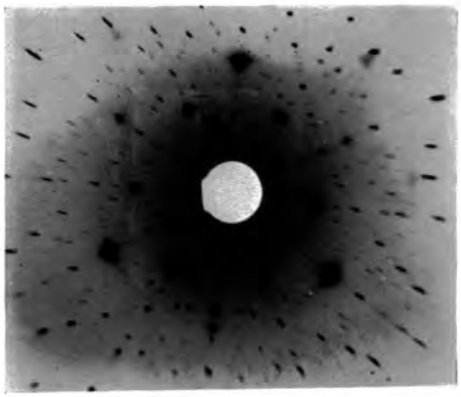

Figure 2. Specimen 1. Central region of ruby boule (concentration 0·35 μg Cr per mg Al_2O_3). Back reflection photograph taken 4·5 mm from boule outer surface. Beam parallel to c axis, CuKα radiation.

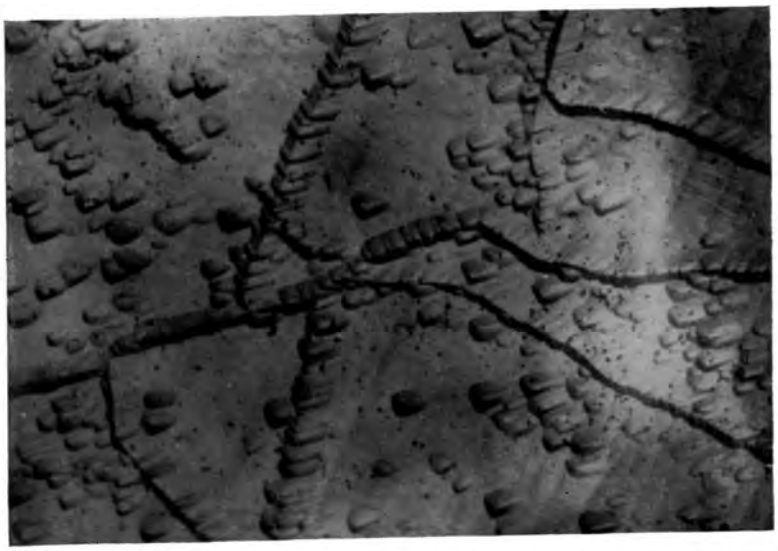

Figure 3. Etch pit pattern on (0001) face in central region of boule. Magnification $\times 160$.

APPENDIX TWO.

THE CALCULATION OF TRANSITION PROBABILITIES IN THE GENERAL CASE

The experimental arrangement deviated in two respects from the perfect arrangement assumed in chapter four for the calculation of the transition probabilities. The c-axis of the specimen was not parallel to OX nor was the guide parallel to Oy. The situation is shown in figure 23.

The components of H_X and H_Z along x,y and z are

$$\begin{aligned} H_x &= H_X \sin\gamma \cos\delta, & H_x &= H_Z \sin\epsilon \cos i, \\ H_y &= H_X \sin\gamma \sin\delta, & H_y &= H_Z \sin\epsilon \sin i, \\ H_z &= H_X \cos\gamma, & H_z &= H_Z \cos\epsilon. \end{aligned} \qquad \text{A2.1}$$

These components cause the transitions and by combining them, taking account of the phases, the transition probabilities can be calculated. However, by careful adjustment of the waveguide so that it is perpendicular to the x-z plane, $\alpha = 0^\circ$, $\epsilon = i = 90^\circ$ and $\delta = 0^\circ$ because OX is then in the x-z plane. Therefore, the expressions in A2.1 simplify considerably to

$$H_x = H_X \sin\gamma, \quad H_y = H_Z, \quad H_z = H_X \cos\gamma. \qquad \text{A2.2}$$

It is known from the X-ray and etching work that $\beta < 5^\circ$. The mean direction of the c-axis can be resolved onto the walls defined by rs and by rt where it has the values λ and μ respectively. Then $\theta = \gamma \pm \lambda$ as rs is in the x-z plane because $\alpha = 0^\circ$. Then expressions A2.2 become

$$H_x = H_X \sin(\theta \pm \lambda), \quad H_y = H_Z, \quad H_z = H_X \cos(\theta \pm \lambda). \qquad \text{A2.3}$$

KEY TO FIGURE 23.

c is the c-axis, r is OX, s is OY and t is OZ.

Oz is the magnetic field direction.

The coordinates of c are θ , ϕ ; the coordinates of r are γ , δ ; the coordinates of t are ϵ , i.

The angle between t and Oy is α.

The angle between c and r is β.

γ is the angle between the magnetic field direction and OX (the broad dimension of the guide).

δ is the angle between Ox and the intercept of the plane Oz OX with the vertical plane containing Ox. (Horizontals and verticals are with respect to the floor.)

ϵ and i are similar for OZ.

H_X is parallel to r and H_Z is parallel to t.

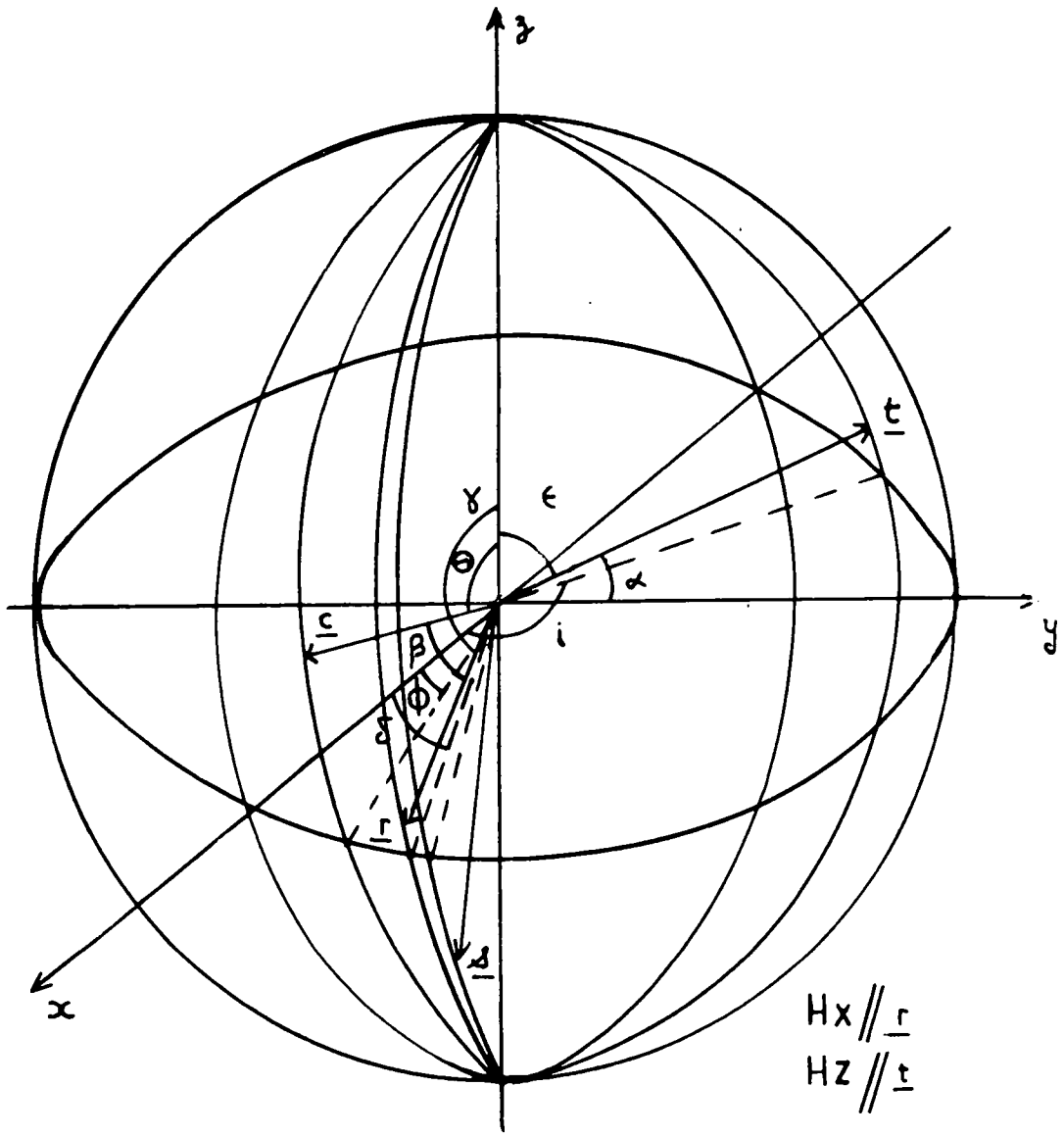

COORDINATE SYSTEM FOR CALCULATING TRANSITION PROBABILITIES.

FIGURE 23 .

In the calculations performed in chapter four the effects of λ were neglected because it was desired only to compare the probabilities at two neighbouring polar angles and not to calculate the absolute probabilities at these polar angles. The angle μ means that the c-axis is not in the x-z plane even if rs, the waveguide, is. μ projects into the x-y plane and it indicates the permanent misorientation of the c-axis about Oz and is the ϕ coordinate of the system. The variations in ϕ are about this direction μ but in the case of the calculation in chapter four this is not of importance because, through the eigenvectors, μ will affect the transition probabilities at each angle θ by the same amount. For comparison purposes it is adequate to take $\mu = 0^\circ$.

The assumptions given above concerning the neglecting of terms are not always correct, especially if α is not exactly equal to zero. H_x has two terms, one is $H_x \sin\gamma\cos\delta$ and the other is $H_z \sin\epsilon \sin i$. For $\alpha \simeq 0^\circ$, $\epsilon \simeq i \simeq 90^\circ$, $\delta \simeq 0^\circ$ and $\gamma = 90^\circ$ the term in H_Z is very much smaller than the term in H_X. For $\gamma = 0^\circ$ however, the term in H_X is zero so the term in H_Z is the important term. Similar comments apply to H_y and H_z and they should be allowed for in the complete calculation of the probabilities.

The importance of aligning the waveguide as

accurately as possible in order to make $\alpha = 0^{\circ}$ and so make the above assumptions valid, can now be seen. In this case the simple calculations made to check whether the transition probabilities vary rapidly with angle are reliable. Also, when $\alpha = 0^{\circ}$ the angle at which the magnet is set is the polar angle. If β is made as small as possible, further simplifications can be made. A second reason for having a small value of β is that the specimens were more easily examined by the X-ray and etching techniques in this orientation.

REFERENCES.

Altshuler, S.A., and Mineeva, R.M., 1963, Sov. Phys. Sol. State, 5, 1234.

Anderson, P.W., and Weiss, P.R., 1953, Rev. Mod. Phys., 25, 269.

Barrett, C.S., 1952, Structure of Metals, p.187, McGraw-Hill.

Bell, D.A., 1960, Electrical Noise, p.225, Van Nostrand.

Bersohn, R., and Das, T.P., 1963, Phys. Rev., 130, 98.

Bleaney, B., and Stevens, K.W.H., 1953, Rep. on Prog. in Phys., 16, 108.

Bloch, F., 1946, Phys. Rev., 70, 460.

Bloembergen, N., Purcell, E.M., and Pound, R.V., 1948, Phys. Rev., 73, 679.

Bloembergen, N., 1956, Phys. Rev., 104, 324.

Combrisson, A., Honig, A., and Townes, C.H., 1956, Compt. Rend. Acad. Fran., 242, 2451.

Ellis, S.G., 1955, Jour. App. Phys., 26, 1140.

Elliston, P.R., Troup, G.J., and Hutton, D.R., 1963, Jour. Sci. Inst., 40, 586.

Feher, G., 1957, B.S.T.J., 36, 449.

Flynn, C.P., and Seymour, E.F.W., 1960, Proc. Phys. Soc., 75, 337.

Goldsborough, J.P., and Mandel, M., 1960, Rev. Sci. Inst., 31, 1044.

Gordon, J.P., Zeiger, H.Z., and Townes, C.H., 1954, Phys. Rev., 95, 282.

Guinier, A., and Tennevin, J., 1949, Acta Cryst., 2, 133.

Hirsch, P.B., 1956, Prog. in Met. Phys., 6, 236.

Horn, F.H., 1952, Phil. Mag., 43, 1210.

Ingram, D.J.E., 1955, Spectroscopy at Radio and Microwave Frequencies, p.76, Butterworths.

REFERENCES (Cont.)

Klauder, J.R., and Anderson, P.W., 1962, Phys. Rev., 125, 912.

Klyshko, D.N., 1964, Sov. Phys. Sol. State, 5, 2066.

Lambot, H., Vassamillet, L., and Dejace, J., 1953, Acta Met., 1, 711.

Lang, A.R., 1958, Jour. App. Phys., 29, 597.

Lonsdale, K., Editor, 1959, Int. Tables for X-Ray Cryst., Vol. 2, p. 161, The Kynoch Press.

Manenkov, A.A., and Fedorov, V.B., 1960, Sov. Phys. J.E.T.P., 11, 751.

Manenkov, A.A., Popova, A.A. and Khaimov-Malkov, V.Y., 1963, Sov. Phys. Sol. State, 5, 1194.

Méléka, A.H.A., 1958, Phil. Mag., 1, 803.

Misra, H., 1963, Ind. Jour. of Pure and App. Phys., 1, 37.

Montgomery, C.G., Dicke, R.H., and Purcell, E.M., 1947, M.I.T. Rad. Lab. Series, Vol.8, p.225, McGraw-Hill.

O'Reilly, D.E., and Tsang. T., 1962, Phys. Rev., 128, 2639.

Pace, J.H., Sampson, D.F., and Thorp, J.S., 1960, Proc. Phys. Soc., 76, 697.

Pryce, M.H.L., and Stevens, K.W.H., 1950, Proc. Phys. Soc., 63A, 36.

Richardson, D., 1964, Mic. Jour., 7, 92.

Scheuplein, R. and Gibbs, P., 1960, Jour. Amer. Cer. Soc., 43, 458.

Schulz-du Bois, E.O., 1959, B.S.T.J., 38, 271.

Shaltiel, D., and Low, W., 1961, Phys. Rev., 124, 1062.

Statz, H., Rimai, L., Weber, M.J., de Mars, G.A., and Koster, G.F., 1961, Jour. App. Phys. (Supp.), 32, 2188.

Thorp, J.S., Curtis, D.A., and Mason, D.R., 1964, B.J.A.P., 15, 775.

REFERENCES (Cont.)

Topping, J., 1958, Errors of Observation and Their Treatment, p. 82, Chapman and Hall.

Torrey, H.B., and Whitmer, C.A., 1947, M.I.T. Rad. Lab. Series, Vol. 15, (a) p.28, (b) p.181, (c) p.346, McGraw-Hill.

Uhlir, A., 1963, Mic. Jour., 6, 59.

Van Vleck J.H., 1948, Phys. Rev., 74, 1168.

Woods, J., 1960, B.J.A.P., 11, 296.